

Dynamical stability of systems with long-range interactions: application of the Nyquist method to the HMF model

P.H. Chavanis and L. Delfini

¹ Université de Toulouse, UPS, Laboratoire de Physique Théorique (IRSAMC), F-31062 Toulouse, France

² CNRS, Laboratoire de Physique Théorique (IRSAMC), F-31062 Toulouse, France

e-mail: chavanis@irsamc.ups-tlse.fr; Luca.Delfini@irsamc.ups-tlse.fr

To be included later

Abstract. We apply the Nyquist method to the Hamiltonian Mean Field (HMF) model in order to settle the linear dynamical stability of a spatially homogeneous distribution function with respect to the Vlasov equation. We consider the case of Maxwell (isothermal) and Tsallis (polytropic) distributions and show that the system is stable above a critical kinetic temperature T_c and unstable below it. Then, we consider a symmetric double-humped distribution, made of the superposition of two decentered Maxwellians, and show the existence of a re-entrant phase in the stability diagram. When we consider an asymmetric double-humped distribution, the re-entrant phase disappears above a critical value of the asymmetry factor $\Delta > 1.09$. We also consider the HMF model with a repulsive interaction. In that case, single-humped distributions are always stable. For asymmetric double-humped distributions, there is a re-entrant phase for $1 < \Delta < 25.6$, a double re-entrant phase for $25.6 < \Delta < 43.9$ and no re-entrant phase for $\Delta > 43.9$. Finally, we extend our results to arbitrary potentials of interaction and mention the connexion between the HMF model, Coulombian plasmas and gravitational systems. We discuss the relation between linear dynamical stability and formal nonlinear dynamical stability and show their equivalence for spatially homogeneous distributions. We also provide a criterion of dynamical stability for inhomogeneous systems.

PACS. 0 5.20.-y Classical statistical mechanics - 05.45.-a Nonlinear dynamics and chaos - 05.20.Dd Kinetic theory - 64.60.De Statistical mechanics of model systems

1 Introduction

Systems with long-range interactions have recently been the object of considerable interest [1,2]. These systems have applications in different areas of physics, astrophysics, hydrodynamics and biology ¹. Furthermore, they display very peculiar phenomena with respect to ordinary systems with short-range interactions such as negative specific heats [6-9], inequivalence of statistical ensembles [10-16], numerous types of phase transitions persisting at the thermodynamic limit [17,18], slow collisional relaxation [19-25], kinetic blocking due to the absence of resonances [26-30,25], non-trivial dependence of the collisional relaxation time with the number N of particles [31-33], long-lived metastable states whose lifetimes increase exponentially with N [34,35], algebraic decay of the correlation functions [36,37,28,30,38], front structure and slow relaxation of the velocity tails [39,30], long-lived quasi stationary states (QSS) [20-23,31,32,40,41,24,25,42], violent collisionless relaxation of the Vlasov equation [43-47,29,48-51], out-of-equilibrium phase transitions [52-59],

re-entrant phases [55,58], dynamical phase transitions [60], curious effects due to spatial inhomogeneity [61], non-ergodic behaviors [62,31,63,64], glassy dynamics [65], non-ideal effects due to the influence of a thermal bath [29,66-68] etc... Certainly, the physical richness of these systems (Pandora box) will lead to further investigations and applications.

For systems with long-range interactions, the mean field approximation is exact in a proper thermodynamic limit where the number of particles $N \rightarrow +\infty$ while the strength of the interaction $k \sim 1/N$ (coupling constant) goes to zero and the volume $V \sim 1$ remains fixed [1,2,69]. For a fixed interval of times $[0, T]$ and $N \rightarrow +\infty$, the evolution of the distribution function $f(\mathbf{r}, \mathbf{v}, t)$ is governed by the (mean field) Vlasov equation. The Vlasov equation describes the collisionless dynamics of the system for sufficiently “short” times with respect to the collisional relaxation time: $t \ll t_R(N)$. In fact, the relaxation time $t_R(N)$ increases rapidly with the number of particles N so that, in practice, the domain of validity of the Vlasov equation is huge [69]. Since the Vlasov equation admits an infinite number of steady states, the system can be found in quasi stationary states (QSS) that differ from the Boltzmann distribution. These are long-lived stable

¹ For example, there exists beautiful analogies between self-gravitating systems, two-dimensional vortices and bacterial populations investigated by one of the authors [3-5].

steady states of the Vlasov equation. For example, if we place initially the system in a stable steady state of the Vlasov equation $f_0(\mathbf{r}, \mathbf{v})$, it will remain in that state for a very long time until “collisions” (more precisely correlations due to finite N effects) make it slowly evolve [69]. On the other hand, if we start from an unstable steady state of the Vlasov equation, or from an unsteady initial condition, the system will spontaneously evolve through phase mixing and violent relaxation towards a QSS on the coarse-grained scale (see, e.g., [21,3]). This distribution function $\bar{f}_{QSS}(\mathbf{r}, \mathbf{v})$ is a stable steady state of the Vlasov equation that can be predicted by the statistical theory of Lynden-Bell [43] if the evolution is ergodic (i.e. if the system “mixes” efficiently [69]). As a result, it is important on general grounds to study the dynamical stability of stationary solutions of the Vlasov equation and devise general stability criteria.

This problem has been first considered in plasma physics [70-72] and astrophysics [20-23]. In plasma physics, the interaction between like-sign charges is repulsive. However, in neutral plasmas, the presence of opposite charges screens the interaction between like-sign charges (Debye shielding) so that the system is spatially homogeneous. Several methods have been developed to study the dynamical stability of spatially homogeneous distribution functions $f(\mathbf{v})$ with respect to the Vlasov equation. One approach is to determine criteria of nonlinear dynamical stability or formal nonlinear stability by minimizing an energy-Casimir functional [73]. Another approach is to determine criteria of linear stability by linearizing the Vlasov equation around a steady state, taking the Laplace-Fourier transform to obtain the dispersion relation and studying the sign of the imaginary part of the complex pulsation [70-72]. In some cases, the dispersion relation can be solved analytically and the pulsation can be obtained explicitly. In more complicated cases, the dispersion relation must be solved numerically. We can also have recourse to other methods to settle the linear stability of the system without being required to solve the dispersion relation. In this respect, Nyquist [74] has introduced a powerful method to investigate the linear stability of a spatially homogeneous distribution of the Vlasov equation. This is based on a graphical construction that can be easily implemented in practice. This method tells whether the distribution is linearly stable (or unstable) but it does not give the value of the decay rate (or growth rate) of the perturbation. Using this criterion, it can be shown with almost no calculation that the Maxwellian distribution is always dynamically stable in a plasma for perturbations with arbitrary wavenumbers.

For gravitational systems, the interaction between masses is attractive leading to possible collapse (Jeans instability). We could imagine using the Nyquist method to settle the dynamical stability of a galaxy described by the Vlasov equation. However, we are rapidly confronted to the difficulty that a realistic stellar system is spatially inhomogeneous [20-23]. This considerably complicates the stability analysis and precludes the direct application of the Nyquist method. In that case, we must use other meth-

ods like the Antonov [75-77] criterion of linear dynamical stability or methods of nonlinear dynamical stability [78]. Using these methods, it can be shown that any distribution function of the form $f = f(\epsilon)$ with $f'(\epsilon) < 0$ where $\epsilon = v^2/2 + \Phi(\mathbf{r})$ is the individual energy of a star is linearly [21], and even nonlinearly [78], dynamically stable with respect to the Vlasov equation. The Nyquist method can be used (see Appendix D) to investigate the linear dynamical stability of a rather unrealistic infinite and homogeneous distribution of stars making the Jeans swindle [21]. For a Maxwellian distribution, it leads to a graphical illustration of the Jeans instability showing that the system is unstable with respect to perturbations of sufficiently low wavenumbers $k < k_J$, where $k_J = (4\pi G\beta n)^{1/2}$ is the Jeans wavenumber.

In this paper, we consider the Hamiltonian Mean Field (HMF) model which is a very much studied toy model of systems with long-range interactions [79,29]. In this model, the interaction between particles is attractive like gravity but, unlike gravity, the system can be spatially homogeneous. Therefore, for the HMF model, it is possible to use the Nyquist method of plasma physics to investigate the linear stability of a homogeneous distribution. However, since the interaction is attractive, a crucial sign changes in the dispersion relation and this leads to new results with respect to plasma physics. As a direct application of this method, we can recover by a graphical construction the fact that the Maxwellian distribution is linearly stable with respect to the Vlasov equation if $T > T_c$ and linearly unstable if $T < T_c$ where $T_c = \frac{kM}{4\pi}$ is a critical temperature. This instability is similar to the Jeans instability in astrophysics where the temperature T plays the role of the wavenumber k .

The paper is organized as follows. In Sec. 2, we recall basic results concerning the Vlasov equation, the dispersion relation and the Nyquist method in relation to the HMF model. We first consider the HMF model with an attractive interaction (ferromagnetic). Using the Nyquist method, we establish general linear stability criteria for single-humped and double-humped distributions. In Secs. 3 and 4, we apply the Nyquist method to the Maxwell (isothermal) and the Tsallis (polytropic) distributions. We show that the system is linearly stable if $T > T_c$ and linearly unstable if $T < T_c$ where $T_c = \frac{n}{n+1} \frac{kM}{4\pi}$ is a critical kinetic temperature depending on the polytropic index n (the Maxwellian distribution is recovered for $n \rightarrow +\infty$). In Sec. 5, we consider a symmetric double-humped distribution made of the superposition of two decentered Maxwellians (with separation v_a). We show that this distribution has a rich stability diagram in the (v_a, T) plane exhibiting a re-entrant phase. In Sec. 6, we generalize our study to the case of an asymmetric double-humped distribution where the amplitude of one maximum is larger than the other by a factor $\Delta > 1$. We determine how the stability diagram in the (v_a, T) plane changes as a function of Δ and show that the re-entrant phase disappears above a very small asymmetry $\Delta > \Delta_c = 1.09$. In Sec. 7, we consider the HMF model with a repulsive interaction (antiferromagnetic). We show that single-humped

distributions (like the Maxwell and the Tsallis distributions) are always linearly stable. We also establish general linear stability criteria for double-humped distributions. More specifically, we investigate the linear stability of a double-humped distribution made of two Maxwellian distributions. For $\Delta = 1$ (symmetric case), we show the existence of a re-entrant phase. A double re-entrant phase appears for $\Delta > \Delta_c^{(1)} = 25.6$ and they both disappear for $\Delta > \Delta_c^{(2)} = 43.9$. In Sec. 8 we discuss the extension of our results to arbitrary attractive or repulsive potentials of interaction and make the connexion between the HMF model, Coulombian plasmas and gravitational systems. We also discuss the relation between linear and formal nonlinear stability and show their equivalence for spatially homogeneous systems.

2 Dynamical stability of the HMF model

2.1 The Vlasov equation

The HMF model consists in N particles of unit mass $m = 1$ moving on a circle and interacting via a cosine potential [79,29]. The microscopic dynamics of this system is governed by the Hamiltonian equations

$$\frac{d\theta_i}{dt} = \frac{\partial H}{\partial v_i}, \quad \frac{dv_i}{dt} = -\frac{\partial H}{\partial \theta_i}, \quad (1)$$

$$H = \sum_{i=1}^N \frac{v_i^2}{2} - \frac{k}{2\pi} \sum_{i<j} \cos(\theta_i - \theta_j), \quad (2)$$

where θ_i is the angle that particle i makes with an axis of reference, $v_i = d\theta_i/dt$ is its velocity and $k > 0$ is the coupling constant. This system conserves the energy $E = H$ and the total mass $M = Nm = N$.

The evolution of the N -body distribution $P_N(\theta_1, v_1, \dots, \theta_N, v_N, t)$ is governed by the Liouville equation

$$\frac{\partial P_N}{\partial t} + \sum_{i=1}^N \left(v_i \frac{\partial P_N}{\partial \theta_i} + F_i \frac{\partial P_N}{\partial v_i} \right) = 0 \quad (3)$$

where

$$F_i = -\frac{\partial \Phi}{\partial \theta_i} = -\frac{k}{2\pi} \sum_{j \neq i} \sin(\theta_i - \theta_j) = \sum_{j \neq i} F(j \rightarrow i) \quad (4)$$

is the total force experienced by particle i due to the interaction with the other particles. From the Liouville equation, we can construct the BBGKY hierarchy for the reduced distributions $P_j(\theta_1, v_1, \dots, \theta_j, v_j, t) = \int P_N(\theta_1, v_1, \dots, \theta_N, v_N, t) \prod_{k=j+1}^N d\theta_k dv_k$ [24].

We consider the thermodynamic limit $N \rightarrow +\infty$ in such a way that the dimensionless energy $\epsilon = 8\pi E/kM^2$ and the dimensionless temperature $\eta = kM/4\pi T$ are of order unity (these scalings are obtained by comparing

the kinetic and the potential energies in Eq. (2) yielding $E \sim N\langle v^2 \rangle \sim NT \sim kN^2$). We can renormalize the parameters so that the coupling constant $k \sim 1/N$ while $\beta \sim 1$, $E/N \sim 1$ and $V = 2\pi \sim 1$. The dynamical time $t_D \sim 2\pi/\sqrt{\langle v^2 \rangle} \sim 1/\sqrt{k\rho}$ is also of order unity². In the thermodynamic limit $N \rightarrow +\infty$, it can be shown from scaling arguments [24] that the N -body distribution factorizes in a product of N one-body distributions

$$P_N(\theta_1, v_1, \dots, \theta_N, v_N, t) = \prod_{i=1}^N P_1(\theta_i, v_i, t). \quad (5)$$

Substituting this result in the first equation of the BBGKY hierarchy, we find that the one-body distribution $P_1(\theta, v, t)$, or equivalently the smooth distribution function $f(\theta, v, t) = NP_1(\theta, v, t)$, satisfies the Vlasov equation³

$$\frac{\partial f}{\partial t} + v \frac{\partial f}{\partial \theta} - \frac{\partial \Phi}{\partial \theta} \frac{\partial f}{\partial v} = 0, \quad (6)$$

where

$$\Phi(\theta, t) = -\frac{k}{2\pi} \int_0^{2\pi} \cos(\theta - \theta') \rho(\theta', t) d\theta', \quad (7)$$

is the mean field potential and $\rho(\theta, t) = \int f(\theta, v, t) dv$ is the spatial density. The mean field average force experienced by a particle located in θ is $\langle F \rangle = -\Phi'(\theta)$.

The Vlasov equation admits an infinite number of stationary solutions. A spatially homogeneous system ($\Phi = 0$) with distribution function (DF) $f = f(v)$ is always a steady state of the Vlasov equation. If the system is spatially inhomogeneous ($\Phi \neq 0$), the general form of steady distributions of the Vlasov equation is $f = f(\epsilon)$ where $\epsilon = v^2/2 + \Phi(\theta)$ is the individual energy. In this paper, we shall only consider spatially homogeneous distributions so that $f = f(v)$.

2.2 The dispersion relation

We want to study the linear dynamical stability⁴ of a spatially homogeneous stationary solution of the Vlasov equation described by a distribution function $f = f(v)$. Linearizing the Vlasov equation around the steady state and taking the Laplace-Fourier transform (writing the perturbation as $\delta f_{n\omega} \sim \delta \Phi_{n\omega} \sim e^{i(n\theta - \omega t)}$), we obtain the dispersion relation [81,82,29]:

$$\epsilon(n, \omega) \equiv 1 + \frac{k}{2} (\delta_{n,1} - \delta_{n,-1}) \int_C \frac{f'(v)}{nv - \omega} dv = 0, \quad (8)$$

² In this paper, we use the notations of [29] that are similar to those introduced in astrophysics. The link with the notations of [32] is made by taking $k = 2\pi/N$, $\eta = \beta/2$ and $\epsilon = 4(U - 1/2)$.

³ A rigorous derivation of the Vlasov equation is given by Braun & Hepp [80].

⁴ In fact, we consider here the *spectral* stability of a distribution function $f = f(v)$. For infinite dimensional systems, spectral stability does not necessarily imply *linear* stability [73]. However, by an abuse of language, we shall often say “linearly stable” instead of “spectrally stable”.

where $\epsilon(n, \omega)$ is the dielectric function and the integral must be performed along the Landau contour (C) [72]. There exists solutions only for $n = \pm 1$ so that only these modes can propagate⁵. For the mode $n = +1$ ($n = -1$ gives the same result), Eq. (8) reduces to

$$\epsilon(\omega) \equiv 1 + \frac{k}{2} \int_C \frac{f'(v)}{v - \omega} dv = 0, \quad (9)$$

which is the fundamental equation studied in this paper. For a given distribution $f(v)$, this equation determines the complex pulsation(s) $\omega = \omega_r + i\omega_i$ of the linearized perturbation δf . Since $\delta f \sim e^{\omega_i t}$, the system is linearly stable if $\omega_i < 0$ and linearly unstable if $\omega_i > 0$. For future reference, let us recall that

$$\int_C \frac{f'(v)}{v - \omega} dv = \int_{-\infty}^{+\infty} \frac{f'(v)}{v - \omega} dv, \quad (\omega_i > 0), \quad (10)$$

$$\int_C \frac{f'(v)}{v - \omega} dv = P \int_{-\infty}^{+\infty} \frac{f'(v)}{v - \omega} dv + i\pi f'(\omega), \quad (\omega_i = 0), \quad (11)$$

$$\int_C \frac{f'(v)}{v - \omega} dv = \int_{-\infty}^{+\infty} \frac{f'(v)}{v - \omega} dv + 2\pi i f'(\omega), \quad (\omega_i < 0). \quad (12)$$

2.3 The condition of marginal stability

The condition of marginal stability corresponds to

$$\omega_i = 0, \quad (13)$$

where ω_i is the imaginary part of ω . In that case, $\omega = \omega_r$ is real and the integral in Eq. (9) can be evaluated along the real axis by using the Plemelj formula [72]:

$$\frac{1}{u - a} = P \frac{1}{u - a} + i\pi \delta(u - a), \quad (14)$$

where P denotes the principal value. We obtain

$$1 + \frac{k}{2} P \int_{-\infty}^{+\infty} \frac{f'(v)}{v - \omega_r} dv + i\pi \frac{k}{2} f'(\omega_r) = 0. \quad (15)$$

Identifying the real and the imaginary parts, it follows that the marginal mode is determined by the equations [29]:

$$1 + \frac{k}{2} \int_{-\infty}^{+\infty} \frac{f'(v)}{v - \omega_r} dv = 0, \quad (16)$$

$$f'(\omega_r) = 0. \quad (17)$$

The second relation fixes the pulsation ω_r of the perturbation and the first relation determines the point of marginal

stability in the series of equilibria⁶. Note that the distribution $f(v)$ can be relatively arbitrary. However, if $f(v)$ has a single maximum at $v = 0$, then $\omega_r = 0$ (implying $\omega = 0$) and the condition of marginal stability becomes

$$1 + \frac{k}{2} \int_{-\infty}^{+\infty} \frac{f'(v)}{v} dv = 0. \quad (18)$$

2.4 The Nyquist Method

To determine whether the distribution $f = f(v)$ is stable or unstable, one possibility is to solve the dispersion relation (9) and determine the sign of the imaginary part of the complex pulsation. This can be done analytically in some simple cases [29]. In this paper, we use another strategy. We shall apply the Nyquist method introduced in plasma physics. This is a graphical method that does not require to solve the dispersion relation. The details of the method are explained in [72] and we just recall how it works in practice. In the ϵ -plane, we plot the Nyquist curve⁷ ($\epsilon_r(\omega_r), \epsilon_i(\omega_r)$) parameterized by ω_r going from $-\infty$ to $+\infty$. This curve is closed and always rotates in the counterclockwise sense. If the Nyquist curve does not encircle the origin, the system is stable. If the Nyquist curve encircles the origin one or more times, the system is unstable. The number N of tours around the origin gives the number of zeros of $\epsilon(\omega)$ in the upper half plane, i.e. the number of unstable modes with $\omega_i > 0$. The Nyquist method by itself does not give the growth rate of the instability.

2.5 General properties

Let us determine some general properties of the Nyquist curve for the HMF model. Taking $\omega_i = 0$, we have

$$\epsilon(\omega_r) = 1 + \frac{k}{2} P \int_{-\infty}^{+\infty} \frac{f'(v)}{v - \omega_r} dv + i\pi \frac{k}{2} f'(\omega_r). \quad (19)$$

Therefore, the real and imaginary parts of the dielectric function $\epsilon(\omega_r) = \epsilon_r(\omega_r) + i\epsilon_i(\omega_r)$ are

$$\epsilon_r(\omega_r) = 1 + \frac{k}{2} P \int_{-\infty}^{+\infty} \frac{f'(v)}{v - \omega_r} dv, \quad (20)$$

$$\epsilon_i(\omega_r) = \pi \frac{k}{2} f'(\omega_r). \quad (21)$$

To apply the Nyquist method, we have to plot the curve ($\epsilon_r(\omega_r), \epsilon_i(\omega_r)$) parameterized by ω_r going from $-\infty$ to $+\infty$. Let us consider the asymptotic behavior for $\omega_r \rightarrow \pm\infty$. Since $f(v)$ tends to zero for $v \rightarrow \pm\infty$, we conclude that $\epsilon_i(\omega_r) \rightarrow 0$ for $\omega_r \rightarrow \pm\infty$ and that $\epsilon_r(\omega_r) > 0$ for

⁵ This differs from the case of gaseous systems described by the dispersion relation (160).

⁶ When condition (17) is fulfilled the integral is convergent in $v = \omega_r$ so that the principal part is not necessary.

⁷ This curve is also called an hodograph.

$\omega_r \rightarrow -\infty$ while $\epsilon_i(\omega_r) < 0$ for $\omega_r \rightarrow +\infty$. On the other hand, integrating by parts in Eq. (20), we obtain

$$\epsilon_r(\omega_r) = 1 + \frac{k}{2} P \int_{-\infty}^{+\infty} \frac{f(v)}{(v - \omega_r)^2} dv, \quad (22)$$

provided that $f(v)$ decreases sufficiently rapidly. Therefore, for $\omega_r \rightarrow \pm\infty$, we obtain at leading order

$$\epsilon_r(\omega_r) \simeq 1 + \frac{k}{2} \frac{\rho}{\omega_r^2}, \quad (\omega_r \rightarrow \pm\infty). \quad (23)$$

In particular, $\epsilon_r(\omega_r) \rightarrow 1$ for $\omega_r \rightarrow \pm\infty$. From these results, we conclude that the behavior of the Nyquist curve close to the limit point $(1, 0)$ is the one represented in Fig. 1. In addition, according to Eq. (21), the Nyquist curve crosses the x -axis at each value of ω_r corresponding to an extremum of $f(v)$. For $\omega_r = v_{ext}$, where v_{ext} is a velocity at which the distribution is extremum ($f'(v_{ext}) = 0$), the imaginary part of the dielectric function $\epsilon_i(v_{ext}) = 0$ and the real part of the dielectric function

$$\epsilon_r(v_{ext}) = 1 + \frac{k}{2} \int_{-\infty}^{\infty} \frac{f'(v)}{v - v_{ext}} dv. \quad (24)$$

Subtracting the value $f'(v_{ext}) = 0$ in the numerator of the integrand, and integrating by parts, we obtain

$$\epsilon_r(v_{ext}) = 1 - \frac{k}{2} \int_{-\infty}^{\infty} \frac{f(v_{ext}) - f(v)}{(v - v_{ext})^2} dv. \quad (25)$$

If v_{Max} denotes the velocity corresponding to the global maximum of the distribution, we clearly have

$$\epsilon_r(v_{Max}) < 1. \quad (26)$$

Finally, for an attractive interaction, we note that if the zero of $f'(v)$ corresponds to a maximum (resp. minimum) of f then the hodograph crosses the real axis downward (resp. upward). On the other hand, if $f(v)$ is symmetric with respect to $v = 0$, then $\epsilon_i(\omega_r = 0) = \pi \frac{k}{2} f'(0) = 0$ and $\epsilon'_r(\omega_r = 0) = \frac{k}{2} P \int_{-\infty}^{+\infty} \frac{f'(v)}{v^2} dv = 0$ so that the Nyquist curve has a vertical tangent at $(\epsilon_r(0), 0)$ when $\omega_r = 0$ provided that $\epsilon'_i(\omega_r = 0) \propto f''(0) \neq 0$.

2.6 Single-humped distributions

Let us assume that the distribution $f(v)$ has a single maximum at $v = v_0$ (so that $f'(v_0) = 0$) and tends to zero for $v \rightarrow \pm\infty$. Then, the Nyquist curve cuts the x -axis ($\epsilon_i(\omega_r)$ vanishes) at the limit point $(1, 0)$ when $\omega_r \rightarrow \pm\infty$ and at the point $(\epsilon_r(v_0), 0)$ when $\omega_r = v_0$. Due to its behavior close to the limit point $(1, 0)$, the fact that it rotates in the counterclockwise sense, and the property that $\epsilon_r(v_0) < 1$ according to Eq. (26), the Nyquist curve must necessarily behave like in Fig. 1. Therefore, the Nyquist curve starts on the real axis at $\epsilon_r(\omega_r) = 1$ for $\omega_r \rightarrow -\infty$, then going in counterclockwise sense it crosses the real axis at the point $\epsilon_r(v_0) < 1$ and returns on the real axis at $\epsilon_r(\omega_r) = 1$ for

$\omega_r \rightarrow +\infty$. According to the Nyquist criterion exposed in Sec. 2.4, we conclude that a single-humped distribution is linearly stable if

$$\epsilon_r(v_0) = 1 + \frac{k}{2} \int_{-\infty}^{+\infty} \frac{f'(v)}{v - v_0} dv > 0, \quad (27)$$

and linearly unstable if $\epsilon_r(v_0) < 0$. The equality corresponds to the marginal stability condition (16)-(17). When the system is unstable, there is only one mode of instability since the Nyquist curve rotates only one time around the origin. This stability criterion, which is valid for single-humped distributions, was stated without proof in [29]. It is here *justified* from the Nyquist method. In particular, a symmetric distribution $f = f(v)$ with a single maximum at $v_0 = 0$ is linearly dynamically stable iff

$$1 + \frac{k}{2} \int_{-\infty}^{+\infty} \frac{f'(v)}{v} dv > 0. \quad (28)$$

This coincides with the criterion of formal stability given in [32,29]. Therefore, for spatially homogeneous distributions, the criterion of linear dynamical stability coincides with the criterion of formal nonlinear dynamical stability (see Sec. 8).

2.7 Double-humped distributions

Let us consider a double-humped distribution with a global maximum at v_{Max} , a minimum at v_{min} and a local maximum at v_{max} . We assume that $v_{Max} < v_{min} < v_{max}$. The Nyquist curve will cut the x -axis at the limit point $(1, 0)$ and at three other points $(\epsilon_r(v_{Max}), 0)$, $(\epsilon_r(v_{min}), 0)$ and $(\epsilon_r(v_{max}), 0)$. We also know that the Nyquist curve can only rotate in the counterclockwise sense and that $\epsilon_r(v_{Max}) < 1$ according to Eq. (26). Then, we can convince ourselves by making drawings of the following results. If

$$\begin{aligned} (+ + +): & \epsilon_r(v_{Max}) > 0, \epsilon_r(v_{min}) > 0, \epsilon_r(v_{max}) > 0, \\ (+ - -): & \epsilon_r(v_{Max}) > 0, \epsilon_r(v_{min}) < 0, \epsilon_r(v_{max}) > 0, \\ (- - +): & \epsilon_r(v_{Max}) < 0, \epsilon_r(v_{min}) < 0, \epsilon_r(v_{max}) < 0, \\ (+ - +)^8: & \epsilon_r(v_{Max}) > 0, \epsilon_r(v_{min}) < 0, \epsilon_r(v_{max}) > 0, \end{aligned}$$

the Nyquist curve does not encircle the origin so the system is stable. If

$$\begin{aligned} (- - -): & \epsilon_r(v_{Max}) < 0, \epsilon_r(v_{min}) < 0, \epsilon_r(v_{max}) < 0, \\ (- + +): & \epsilon_r(v_{Max}) < 0, \epsilon_r(v_{min}) > 0, \epsilon_r(v_{max}) > 0, \\ (+ + -): & \epsilon_r(v_{Max}) > 0, \epsilon_r(v_{min}) > 0, \epsilon_r(v_{max}) < 0, \end{aligned}$$

the Nyquist curve rotates one time around the origin so that there is one mode of instability. Finally, if

$$(- + -): \epsilon_r(v_{Max}) < 0, \epsilon_r(v_{min}) > 0, \epsilon_r(v_{max}) < 0,$$

the Nyquist curve rotates two times around the origin so that there are two modes of instability. Cases $(+ + +)$, $(- - -)$, $(- + +)$ and $(- + -)$ are observed in Sec. 6 for

⁸ This case is relatively tricky. It is obtained by making two loops in the S-E and N-W quadrants of the ϵ -plane (assuming that this is possible for some double-humped distributions). The origin is then encircled by a sort of triangle but since the curve rotates clockwise along this triangle, the origin is in fact exterior to the Nyquist curve. Thus the system is stable.

an asymmetric double-humped distribution made of two Maxwellians. The other cases cannot be obtained from this distribution but they may be obtained from other distributions.

If the double-humped distribution is symmetric with respect to the origin with two maxima at $\pm v_*$ and a minimum at $v = 0$, only three cases can arise. If

$$(+ + +): \epsilon_r(v_*) > 0, \epsilon_r(0) > 0,$$

$$(+ - +): \epsilon_r(v_*) > 0, \epsilon_r(0) < 0,$$

the Nyquist curve does not encircle the origin so the system is stable. If

$$(- - -): \epsilon_r(v_*) < 0, \epsilon_r(0) < 0,$$

the Nyquist curve rotates one time around the origin so that there is one mode of instability. Finally, if

$$(- + -): \epsilon_r(v_*) < 0, \epsilon_r(0) > 0,$$

the Nyquist curve rotates two times around the origin so that there are two modes of instability. Cases $(+ + +)$, $(- - -)$ and $(- + -)$ are observed in Sec. 5 for a symmetric double-humped distribution made of two Maxwellians.

2.8 A particular solution of $\epsilon(\omega) = 0$

For the attractive HMF model we can look for a solution of the equation $\epsilon(\omega) = 0$ in the form $\omega = i\omega_i$ corresponding to $\omega_r = 0$. In that case, the perturbation grows ($\omega_i > 0$) or decays ($\omega_i < 0$) without oscillating. For $\omega_i > 0$, the equation $\epsilon(\omega) = 0$ becomes

$$1 + \frac{k}{2} \int_{-\infty}^{+\infty} \frac{f'(v)}{v - i\omega_i} dv = 0. \quad (29)$$

Multiplying the numerator by $v + i\omega_i$ and separating real and imaginary parts, we obtain

$$1 + \frac{k}{2} \int_{-\infty}^{+\infty} \frac{vf'(v)}{v^2 + \omega_i^2} dv = 0, \quad (30)$$

$$\int_{-\infty}^{+\infty} \frac{f'(v)}{v^2 + \omega_i^2} dv = 0. \quad (31)$$

If we consider distribution functions $f(v)$ that are symmetric with respect to $v = 0$, Eq. (31) is always satisfied. Then, the growth rate ω_i is given by Eq. (30).

For $\omega_i < 0$, the equation $\epsilon(\omega) = 0$ becomes

$$1 + \frac{k}{2} \int_{-\infty}^{+\infty} \frac{f'(v)}{v - i\omega_i} dv + ik\pi f'(i\omega_i) = 0. \quad (32)$$

Multiplying the numerator by $v + i\omega_i$, assuming that $f(v)$ is even, and separating real and imaginary parts, we obtain

$$1 + \frac{k}{2} \int_{-\infty}^{+\infty} \frac{vf'(v)}{v^2 + \omega_i^2} dv + ik\pi f'(i\omega_i) = 0, \quad (33)$$

and Eq. (31). The equation for the imaginary part is always satisfied. Then, the damping rate ω_i is given by Eq. (33).

Note that the solution $\omega = i\omega_i$ exists only for attractive interactions. Note also that there may exist other solutions to the equation $\epsilon(\omega) = 0$. However, for unstable single-humped distributions, the Nyquist curve encircles the origin only once (see Sec. 2.6) so that $\omega = i\omega_i$ with $\omega_i > 0$ is the only solution of $\epsilon(\omega) = 0$ (for stable single-humped distributions there may be other solutions of $\epsilon(\omega) = 0$ with $\omega_r \neq 0$ and $\omega_i < 0$). Explicit solutions of $\epsilon(\omega) = 0$ with $\omega = i\omega_i$ are given in [29] for the Maxwell and Tsallis distributions.

3 The Maxwell distribution

We consider the Maxwell (or isothermal) distribution

$$f(v) = \left(\frac{\beta}{2\pi}\right)^{1/2} \rho e^{-\beta \frac{v^2}{2}}, \quad (34)$$

where $\rho = M/(2\pi)$ is the spatial density and $T \equiv 1/\beta = \langle v^2 \rangle$ is the kinetic temperature⁹. We justify here the Maxwell distribution as a particular stationary solution of the Vlasov equation [29,83]. The Maxwell distribution represents also the statistical equilibrium state of the system. In that case, T can be interpreted as the thermodynamical temperature.

The Maxwellian distribution has a single maximum at $v = 0$. Therefore, the condition of marginal stability (17) implies $\omega_r = 0$. From Eq. (16), we find that the Maxwellian distribution is marginally stable for $T = T_c$ where we have introduced the critical temperature

$$T_c = \frac{kM}{4\pi}. \quad (35)$$

According to the criterion (28), the Maxwell distribution is linearly dynamically stable if $T > T_c$ and linearly dynamically unstable if $T < T_c$.

The dielectric function (9) associated to the Maxwellian distribution is

$$\epsilon(\omega) = 1 - \frac{k}{2} \left(\frac{\beta}{2\pi}\right)^{1/2} \rho \int_C \frac{\beta v}{v - \omega} e^{-\beta \frac{v^2}{2}} dv. \quad (36)$$

Introducing the dimensionless temperature

$$\eta = \frac{\beta kM}{4\pi}, \quad (37)$$

and the dimensionless pulsation and velocity

$$\Omega = \left(\frac{4\pi}{kM}\right)^{1/2} \omega, \quad V = \left(\frac{4\pi}{kM}\right)^{1/2} v, \quad (38)$$

⁹ For any distribution function $f(\mathbf{v})$, we define the kinetic temperature by the relation $\frac{1}{2}m\langle(\mathbf{v} - \langle\mathbf{v}\rangle)^2\rangle = \frac{d}{2}T_{kin}$ where d is the dimension of space. The energy (conserved control parameter) is then $E = \frac{1}{2}Nm\langle v^2 \rangle = \frac{1}{2}Nm\langle v \rangle^2 + \frac{d}{2}NT_{kin}$. For one dimensional systems ($d = 1$) and particles of unit mass ($m = 1$), the kinetic temperature is equal to the velocity dispersion $T_{kin} = \langle v^2 \rangle$ when $\langle v \rangle = 0$.

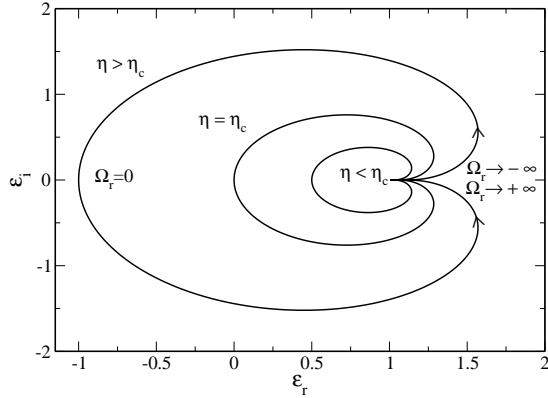


Fig. 1. Nyquist curve for the Maxwellian distribution (34). The DF is stable for $\eta < \eta_c$ ($T > T_c$), marginally stable for $\eta = \eta_c$ ($T = T_c$) and unstable for $\eta > \eta_c$ ($T < T_c$). We have taken $\eta = 2, 1, 0.5$ from the outer to the inner curve.

the dielectric function can be rewritten

$$\epsilon(\Omega) = 1 - \eta W(\sqrt{\eta}\Omega), \quad (39)$$

where

$$W(z) = \frac{1}{\sqrt{2\pi}} \int_C \frac{x}{x-z} e^{-\frac{x^2}{2}} dx \quad (40)$$

is the W -function of plasma physics [70,71]. We note that $W(0) = 1$. For any complex number z , we have the analytical expression

$$W(z) = 1 - ze^{-\frac{z^2}{2}} \int_0^z e^{\frac{x^2}{2}} dx + i\sqrt{\frac{\pi}{2}} ze^{-\frac{z^2}{2}}. \quad (41)$$

When $\Omega_i = 0$, the real and imaginary parts of the dielectric function $\epsilon(\Omega_r) = \epsilon_r(\Omega_r) + i\epsilon_i(\Omega_r)$ can be written

$$\epsilon_r(\Omega_r) = 1 - \eta W_r(\sqrt{\eta}\Omega_r), \quad (42)$$

$$\epsilon_i(\Omega_r) = -\eta W_i(\sqrt{\eta}\Omega_r), \quad (43)$$

with

$$W_r(z) = 1 - ze^{-\frac{z^2}{2}} \int_0^z e^{\frac{x^2}{2}} dx, \quad (44)$$

$$W_i(z) = \sqrt{\frac{\pi}{2}} ze^{-\frac{z^2}{2}}, \quad (45)$$

where z is here a real number. The condition of marginal stability corresponds to $\epsilon_r(\Omega_r) = \epsilon_i(\Omega_r) = 0$. The condition $\epsilon_i(\Omega_r) = 0$, which is equivalent to $f'(\Omega_r) = 0$, implies $\Omega_r = 0$. Then, the condition $\epsilon_r(\Omega_r) = 0$ leads to $\eta = \eta_c$ with

$$\eta_c = 1. \quad (46)$$

To apply the Nyquist method, we need to plot the curve $(\epsilon_r(\Omega_r), \epsilon_i(\Omega_r))$ in the ϵ -plane. For $\Omega_r \rightarrow \pm\infty$, this curve tends to the point $(1, 0)$ in the manner described in Sec. 2.6. On the other hand, for $\Omega_r = 0$, it crosses the x -axis at $(\epsilon_r(0) = 1 - \eta, 0)$. The Nyquist curve is represented in Fig. 1 for several values of the inverse temperature η .

For $\eta < 1$ (i.e. $T > T_c$), the Nyquist curve does not encircle the origin so that the Maxwellian distribution is stable. For $\eta > 1$ (i.e. $T < T_c$) the Nyquist curve encircles the origin so that the Maxwellian distribution is unstable. For $\eta = 1$ (i.e. $T = T_c$) the Nyquist curve passes through the origin so that the Maxwellian distribution is marginally stable.

The stability limits obtained with the Nyquist method for isothermal and polytropic (see next section) distributions coincide with those found in [29]. However, the Nyquist method does not give the value of the growth rate (in the unstable regime) or decay rate (in the stable regime) of the perturbation. These values have been obtained in [29] by solving the dispersion relation (9).

4 The Tsallis distributions

We consider the Tsallis (or polytropic) distributions written in the form (see [29] and Appendix B):

$$f(v) = B_n \frac{\rho}{\sqrt{2\pi T}} \left[1 - \frac{v^2}{2(n+1)T} \right]_+^{n-1/2}, \quad (47)$$

where $\rho = \frac{M}{2\pi}$ is the density, $T \equiv 1/\beta = \langle v^2 \rangle$ is the kinetic temperature and B_n is a normalization constant given by

$$B_n = \frac{\Gamma(n+1)}{\Gamma(n+1/2)(n+1)^{1/2}}, \quad n > \frac{1}{2}, \quad (48)$$

$$B_n = \frac{\Gamma(1/2-n)}{\Gamma(-n)[-(n+1)]^{1/2}}, \quad n < -1. \quad (49)$$

We limit ourselves to these indices so that the distributions are normalizable and their second moments $\langle v^2 \rangle$ exist. Some representative distributions are plotted in Figs. 2, 3 and 4. For $n > 1/2$ the distributions have a compact support since they vanish at $v = \pm v_m$ where

$$v_m = \sqrt{2(n+1)T}. \quad (50)$$

For $v > v_m$, we set $f = 0$. Therefore, the notation $[x]_+ = x$ for $x > 0$ and $[x]_+ = 0$ for $x < 0$. For $n < -1$, the distribution functions remain strictly positive for all v and they decrease algebraically like $|v|^{-(1-2n)}$ for $v \rightarrow \pm\infty$. For $n \rightarrow \pm\infty$, we recover the Maxwell distribution (34). We justify here the Tsallis distributions (47) as particular stationary solutions of the Vlasov equation [29,83]. These distributions possess a lot of interesting mathematical properties so that their study is interesting in its own right¹⁰. We also note that the Tsallis distributions (47)

¹⁰ Such distributions have been extensively studied in astrophysics because they represent an important class of stationary solutions of the Vlasov-Poisson system called stellar polytropes [21]. Stellar polytropes have been introduced by Plummer [84] and Eddington [85]. However, these distributions were written in a form that is less convenient than the ‘‘Tsallis form’’ (215) or (47). The nice forms (215) or (47) allow us to make a smooth connexion between polytropic and isothermal distributions for $q \rightarrow 1$ or $n \rightarrow \infty$. See [83] for further discussion on these historical issues.

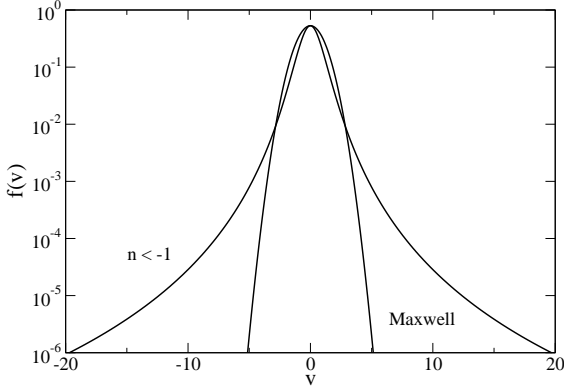


Fig. 2. Tsallis distribution with $n < -1$ (power-law tail) and Maxwell distribution (corresponding to $n = \pm\infty$).

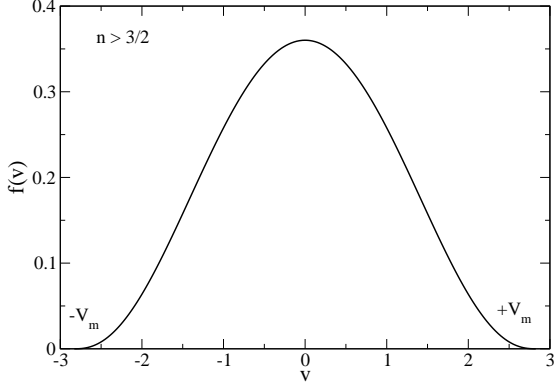


Fig. 3. Tsallis distribution with $n > 3/2$ (specifically $n = 3$). It has a compact support with a horizontal tangent at $v = \pm v_m$.

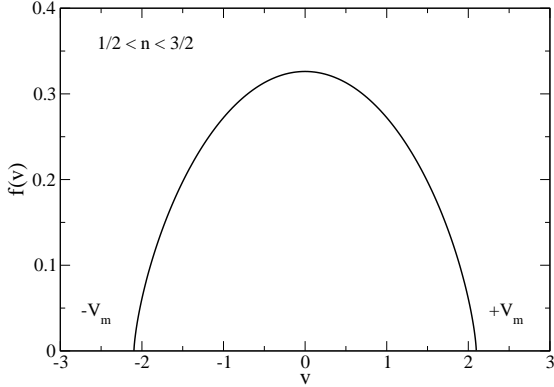


Fig. 4. Tsallis distribution with $1/2 < n < 3/2$ (specifically $n = 1.2$). It has a compact support with a vertical tangent at $v = \pm v_m$.

have been observed in numerical simulations of the HMF model either in case of incomplete relaxation [31,33] or during the collisional evolution of the system [60] (see discussion in Sec. 3.4 of [24]).

The Tsallis distributions have a single maximum at $v = 0$. Therefore, the condition of marginal stability (17) implies $\omega_r = 0$ (it is shown below that the minimum at

$v = \pm v_m$ for $n > 3/2$ does not lead to marginal stability). From Eq. (16), we find that the Tsallis distribution of index n is marginally stable for $T = T_c$ where we have introduced the critical temperature

$$T_c = \frac{n}{n+1} \frac{kM}{4\pi}. \quad (51)$$

For $n \rightarrow \pm\infty$, we recover the critical temperature (35) corresponding to the Maxwell distribution. On the other hand, according to the criterion (28), the Tsallis distribution of index n is linearly dynamically stable if $T > T_c$ and linearly dynamically unstable if $T < T_c$.

The dielectric function associated to the Tsallis distribution of index n is

$$\begin{aligned} \epsilon(\omega) = 1 - \frac{k}{2} \frac{\rho}{\sqrt{2\pi}T} B_n \left(n - \frac{1}{2} \right) \frac{1}{(n+1)T} \\ \times \int_C \frac{v \left[1 - \frac{v^2}{2(n+1)T} \right]_+^{n-3/2}}{v - \omega} dv. \end{aligned} \quad (52)$$

Introducing the dimensionless temperature (37) and the dimensionless pulsation (38) it can be rewritten

$$\epsilon(\Omega) = 1 - \frac{n}{n+1} \eta W^{(n)}(\sqrt{\eta}\Omega), \quad (53)$$

where

$$W^{(n)}(z) = \frac{1}{\sqrt{2\pi}} \frac{B_n}{n} \left(n - \frac{1}{2} \right) \int_C \frac{x \left[1 - \frac{x^2}{2(n+1)} \right]_+^{n-3/2}}{x - z} dx, \quad (54)$$

generalizes the W function of plasma physics to the case of Tsallis distributions [29]. We note that $W^{(n)}(0) = 1$.

When $\Omega_i = 0$, the real and imaginary parts of the dielectric function $\epsilon(\Omega_r) = \epsilon_r(\Omega_r) + i\epsilon_i(\Omega_r)$ can be written

$$\epsilon_r(\Omega_r) = 1 - \frac{n}{n+1} \eta W_r^{(n)}(\sqrt{\eta}\Omega_r), \quad (55)$$

$$\epsilon_i(\Omega_r) = -\frac{n}{n+1} \eta W_i^{(n)}(\sqrt{\eta}\Omega_r), \quad (56)$$

with

$$W_r^{(n)}(z) = \frac{1}{\sqrt{2\pi}} \frac{B_n}{n} \left(n - \frac{1}{2} \right) P \int_{-\infty}^{+\infty} \frac{x \left[1 - \frac{x^2}{2(n+1)} \right]_+^{n-3/2}}{x - z} dx, \quad (57)$$

$$W_i^{(n)}(z) = \sqrt{\frac{\pi}{2}} \frac{B_n}{n} \left(n - \frac{1}{2} \right) z \left[1 - \frac{z^2}{2(n+1)} \right]_+^{n-3/2}, \quad (58)$$

where z is here a real number. The condition of marginal stability corresponds to $\epsilon_r(\Omega_r) = \epsilon_i(\Omega_r) = 0$. The condition $\epsilon_i(\Omega_r) = 0$, which is equivalent to $f'(\Omega_r) = 0$, implies $\Omega_r = 0$. Then, the relation $\epsilon_r(\Omega_r) = 0$ leads to $\eta = \eta_c$ with

$$\eta_c = \frac{n+1}{n}. \quad (59)$$

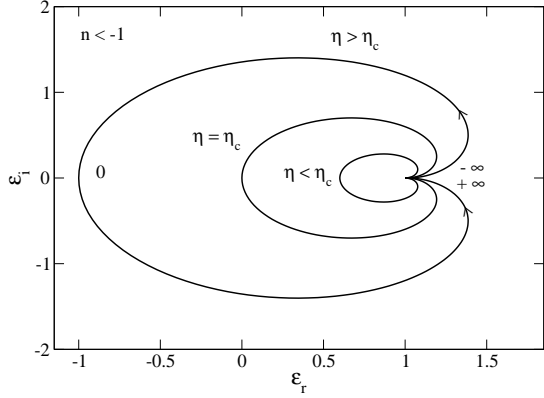


Fig. 5. Nyquist curve for the Tsallis distributions with $n < -1$ (specifically $n = -2$ yielding $\eta_c = 1/2$). The DF is stable for $\eta < \eta_c$, marginally stable for $\eta = \eta_c$ and unstable for $\eta > \eta_c$. We have taken $\eta = 1, 0.5, 0.4$ from the outer to the inner curve.

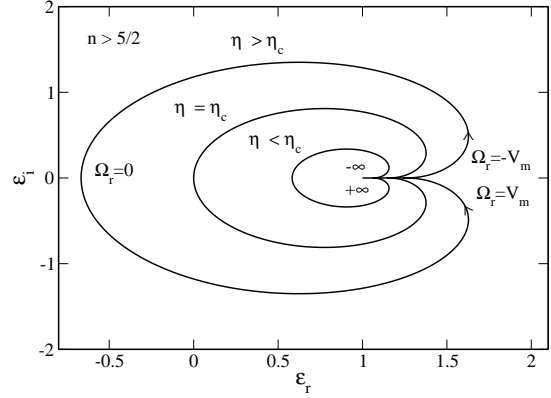


Fig. 6. Nyquist curve for the Tsallis distribution with $n > 5/2$ (specifically $n = 5$ yielding $\eta_c = 6/5$). The DF is stable for $\eta < \eta_c$, marginally stable for $\eta = \eta_c$ and unstable for $\eta > \eta_c$. We have taken $\eta = 2, 6/5, 0.5$ from the outer to the inner curve. The curve has a horizontal tangent at $(\epsilon_r(V_m), 0)$.

To apply the Nyquist method, we need to plot the curve $(\epsilon_r(\Omega_r), \epsilon_i(\Omega_r))$ in the ϵ -plane. We have to distinguish different cases:

- For $n < -1$, the Tsallis distributions have a single maximum at $v = 0$ and they decrease algebraically at infinity. For $\Omega_r \rightarrow \pm\infty$, the curve $(\epsilon_r(\Omega_r), \epsilon_i(\Omega_r))$ tends to the point $(1, 0)$ in the manner described in Sec. 2.6. On the other hand, for $\Omega_r = 0$, it crosses the x -axis at $(\epsilon_r(0) = 1 - \eta/\eta_c, 0)$. The Nyquist curve is represented in Fig. 5 for several values of the inverse temperature η . For $\eta < \eta_c$ (i.e. $T > T_c$), the Nyquist curve does not encircle the origin so that the Tsallis distribution is stable. For $\eta > \eta_c$ (i.e. $T < T_c$) the Nyquist curve encircles the origin so that the Tsallis distribution is unstable. For $\eta = \eta_c$ (i.e. $T = T_c$) the Nyquist curve passes through the origin so that the Tsallis distribution is marginally stable. Therefore, the Nyquist curve of polytropic distributions with index $n < -1$ is very similar to the Nyquist curve of Maxwellian distributions (recovered for $n = -\infty$). They essentially differ in the value of the critical temperature η_c .

- For $n > 3/2$, the Tsallis distributions have a single maximum at $v = 0$ and they vanish at $v = \pm v_m$ with a horizontal tangent: $f'(\pm v_m) = 0$ (see Fig. 3). Therefore, when $\Omega_r \rightarrow \pm V_m$, the Nyquist curve $(\epsilon_r(\Omega_r), \epsilon_i(\Omega_r))$ tends to the point $(\epsilon_r(V_m) = 1 + (\eta/\eta_c)\zeta_n, 0)$ where $\zeta_n \equiv -W_r^{(n)}(\sqrt{2(n+1)}) \geq 0$ ¹¹. This parameter is plotted as a function of n in Fig. 65 of Appendix C. We note that $\epsilon_i(\Omega_r) > 0$ for $\Omega_r \rightarrow -V_m^+$ and $\epsilon_i(\Omega_r) < 0$ for $\Omega_r \rightarrow V_m^-$. We need now to distinguish three sub-cases. For $n > 5/2$, $f''(v_m) = 0$: this implies $\epsilon'_i(V_m) = 0$ so that the Nyquist curve has a horizontal tangent at $(\epsilon_r(V_m), 0)$. For $3/2 < n < 5/2$, $f''(v_m) = +\infty$: this implies $\epsilon'_i(V_m) = \infty$, so that the Nyquist curve has a vertical tangent at $(\epsilon_r(V_m), 0)$. For $n = 5/2$, $f''(v_m) = 15\rho/(14\sqrt{7}T^{3/2})$ and $\epsilon'_i(V_m) = 15\pi\eta^{3/2}/(14\sqrt{7})$ are finite so that the Nyquist

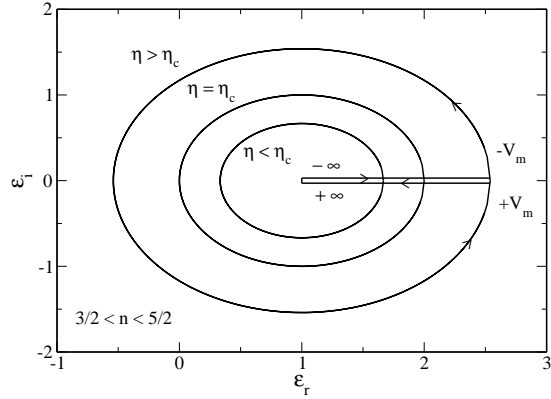


Fig. 7. Nyquist curve for the Tsallis distribution with $3/2 < n < 5/2$ (specifically $n = 2$ yielding $\eta_c = 3/2$). The DF is stable for $\eta < \eta_c$, marginally stable for $\eta = \eta_c$ and unstable for $\eta > \eta_c$. We have taken $\eta = 2, 3/2, 0.5$ from the outer to the inner curve. The curve has a vertical tangent at $(\epsilon_r(V_m), 0)$.

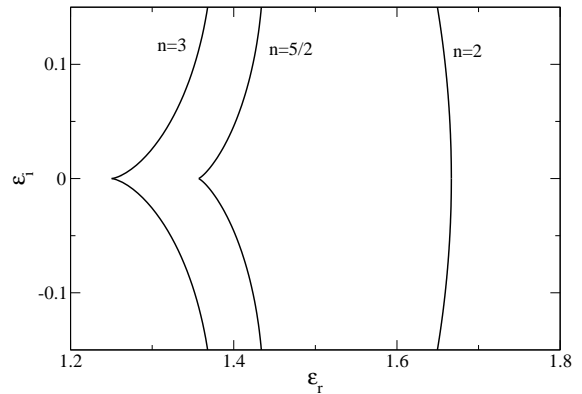


Fig. 8. Behavior of the Nyquist curve close to the point $(\epsilon_r(V_m), 0)$. For $n > 5/2$ (specifically $n = 3$) the tangent is horizontal, for $n = 5/2$ the tangent has a finite slope and for $3/2 < n < 5/2$ (specifically $n = 2$) the tangent is vertical.

¹¹ We note that $\epsilon_r(V_m) \geq 1$ (it is equal to unity for $n \rightarrow \infty$) so that $\Omega_r = \pm V_m$ can never correspond to a marginal mode (it satisfies $\epsilon_i = 0$ but it can never satisfy $\epsilon_r = 0$).

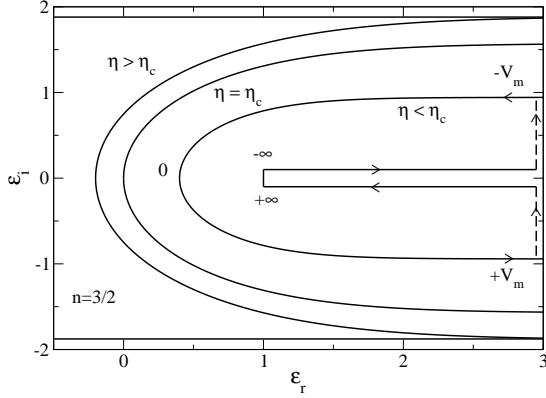


Fig. 9. Nyquist curve for the Tsallis distribution with $n = 3/2$ yielding $\eta_c = 5/3$. The DF is stable for $\eta < \eta_c$, marginally stable for $\eta = \eta_c$ and unstable for $\eta > \eta_c$. We have taken $\eta = 2, 5/3, 0.5$ from the outer to the inner curve.

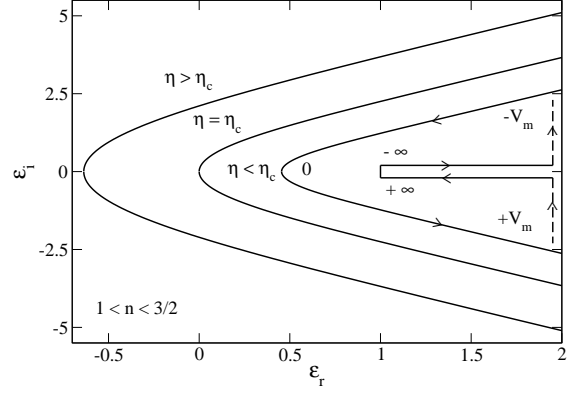


Fig. 10. Nyquist curve for the Tsallis distribution with $1 < n < 3/2$ (specifically $n = 1.2$). The DF is stable for $\eta < \eta_c$, marginally stable for $\eta = \eta_c$ and unstable for $\eta > \eta_c$.

curve has a finite slope at $(\epsilon_r(V_m), 0)$. These three behaviors are represented in Figs. 6, 7 and 8. On the other hand, for $\Omega_r < -V_m$, the imaginary part of the dielectric function $\epsilon_i(\Omega_r) = 0$ and the real part $\epsilon_r(\Omega_r)$ varies from 1 (for $\Omega_r \rightarrow -\infty$) to $\epsilon_r(V_m) = 1 + (\eta/\eta_c)\zeta_n$ (for $\Omega_r \rightarrow -V_m^-$); see Appendix C. For $\Omega_r > V_m$, the imaginary part of the dielectric function $\epsilon_i(\Omega_r) = 0$ and the real part $\epsilon_r(\Omega_r)$ varies from $\epsilon_r(V_m) = 1 + (\eta/\eta_c)\zeta_n$ (for $\Omega_r \rightarrow +V_m^+$) to 1 (for $\Omega_r \rightarrow +\infty$). This corresponds to a segment on the x -axis between $(1, 0)$ and $(1 + (\eta/\eta_c)\zeta_n, 0)$ in Figs. 6 and 7 (for clarity, we have slightly shifted the segment from the x -axis in Fig. 7 to show the complete path). Finally, considering the value $\Omega_r = 0$, we see that the Nyquist curve crosses the x -axis at $(\epsilon_r(0) = 1 - \eta/\eta_c, 0)$. For $\eta < \eta_c$ (i.e. $T > T_c$), the Nyquist curve does not encircle the origin so that the Tsallis distribution is stable. For $\eta > \eta_c$ (i.e. $T < T_c$) the Nyquist curve encircles the origin so that the Tsallis distribution is unstable. For $\eta = \eta_c$ (i.e. $T = T_c$) the Nyquist curve passes through the origin so that the Tsallis distribution is marginally stable. The Nyquist curve of polytropic distributions with index $n > 5/2$ is very similar to the Nyquist curve of Maxwellian distributions (recovered for $n = +\infty$). They essentially differ in the presence of a segment between $(1, 0)$ and $(1 + (\eta/\eta_c)\zeta_n, 0)$ and in the value of the critical temperature η_c . For $n \leq 5/2$, the Nyquist curves of polytropic and isothermal distributions become sensibly different.

- For $1/2 < n \leq 3/2$, the Tsallis distributions have a single maximum at $v = 0$ and they vanish at $v = \mp v_m$ with a vertical tangent: $f'(\mp v_m) = \pm\infty$ (see Fig. 4; for $n = 3/2$, the slope $f'(\mp v_m) = \pm 3\rho/(10T)$ is finite). Therefore, the imaginary part of the dielectric function $\epsilon_i(\Omega_r) \rightarrow \pm\infty$ when $\Omega_r \rightarrow \mp V_m$ (for $n = 3/2$, the imaginary part of the dielectric function $\epsilon_i(\Omega_r) \rightarrow \pm 3\pi\eta/10$ when $\Omega_r \rightarrow \mp V_m$). We need now to distinguish three subcases. For $1 < n \leq 3/2$, the real part of the dielectric function $\epsilon_r(\Omega_r) \rightarrow +\infty$ when $\Omega_r \rightarrow \pm V_m$. For $n = 1$, the dielectric function $\epsilon_r(\Omega_r)$ is independent on

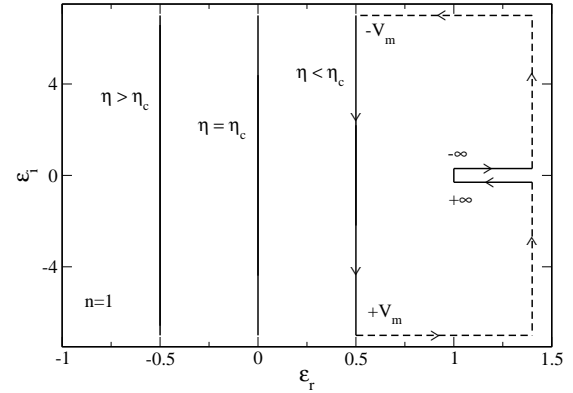


Fig. 11. Nyquist curve for the Tsallis distribution with $n = 1$ yielding $\eta_c = 2$. The DF is stable for $\eta < \eta_c$, marginally stable for $\eta = \eta_c$ and unstable for $\eta > \eta_c$. We have taken $\eta = 3, 2, 0.5$ from the outer to the inner curve.

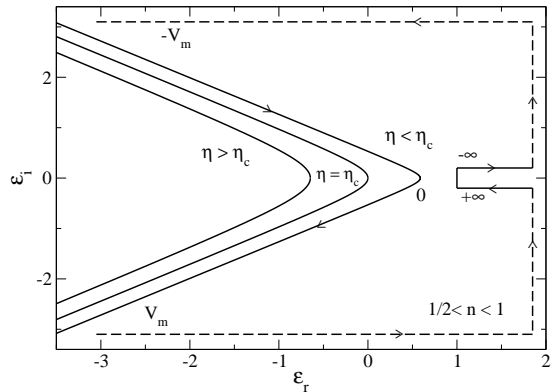


Fig. 12. Nyquist curve for the Tsallis distribution with $1/2 < n < 1$ (specifically $n = 0.7$). The DF is stable for $\eta < \eta_c$, marginally stable for $\eta = \eta_c$ and unstable for $\eta > \eta_c$.

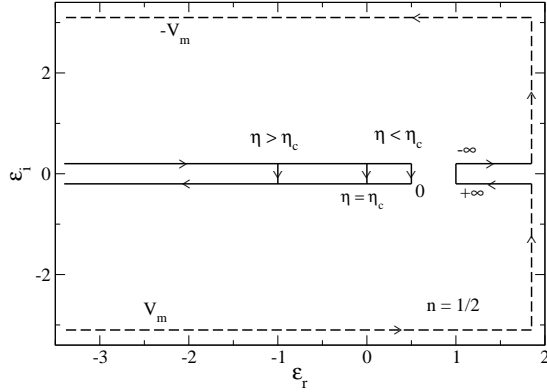


Fig. 13. Nyquist curve for the Tsallis distribution with $n = 1/2$ yielding $\eta_c = 3$. The DF is stable for $\eta < \eta_c$, marginally stable for $\eta = \eta_c$ and unstable for $\eta > \eta_c$.

$\Omega_r \in [-V_m, V_m]$. For $1/2 < n < 1$, the dielectric function $\epsilon_r(\Omega_r) \rightarrow -\infty$ when $\Omega_r \rightarrow \pm V_m$; see Appendix C. This leads to the Nyquist curves represented in Figs. 9, 10, 11 and 12. On the other hand, for $\Omega_r < -V_m$, the imaginary part of the dielectric function $\epsilon_i(\Omega_r) = 0$ and the real part $\epsilon_r(\Omega_r)$ varies from 1 (for $\Omega_r \rightarrow -\infty$) to $+\infty$ (for $\Omega_r \rightarrow -V_m^-$). For $\Omega_r > V_m$, the imaginary part of the dielectric function $\epsilon_i(\Omega_r) = 0$ and the real part $\epsilon_r(\Omega_r)$ varies from $+\infty$ (for $\Omega_r \rightarrow +V_m^+$) to 1 (for $\Omega_r \rightarrow +\infty$). This corresponds to a segment on the x -axis between $(1, 0)$ and $(+\infty, 0)$ in Figs. 9, 10, 11 and 12 (for clarity, we have slightly shifted the segment from the x -axis to show the complete path). Finally, considering the value $\Omega_r = 0$, we see that the Nyquist curve crosses the x -axis at $(\epsilon_r(0) = 1 - \eta/\eta_c, 0)$. For $\eta < \eta_c$ (i.e. $T > T_c$), the Nyquist curve does not encircle the origin so that the Tsallis distribution is stable. For $\eta > \eta_c$ (i.e. $T < T_c$) the Nyquist curve encircles the origin so that the Tsallis distribution is unstable. For $\eta = \eta_c$ (i.e. $T = T_c$) the Nyquist curve passes through the origin so that the Tsallis distribution is marginally stable. Note that it is important to determine the complete path of evolution, from $\Omega_r = -\infty$ to $\Omega_r = +\infty$, in order to apply the Nyquist criterion.

• The index $n = 1/2$ deserves a particular attention. In that case, $f = \eta_0$ for $|v| \leq v_m$ and $f = 0$ otherwise. It corresponds to the Fermi distribution or to the water-bag model. The constant η_0 is determined by the normalization condition $\rho = \int f dv$ yielding $\rho = 2\eta_0 v_m$. The kinetic temperature $T = \langle v^2 \rangle$ is given by $T = v_m^2/3$. The derivative of the distribution function is $f'(v) = \eta_0 [\delta(v + v_0) - \delta(v - v_0)]$. According to Eq. (18), the critical temperature is $T_c = kM/12\pi$ i.e. $\eta_c = 3$ in complete agreement with Eqs. (51) and (59). More precisely, for $n = 1/2$, we can obtain an analytical expression of the dielectric function in the form [29]:

$$\epsilon(\Omega) = 1 - \frac{1}{3}\eta W^{(1/2)}(\sqrt{\eta}\Omega), \quad (60)$$

with

$$W^{(1/2)}(z) = \frac{1}{1 - \frac{1}{3}z^2}. \quad (61)$$

The condition $\epsilon(\omega) = 0$ determines the complex pulsation. For $T > T_c$, the system is stable and

$$\omega = \pm\sqrt{3}(T - T_c)^{1/2}. \quad (62)$$

For $T < T_c$, the system is unstable and

$$\omega = \pm i\sqrt{3}(T_c - T)^{1/2}. \quad (63)$$

On the other hand, for $\Omega_i = 0$, we get

$$\epsilon_r(\Omega_r) = 1 - \frac{1}{3}\eta \frac{1}{1 - \frac{1}{3}\eta\Omega_r^2}, \quad \epsilon_i(\Omega_r) = 0. \quad (64)$$

Therefore, the Nyquist curve is made of two segments $] -\infty, 1 - \eta/3]$ and $[1, +\infty[$ as represented in Fig. 13.

5 The symmetric double-humped distribution

5.1 Determination of the extrema

We consider a symmetric double-humped distribution of the form

$$f(v) = \sqrt{\frac{\beta}{2\pi}} \frac{\rho}{2} \left[e^{-\frac{\beta}{2}(v-v_a)^2} + e^{-\frac{\beta}{2}(v+v_a)^2} \right]. \quad (65)$$

It corresponds to the superposition of two Maxwellian distributions with temperature $T = 1/\beta$ centered in v_a and $-v_a$ respectively (see Fig. 14). This distribution models two streams of particles in opposite direction. The average velocity is $\langle v \rangle = 0$ and the kinetic temperature $T_{kin} \equiv \langle v^2 \rangle = T + v_a^2$. The velocities v_0 at which the distribution function $f(v)$ is extremum satisfy $f'(v_0) = 0$. They are determined by the equation

$$e^{-2\beta v_a v_0} = \frac{v_a - v_0}{v_a + v_0}. \quad (66)$$

Introducing the dimensionless temperature (37), the dimensionless velocity (38) and the dimensionless separation

$$a = v_a \left(\frac{4\pi}{kM} \right)^{1/2}, \quad (67)$$

Eq. (66) can be rewritten

$$\eta = \frac{1}{2aV_0} \ln \left(\frac{a + V_0}{a - V_0} \right). \quad (68)$$

For a given value of the inverse temperature η and separation a , this equation determines the velocities V_0 where $f(V)$ is extremum. We note that $V_0 \in [-a, +a]$. It is convenient to introduce the variables

$$x = V_0/a, \quad y = \eta a^2. \quad (69)$$

For fixed a , the parameter y plays the role of the inverse temperature and the parameter x plays the role of the velocity. Then, we have to study the function

$$y(x) = \frac{1}{2x} \ln \left(\frac{1+x}{1-x} \right), \quad (70)$$

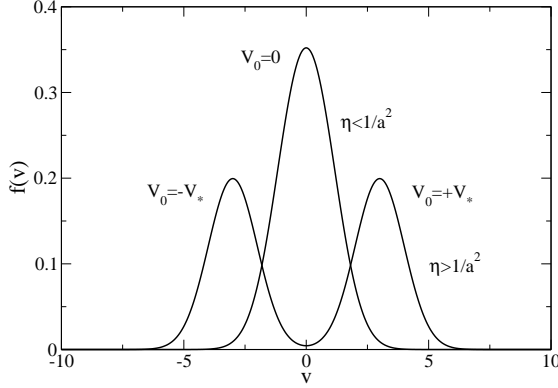


Fig. 14. Symmetric double-humped distribution made of two Maxwellian with separation a . If $\eta > 1/a^2$, the distribution has two maxima at $\pm V_*$ and one minimum at $V_0 = 0$ while for $\eta < 1/a^2$, it has only one maximum at $V_0 = 0$.

for $x \in]-1, +1[$. This function is plotted in Fig. 15. It has the following properties:

$$y(-x) = y(x), \quad (71)$$

$$y(x) \sim -\frac{1}{2} \ln(1-x), \quad (x \rightarrow 1^-), \quad (72)$$

$$y(0) = 1. \quad (73)$$

The extrema of the distribution function (65) can be determined from the study of this function. First, considering Eq. (68), we note that $f(V)$ always has an extremum at $V_0 = 0$, for any value of η and a . This is a “degenerate” solution of Eq. (70) corresponding to the vertical line $x = 0$ in Fig. 15. On the other hand, if $y > 1$, i.e. $\eta > 1/a^2$, there exists two other extrema $V_0 = \pm V_*$ where $V_* = ax_*$ with $x_* = y^{-1}(\eta a^2)$.

In conclusion, for a given separation a :

- if $\eta > 1/a^2$, the distribution function $f(V)$ has two maxima at $V_0 = \pm V_*$ and one minimum at $V_0 = 0$.

- if $\eta \leq 1/a^2$, the distribution function $f(V)$ has only one maximum at $V_0 = 0$ (the limit case $\eta = 1/a^2$ corresponds to $f''(0) = 0$).

Remark: We can note the formal analogy with the mean field theory (ferromagnetic transition) of the one dimensional Ising model without magnetic field (compare Eq. (68) with Eq. (14) of [86]).

5.2 The condition of marginal stability

The dielectric function associated to the symmetric double-humped distribution (65) is

$$\epsilon_r(\Omega) = 1 - \frac{\eta}{2} [W(\sqrt{\eta}(\Omega - a)) + W(\sqrt{\eta}(\Omega + a))], \quad (74)$$

where $W(z)$ is defined in Eq. (40). When $\Omega_i = 0$, the real and imaginary parts of the dielectric function $\epsilon_r(\Omega_r) = \epsilon_r(\Omega_r) + i\epsilon_i(\Omega_r)$ can be written

$$\epsilon_r(\Omega_r) = 1 - \frac{\eta}{2} [W_r(\sqrt{\eta}(\Omega_r - a)) + W_r(\sqrt{\eta}(\Omega_r + a))], \quad (75)$$

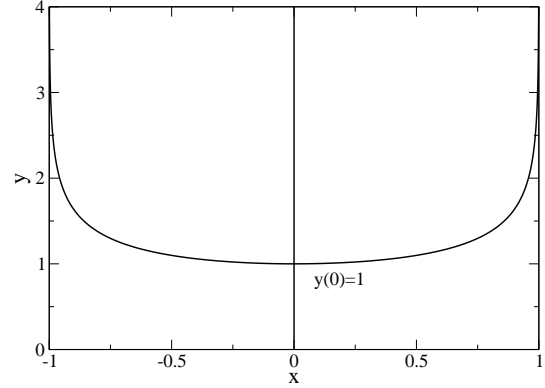


Fig. 15. The function $y(x)$ for the symmetric double-humped distribution.

$$\epsilon_i(\Omega_r) = -\frac{\eta}{2} [W_i(\sqrt{\eta}(\Omega_r - a)) + W_i(\sqrt{\eta}(\Omega_r + a))], \quad (76)$$

where $W_r(z)$ and $W_i(z)$ are defined in Eqs. (44)-(45) where z is here a real number. The condition of marginal stability corresponds to $\epsilon_r(\Omega_r) = \epsilon_i(\Omega_r) = 0$. The condition $\epsilon_i(\Omega_r) = 0$ is equivalent to

$$f'(\Omega_r) = 0. \quad (77)$$

The condition $\epsilon_r(\Omega_r) = 0$ leads to

$$1 - \frac{\eta}{2} [W_r(\sqrt{\eta}(\Omega_r - a)) + W_r(\sqrt{\eta}(\Omega_r + a))] = 0. \quad (78)$$

Therefore, according to Eq. (77), the real pulsation Ω_r is equal to a velocity V_0 at which the distribution (65) is extremum. The second equation (78) determines the value(s) $\eta_c(a)$ of the temperature at which the distribution is marginally stable.

5.2.1 The case $\omega_r = 0$

Let us first consider the value $\Omega_r = 0$ that is solution of Eq. (77) for any a and η . In that case, Eq. (78) becomes

$$\eta W_r(\sqrt{\eta}a) = 1, \quad (79)$$

where we have used Eq. (207). For fixed a , this equation determines the temperature(s) $\eta_c^{(0)}(a)$ corresponding to a mode of marginal stability with $\Omega_r = 0$. Introducing $y = \eta a^2 \geq 0$, the foregoing equation can be rewritten in the parametric form

$$a^2 = y W_r(\sqrt{y}), \quad (80)$$

$$\eta = \frac{1}{W_r(\sqrt{y})}. \quad (81)$$

The function defined by Eq. (80) is plotted in Fig. 16. It vanishes at $y = y_{max} = z_c^2$ where $z_c = 1.307$ is the zero of $W_r(z)$ (see Appendix A). For $y > y_{max} = 1.708$, the function (80) is negative so we restrict ourselves to

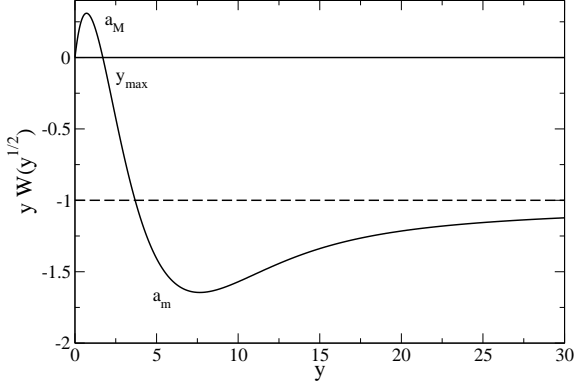


Fig. 16. $a^2 = yW_r(\sqrt{y})$ as a function of $y = \eta a^2$.

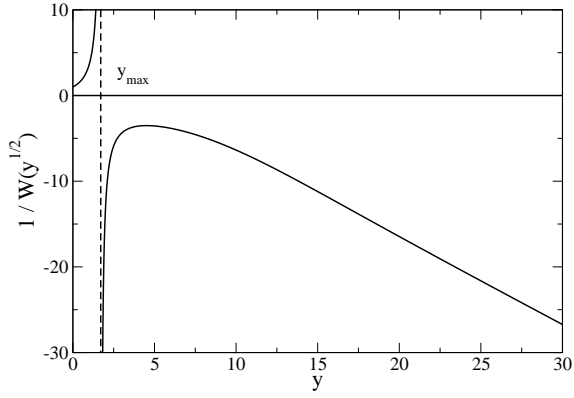


Fig. 17. $\eta = 1/W_r(\sqrt{y})$ as a function of $y = \eta a^2$.

$y \in [0, y_{max}]$. In this interval, it has a maximum at $y = y_M = 0.724$ and its value is $a_M = 0.556$. Therefore, for $a > a_M$, Eq. (80) has no solution. For $a = a_M$, Eq. (80) has one solution $y = y_M$ determining through Eq. (81) a temperature $\eta_c^{(0)(M)} = 2.338$. For $a < a_M$, Eq. (80) has two solutions $y_{1,2}$. Then, Eq. (81) determines two temperatures $\eta_c^{(0)(1,2)}(a)$ as illustrated in Fig. 17. These are the solutions of Eq. (79) for $a \leq a_M$.

Let us consider the limit $a \rightarrow 0$. In that case, we see in Fig. 16 that $y_1 \rightarrow 0$ and $y_2 \rightarrow y_{max}$. In the first case $y_1 \rightarrow 0$, using Eq. (214), we find from Eq. (81) that

$$\eta_c^{(0)(1)}(a) \rightarrow 1, \quad (a \rightarrow 0). \quad (82)$$

This result is to be expected since, for $a = 0$, the distribution (65) reduces to the Maxwellian. We thus recover the critical temperature (46). In the second case $y_2 \rightarrow y_{max}$, we find from Eq. (80) that $a^2 \sim y_{max}W_r(\sqrt{y_2})$. Substituting this equivalent in Eq. (81), and recalling that $y_{max} = z_c^2$, we get

$$\eta_c^{(0)(2)}(a) \sim \frac{z_c^2}{a^2}, \quad (a \rightarrow 0). \quad (83)$$

For $a \rightarrow 0$, this solution $\eta_c^{(0)(2)}(a) \rightarrow +\infty$ so that it does not appear in the study of the Maxwellian distribution corresponding to $a = 0$.

In conclusion:

- if $a < a_M$, there exists two critical temperatures $\eta_c^{(0)(1)}(a)$ and $\eta_c^{(0)(2)}(a)$ determined by Eqs. (80)-(81) corresponding to a marginal mode ($\Omega_r = 0, \Omega_i = 0$). These two branches merge at the point $(a_M, \eta_c^{(0)(M)})$.
- if $a > a_M$, there is no marginal mode ($\Omega_r = 0, \Omega_i = 0$).

The curves $\eta_c^{(0)(1)}(a)$ and $\eta_c^{(0)(2)}(a)$ corresponding to the marginal mode with zero pulsation $\Omega_r = 0$ are plotted in Fig. 18.

5.2.2 The case $\omega_r \neq 0$

We now consider the pulsations $\Omega_r = \pm V_*$ that are solutions of Eq. (77) for $\eta > 1/a^2$. To determine the temperature(s) at which the distribution (65) is marginally stable, we have to solve

$$1 - \frac{\eta}{2} [W_r(\sqrt{\eta}(V_* - a)) + W_r(\sqrt{\eta}(V_* + a))] = 0, \quad (84)$$

where V_* is given by

$$\eta = \frac{1}{2aV_*} \ln \left(\frac{a + V_*}{a - V_*} \right). \quad (85)$$

Eliminating V_* between these two expressions, we obtain the critical temperature(s) $\eta_c^{(\pm)}(a)$ as a function of a . However, it is easier to proceed differently. Setting $x = V_*/a$ and $y = \eta a^2$, we obtain the equations

$$y = \frac{1}{2x} \ln \left(\frac{1+x}{1-x} \right), \quad (86)$$

$$\eta = \frac{2}{[W_r(\sqrt{y}(x-1)) + W_r(\sqrt{y}(x+1))]}, \quad (87)$$

$$a^2 = \frac{y}{\eta}. \quad (88)$$

For given x , we can obtain y from Eq. (86) [see also Fig. 15], η from Eq. (87) and a from Eq. (88). Varying x in the interval $]-1, 1[$ yields the full curve $\eta_c^{(\pm)}(a)$. By symmetry, we can restrict ourselves to the interval $x \in [0, 1[$.

The limit $a \rightarrow +\infty$ (i.e. $y \rightarrow +\infty$) corresponds to $V_* \rightarrow a^-$ (i.e. $x \rightarrow 1^-$). For $x \rightarrow 1^-$, Eqs. (86) and (87) reduce to

$$y \sim -\frac{1}{2} \ln(1-x) \rightarrow +\infty, \quad (89)$$

and

$$\eta \simeq \frac{2}{[W_r(\sqrt{y}(x-1)) + W_r(2\sqrt{y})]}. \quad (90)$$

Using Eqs. (213) and (214), we obtain at leading order

$$\eta \simeq \frac{2}{1 - \frac{1}{4y}} \simeq 2 \left(1 + \frac{1}{4y} \right) \simeq 2 \left(1 + \frac{1}{4\eta a^2} \right), \quad (91)$$

so that

$$\eta_c^{(\pm)}(a) = 2 + \frac{1}{4a^2} + \dots \quad (a \rightarrow +\infty). \quad (92)$$

The result $\eta_c^{(\pm)}(a) \rightarrow 2$ can be understood simply. For $a \rightarrow +\infty$, the two humps are far away from each other so that we expect that the critical temperature $\eta_c^{(\pm)}$ will coincide with the critical temperature of a single Maxwellian since they do not “see” each other. Noting that the mass of a single hump is $M/2$, the corresponding critical temperature is $T_c = \frac{k(M/2)}{4\pi} = \frac{kM}{8\pi}$ leading to $\eta_c^{(\pm)} = 2$.

On the other hand, the branch $\eta_c^{(\pm)}(a)$ starts at the point (a_*, η_*) , corresponding to $\Omega_r = \pm V_* = 0$ (i.e. $x = 0$), connecting the branch $\eta_c^{(0)}(a)$ along which $\Omega_r = 0$. Now, for $x = 0$, we have $y = 1$ leading to $\eta_* = 1/W_r(1) = 3.633$ and $a_* = \sqrt{W_r(1)} = 0.524$. Therefore, the branch $\eta_c^{(\pm)}(a)$ corresponding to $\Omega_r = \pm V_*$ starts at the intersection between the branch $\eta_c^{(0)}(a)$ corresponding to $\Omega_r = 0$ and the hyperbole $\eta = 1/a^2$ separating the regions where the DF has one or two maxima.

In conclusion:

- if $a > a_*$, there exists a single critical temperature $\eta_c^{(\pm)}(a)$ determined by Eqs. (86)-(88) corresponding to a marginal mode ($\Omega_r = \pm V_*$, $\Omega_i = 0$). Note that the modes $\Omega_r = +V_*$ and $\Omega_r = -V_*$ are degenerate. This degeneracy can be raised by a small asymmetry (symmetry breaking) in the distribution (see Sec. 6).
- if $a < a_*$, there is no marginal mode ($\Omega_r = \pm V_*$, $\Omega_i = 0$).

The curve $\eta_c^{(\pm)}(a)$ corresponding to the marginal mode with pulsation $\Omega_r = \pm V_*$ is plotted in Fig. 18.

5.3 The stability diagram

The critical temperatures $\eta_c(a)$ corresponding to marginal stability determined previously are represented as a function of the separation a in Fig. 18. We have also plotted the hyperbole $\eta = 1/a^2$. Below this curve, the DF has a single maximum at $V_0 = 0$ and above this curve, the DF has two maxima at $V_0 = \pm V_*$ and a minimum at $V_0 = 0$. In order to investigate the stability of the solutions in the different regions, we can use the Nyquist method.

For $a < a_*$, there exists two temperatures $\eta_c^{(0)(1)}$ and $\eta_c^{(0)(2)}$ at which the DF is marginally stable. For $\eta = \eta_c^{(0)(1)}$, the DF has a single maximum at $V_0 = 0$ and for $\eta = \eta_c^{(0)(2)}$ the DF has a minimum at $V_0 = 0$ and two maxima at $\pm V_*$. In both cases, the marginal perturbation has zero pulsation $\Omega_r = 0$. By considering the Nyquist curves in this region (see Figs. 19-22), we find that the DF is stable for $\eta < \eta_c^{(0)(1)}$ and unstable for $\eta < \eta_c^{(0)(1)}$.

For $a > a_M$, there exists one temperature $\eta_c^{(\pm)}$ at which the DF is marginally stable. For $\eta = \eta_c^{(\pm)}$, the DF has two maxima at $V_0 = \pm V_*$ and one minimum at $V_0 = 0$. The marginal perturbation evolves with a pulsation $\Omega_r = \pm V_*$. By considering the Nyquist curves in this region (see Figs. 23-25), we find that the DF is stable for $\eta < \eta_c^{(\pm)}$ and unstable for $\eta > \eta_c^{(\pm)}$.

For $a_* < a < a_M$, there exists three temperatures $\eta_c^{(0)(1)}$, $\eta_c^{(0)(2)}$ and $\eta_c^{(\pm)}$ at which the DF is marginally sta-

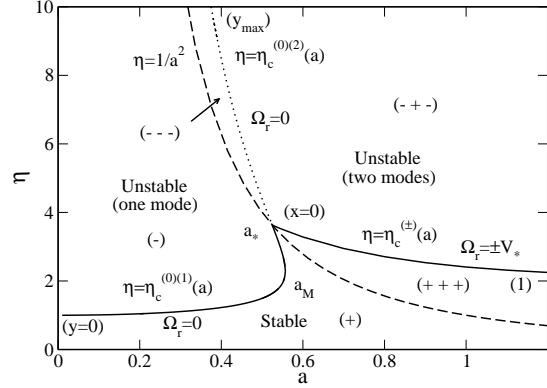


Fig. 18. Stability diagram of the symmetric double-humped distribution (65). The solid line corresponds to the critical line: below this line the DF is stable and above this line the DF is unstable. On the left panel (delimited by the solid line and the dotted line), there is one mode of instability and on the right panel there are two modes of instability. For $a_* < a < a_M$, there exists a “re-entrant” phase as described in the text. The dashed line corresponds to the hyperbole $\eta = 1/a^2$: below this line the DF has one maximum and above this line the DF has two maxima and one minimum. The symbols in parenthesis give the values of x or y that parametrize the marginal curves. The notations like $(-+-)$ give the positions of the $\epsilon_r(v_{ext})$'s in the Nyquist curves as defined in Sec. 2.7.

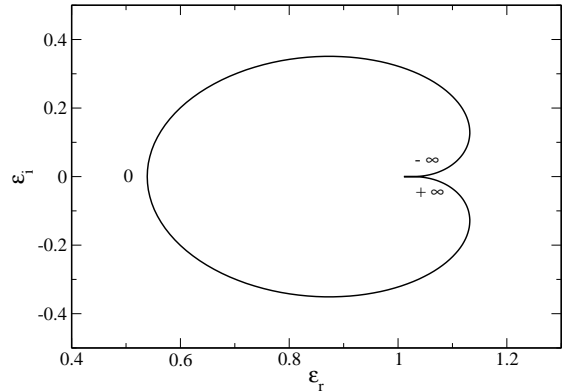


Fig. 19. Nyquist curve for $a < a_*$ and $\eta < \eta_c^{(0)(1)} < 1/a^2$ (specifically $a = 0.4$ and $\eta = 0.5$). The DF has only one maximum at $V_0 = 0$. It is stable because the Nyquist curve does not encircle the origin. Case (+).

ble. For $\eta = \eta_c^{(0)(1)}$ and $\eta = \eta_c^{(0)(2)}$, the DF has a single maximum at $V_0 = 0$. The marginal perturbation has zero pulsation $\Omega_r = 0$. For $\eta = \eta_c^{(\pm)}$, the DF has two maxima at $V_0 = \pm V_*$ and one minimum at $V_0 = 0$. The marginal perturbation has a pulsation $\Omega_r = \pm V_*$. By considering the Nyquist curves in this region (see Figs. 26-30), we find that the DF is stable for $\eta < \eta_c^{(0)(1)}$ unstable for $\eta_c^{(0)(1)} < \eta < \eta_c^{(0)(2)}$, stable again for $\eta_c^{(0)(2)} < \eta < \eta_c^{(\pm)}$

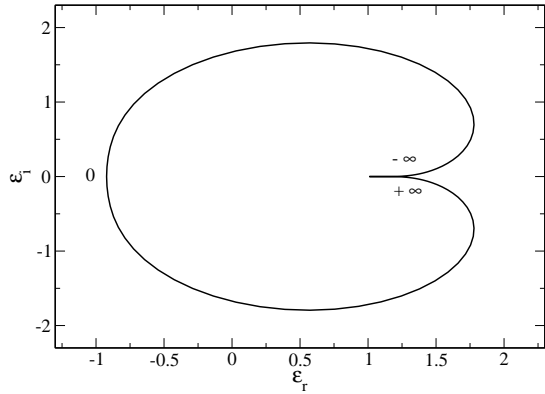


Fig. 20. Nyquist curve for $a < a_*$ and $\eta_c^{(1)(0)} < \eta < 1/a^2 < \eta_c^{(0)(2)}$ (specifically $a = 0.4$ and $\eta = 4$). The DF has only one maximum at $V_0 = 0$. The DF is unstable because the Nyquist curve encircles the origin. Case $(-)$.

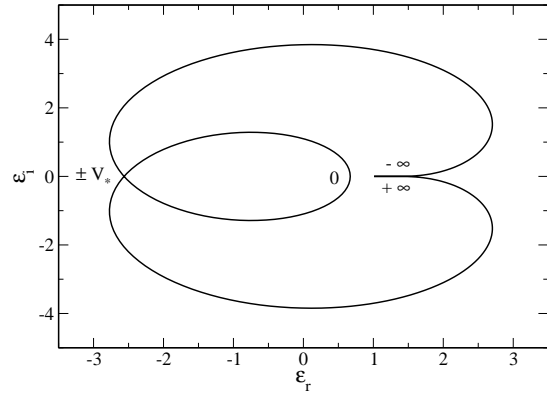


Fig. 22. Nyquist curve for $a < a_*$ and $\eta > \eta_c^{(0)(2)}$ (specifically $a = 0.4$ and $\eta = 10$). The DF has two maxima at $V_0 = \pm V_*$ and one minimum at $V_0 = 0$. The DF is unstable because the Nyquist curve encircles the origin. Since it rotates twice around the origin, this implies that there are $N = 2$ unstable modes (ω_r, ω_i) with $\omega_i > 0$. Case $(-+-)$.

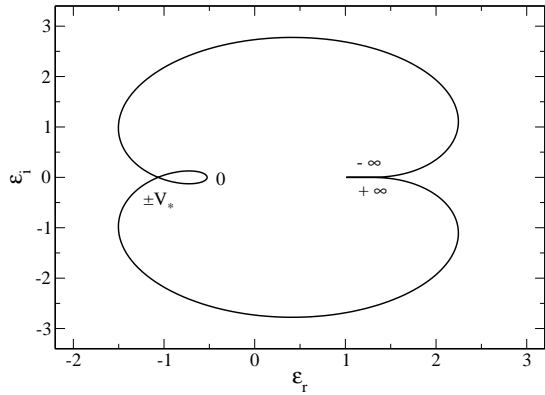


Fig. 21. Nyquist curve for $a < a_*$ and $1/a^2 < \eta < \eta_c^{(0)(2)}$ (specifically $a = 0.4$ and $\eta = 7$). The DF has two maxima at $V_0 = \pm V_*$ and one minimum at $V_0 = 0$. The DF is unstable because the Nyquist curve encircles the origin. Since it rotates only once around the origin, this implies that there is $N = 1$ unstable mode (ω_r, ω_i) with $\omega_i > 0$. Case $(---)$.

and unstable again for $\eta > \eta_c^{(\pm)}$. This corresponds to a re-entrant phase¹².

In conclusion, considering the stability diagram of Fig. 18, the symmetric double-humped distribution is stable below the solid line and unstable above it. When the solution is unstable, we expect that the system will evolve through violent relaxation towards a QSS that corresponds, in case of efficient mixing, to a Lynden-Bell statistical equilibrium state.

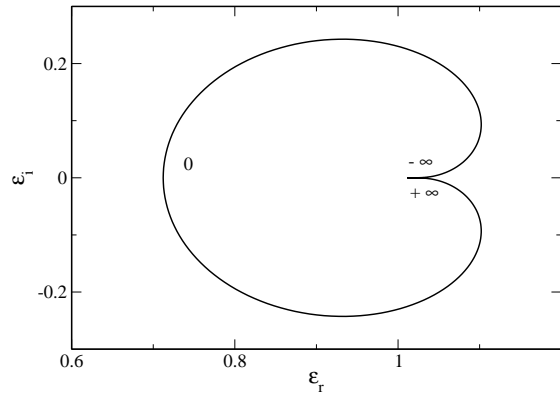


Fig. 23. Nyquist curve for $a > a_M$ and $\eta < 1/a^2 < \eta_c^{(\pm)}$ (specifically $a = 1$ and $\eta = 0.5$). The DF has only one maximum at $V_0 = 0$. The DF is stable because the Nyquist curve does not encircle the origin. Case $(+)$.

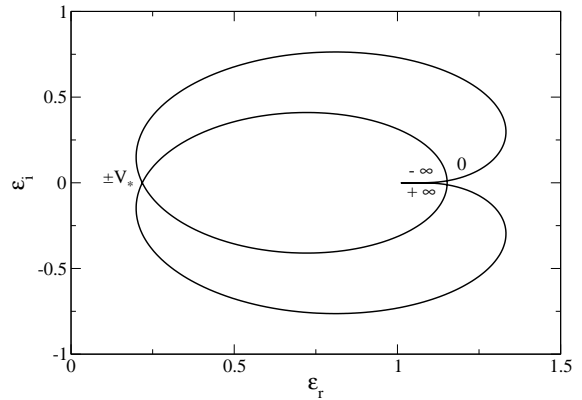


Fig. 24. Nyquist curve for $a > a_M$ and $1/a^2 < \eta < \eta_c^{(\pm)}$ (specifically $a = 1$ and $\eta = 2$). The DF has two maxima at $V_0 = \pm V_*$ and one minimum at $V_0 = 0$. The DF is stable because the Nyquist curve does not encircle the origin. Case $(+++)$.

¹² Interestingly, a re-entrant phase has also been observed in the stability diagram of the Lynden-Bell (or Fermi-Dirac) distributions for the HMF model [55,58].

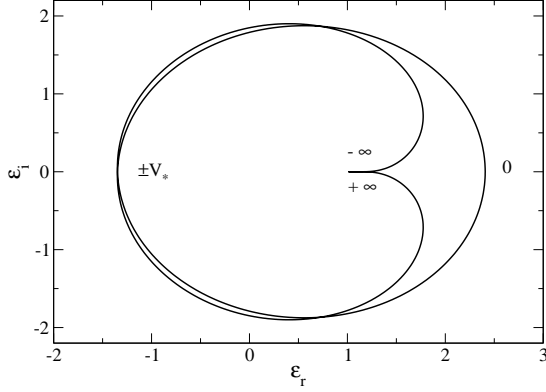


Fig. 25. Nyquist curve for $a > a_M$ and $\eta > \eta_c^{(\pm)} > 1/a^2$ (specifically $a = 1$ and $\eta = 5$). The DF has two maxima at $V_0 = \pm V_*$ and one minimum at $V_0 = 0$. The DF is unstable because the Nyquist curve encircles the origin. Since it rotates twice around the origin, this implies that there are $N = 2$ unstable modes (ω_r, ω_i) with $\omega_i > 0$. Case $(-+-)$.

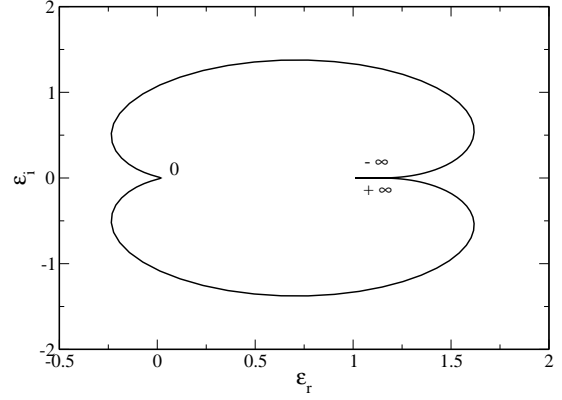


Fig. 28. Nyquist curve for $a_* < a < a_M$ and $\eta_c^{(0)(2)} < \eta < 1/a^2 < \eta_c^{(\pm)}$ (specifically $a = 0.535$ and $\eta = 3.4$). The DF has only one maximum at $V_0 = 0$. The DF is stable because the Nyquist curve does not encircle the origin. Case $(+)$. Note that when $\eta \rightarrow 1/a^2$, the tangent at $(\epsilon_r(\omega_r = 0), 0)$ is no more vertical since $f''(0) = 0$ (see remark at the end of Sec. 2.5). This corresponds precisely the transition between one maximum and two maxima and a minimum.

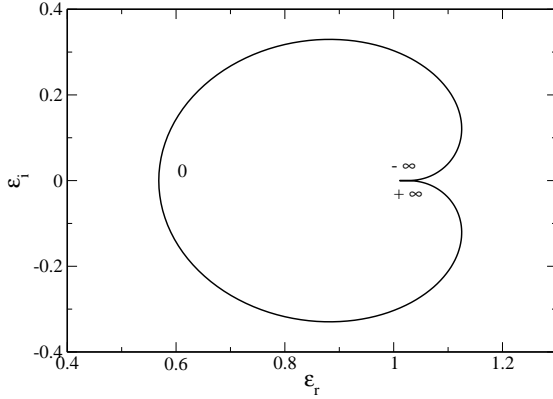


Fig. 26. Nyquist curve for $a_* < a < a_M$ and $\eta < \eta_c^{(0)(1)} < 1/a^2$ (specifically $a = 0.535$ and $\eta = 0.5$). The DF has only one maximum at $V_0 = 0$. The DF is stable because the Nyquist curve does not encircle the origin. Case $(+)$.

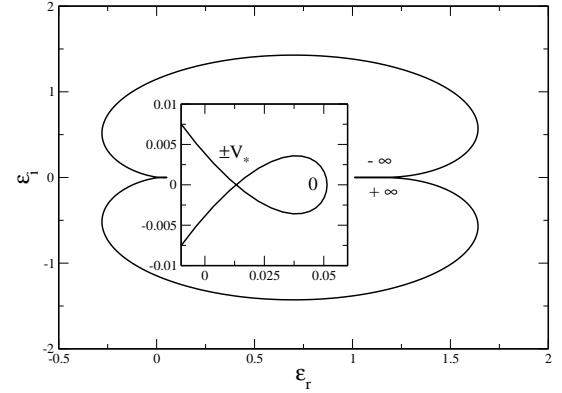


Fig. 29. Nyquist curve for $a_* < a < a_M$ and $\eta_c^{(0)(2)} < 1/a^2 < \eta < \eta_c^{(\pm)}$ (specifically $a = 0.535$ and $\eta = 3.55$). The DF has two maxima at $V_0 = \pm V_*$ and one minimum at $V_0 = 0$. The DF is stable because the Nyquist curve does not encircle the origin. Case $(+++)$.

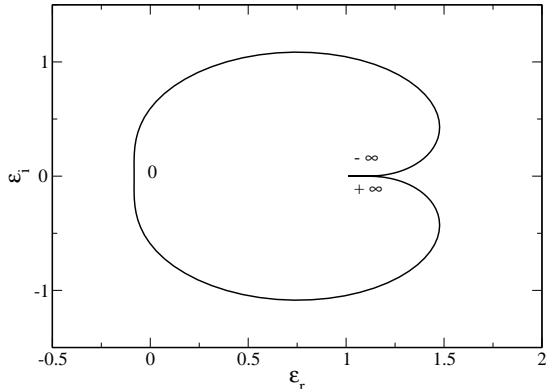


Fig. 27. Nyquist curve for $a_* < a < a_M$ and $\eta_c^{(0)(1)} < \eta < \eta_c^{(0)(2)} < 1/a^2$ (specifically $a = 0.535$ and $\eta = 2.5$). The DF has only one maximum at $V_0 = 0$. The DF is unstable because the Nyquist curve encircles the origin once. There is $N = 1$ mode of instability. Case $(-)$.

6 The asymmetric double-humped distribution

6.1 Determination of the extrema

We consider an asymmetric double-humped distribution of the form

$$f(v) = \sqrt{\frac{\beta}{2\pi}} \frac{\rho}{1 + \Delta} \left[e^{-\frac{\beta}{2}(v-v_a)^2} + \Delta e^{-\frac{\beta}{2}(v+v_a)^2} \right], \quad (93)$$

where $T = 1/\beta$ is the temperature of the Maxwellians and Δ is the asymmetry parameter (we assume here that $\Delta > 1$). This distribution is plotted in Fig. 31. The symmetric case is recovered for $\Delta = 1$. The average velocity is $\langle v \rangle = -[(\Delta - 1)/(\Delta + 1)]v_a$ and the kinetic temperature $T_{kin} \equiv$

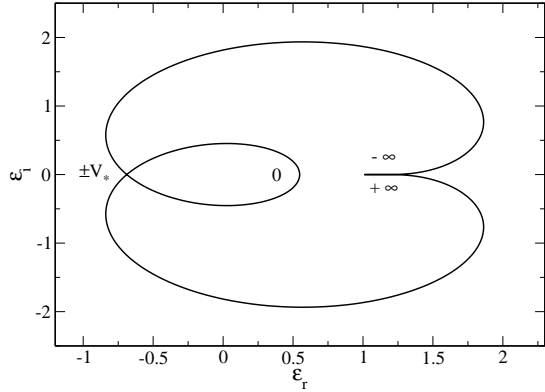


Fig. 30. Nyquist curve for $a_* < a < a_M$ and $\eta > \eta_c^{(\pm)} > 1/a^2$ (specifically $a = 0.535$ and $\eta = 5$). The DF has two maxima at $V_0 = \pm V_*$ and one minimum at $V_0 = 0$. The DF is unstable because the Nyquist curve encircles the origin twice. There are $N = 2$ modes of instability. Case $(-+-)$.

$\langle (v - \langle v \rangle)^2 \rangle = T + [4\Delta/(\Delta + 1)^2]v_a^2$. The velocities v_0 at which the distribution function $f(v)$ is extremum satisfy $f'(v_0) = 0$. They are determined by the equation

$$e^{-2\beta v_a v_0} = \frac{1}{\Delta} \frac{v_a - v_0}{v_a + v_0}. \quad (94)$$

Introducing the dimensionless temperature (37), the dimensionless velocity (38) and the dimensionless separation (67), Eq. (94) can be rewritten

$$\eta = \frac{1}{2aV_0} \ln \left(\frac{a + V_0}{a - V_0} \right) + \frac{\ln(\Delta)}{2aV_0}. \quad (95)$$

For a given value of inverse temperature η , separation a and asymmetry Δ , this equation determines the velocities V_0 where $f(V)$ is extremum. We note that $V_0 \in]-a, +a[$. It is convenient to introduce the variables

$$x = V_0/a, \quad y = \eta a^2. \quad (96)$$

For fixed a , the parameter y plays the role of the inverse temperature and the parameter x plays the role of the velocity. Then, we have to study the function

$$y(x) = \frac{1}{2x} \ln \left(\frac{1+x}{1-x} \right) + \frac{\ln(\Delta)}{2x}, \quad (97)$$

for $x \in]-1, +1[$. This function is plotted in Fig. 32. It has the following properties

$$y(x) \sim -\frac{1}{2} \ln(1-x), \quad (x \rightarrow 1^-), \quad (98)$$

$$y(x) \sim -\frac{1}{2} \ln(1+x), \quad (x \rightarrow -1^+), \quad (99)$$

$$y(x) \sim \frac{\ln(\Delta)}{2x}, \quad (x \rightarrow 0). \quad (100)$$

Considering the negative velocities $x < 0$, we note that $y \geq 0$ iff $x \leq x_0$ with

$$x_0 = \frac{\Delta - 1}{\Delta + 1}. \quad (101)$$

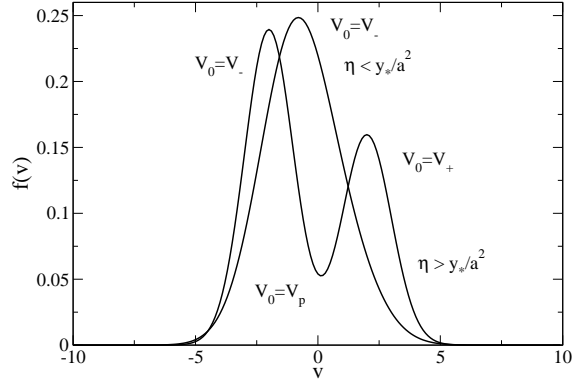


Fig. 31. Asymmetric double-humped distribution made of two Maxwellians with separation a and asymmetry $\Delta > 1$. If $\eta > y_*/a^2$, the DF has one global maximum at $V_0 = V_- < 0$, a minimum at $V_0 = V_p > 0$ and a local maximum at $V_0 = V_+ > 0$. If $\eta < y_*/a^2$, the DF has only one maximum at $V_0 = V_- < 0$.

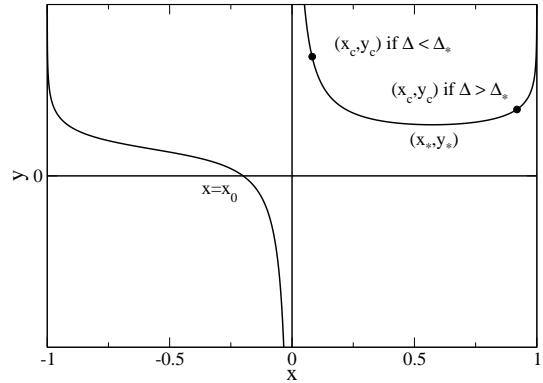


Fig. 32. The function $y(x)$ for the asymmetric double-humped distribution.

Considering the positive velocities $x > 0$, we note that the curve $y(x)$ is minimum at $x = x_*$ where x_* is solution of

$$\frac{2x_*}{1-x_*^2} - \ln \left(\frac{1+x_*}{1-x_*} \right) = \ln(\Delta). \quad (102)$$

This function is represented in Fig. 33. We note that Eq. (102) has a unique solution x_* for each value of $\Delta > 1$. Therefore, the function $y(x)$ has a single minimum at $x = x_*$. The value of this minimum is

$$y_* = \frac{1}{1-x_*^2} > 1. \quad (103)$$

The extrema of the distribution $f(V)$ can be determined from the study of the function (97). If $y < y_*$, i.e. $\eta < y_*/a^2$, the distribution $f(V)$ has a single maximum at $V_0 = V_- < 0$. If $y > y_*$, i.e. $\eta > y_*/a^2$, the distribution $f(V)$ has two maxima at $V_0 = V_- < 0$ and $V_0 = V_+ > 0$ and one minimum at $V_0 = V_p > 0$. These different values are given by $V_0 = ay^{-1}(\eta a^2)$.

In conclusion, for a given asymmetry Δ and separation a :

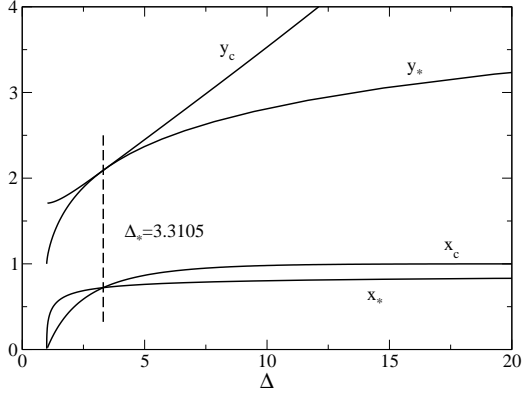


Fig. 33. Evolution of x_* , y_* , x_c and y_c as a function of Δ . The curves intersect each other at $\Delta_* = 3.3105$.

- if $\eta > y_*/a^2$, the distribution function $f(V)$ has a global maximum at $V_0 = V_- < 0$, a local maximum at $V_0 = V_+ > 0$ and one minimum at $V_0 = V_p > 0$.

- if $\eta < y_*/a^2$, the distribution function $f(V)$ has only one maximum at $V_0 = V_- < 0$.

Remark: We can note the formal analogy with the mean field theory (ferromagnetic transition) of the one dimensional Ising model with magnetic field where the asymmetry Δ plays the role of the magnetic field (compare Eq. (95) with Eq. (14) of [86]).

6.2 The condition of marginal stability

The dielectric function associated to the asymmetric double-humped distribution is

$$\epsilon(\Omega) = 1 - \frac{\eta}{1 + \Delta} [W(\sqrt{\eta}(\Omega - a)) + \Delta W(\sqrt{\eta}(\Omega + a))], \quad (104)$$

where $W(z)$ is defined in Eq. (40). When $\Omega_i = 0$, the real and imaginary parts of the dielectric function $\epsilon(\Omega_r) = \epsilon_r(\Omega_r) + i\epsilon_i(\Omega_r)$ can be written

$$\epsilon_r(\Omega_r) = 1 - \frac{\eta}{1 + \Delta} [W_r(\sqrt{\eta}(\Omega_r - a)) + \Delta W_r(\sqrt{\eta}(\Omega_r + a))], \quad (105)$$

$$\epsilon_i(\Omega_r) = -\frac{\eta}{1 + \Delta} [W_i(\sqrt{\eta}(\Omega_r - a)) + \Delta W_i(\sqrt{\eta}(\Omega_r + a))], \quad (106)$$

where $W_r(z)$ and $W_i(z)$ are defined in Eqs. (44)-(45) where z is here a real number. The condition of marginal stability corresponds to $\epsilon_r(\Omega_r) = \epsilon_i(\Omega_r) = 0$. The condition $\epsilon_i(\Omega_r) = 0$ is equivalent to

$$f'(\Omega_r) = 0. \quad (107)$$

The condition $\epsilon_r(\Omega_r) = 0$ leads to

$$1 - \frac{\eta}{1 + \Delta} [W_r(\sqrt{\eta}(\Omega_r - a)) + \Delta W_r(\sqrt{\eta}(\Omega_r + a))] = 0. \quad (108)$$

According to Eq. (107), the real pulsation Ω_r is equal to a velocity V_0 at which the distribution (93) is extremum. The second equation (108) determines the value(s) $\eta_c(a)$ of the temperature at which the distribution is marginally stable. Therefore, we have to solve

$$1 - \frac{\eta}{1 + \Delta} [W_r(\sqrt{\eta}(V_0 - a)) + \Delta W_r(\sqrt{\eta}(V_0 + a))] = 0, \quad (109)$$

where V_0 is given by

$$\eta = \frac{1}{2aV_0} \ln \left(\frac{a + V_0}{a - V_0} \right) + \frac{\ln(\Delta)}{2aV_0}. \quad (110)$$

Eliminating V_0 between these two expressions yields the critical temperature(s) $\eta_c(a)$ as a function of a . However, it is easier to proceed differently. Setting $x = V_0/a$ and $y = \eta a^2$, we obtain the equations

$$y = \frac{1}{2x} \ln \left(\frac{1+x}{1-x} \right) + \frac{\ln(\Delta)}{2x}, \quad (111)$$

$$\eta = \frac{1 + \Delta}{[W_r(\sqrt{y}(x-1)) + \Delta W_r(\sqrt{y}(x+1))]}, \quad (112)$$

$$a^2 = \frac{y}{\eta}. \quad (113)$$

For given x , we can obtain y from Eq. (111) [see also Fig. 32], η from Eq. (112) and a from Eq. (113). Varying x in the interval $] -1, 1[$ yields the full curve $\eta_c(a)$. We have three types of solutions. For $x \in] -1, x_0]$, we obtain a branch $\eta_c^{(-)}(a)$ where the pulsation of the marginal mode is negative: $\Omega_r = V_- < 0$ corresponding to the global maximum of $f(v)$. For $x \in]0, x_*]$, we obtain a branch $\eta_c^{(p)}(a)$ where the pulsation of the marginal mode is positive: $\Omega_r = V_p > 0$ corresponding to the minimum of $f(v)$.

For $x \in [x_*, 1[$, we obtain a branch $\eta_c^{(+)}(a)$ where the pulsation of the marginal mode is positive: $\Omega_r = V_+ > 0$ corresponding to the local maximum of $f(v)$. This leads to the curves reported in Figs. 34, 35 and 36 for three values of the asymmetry factor Δ .

The limit $a \rightarrow +\infty$ (i.e. $y \rightarrow +\infty$) corresponds to $V_0 \rightarrow a^-$ (i.e. $x \rightarrow 1^-$) or $V_0 \rightarrow -a^+$ (i.e. $x \rightarrow -1^+$). For $x \rightarrow 1^-$, Eqs. (111) and (112) reduce to

$$y \sim -\frac{1}{2} \ln(1-x) \rightarrow +\infty, \quad (114)$$

and

$$\eta \simeq \frac{1 + \Delta}{[W_r(\sqrt{y}(x-1)) + \Delta W_r(2\sqrt{y})]}. \quad (115)$$

Using Eqs. (213) and (214), we obtain at leading order

$$\eta \simeq \frac{1 + \Delta}{1 - \frac{\Delta}{4y}} \simeq (1 + \Delta) \left(1 + \frac{\Delta}{4y} \right) \simeq (1 + \Delta) \left(1 + \frac{\Delta}{4\eta a^2} \right), \quad (116)$$

so that

$$\eta_c^{(+)}(a) = 1 + \Delta + \frac{\Delta}{4a^2} + \dots \quad (a \rightarrow +\infty). \quad (117)$$

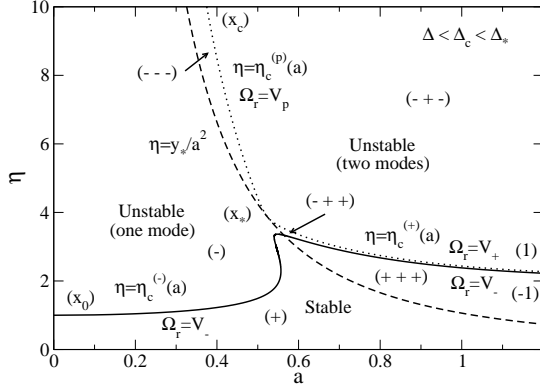


Fig. 34. Stability diagram of the asymmetric double-humped distribution for $\Delta < \Delta_c < \Delta_*$ (specifically $\Delta = 1.02$) showing a re-entrant phase in continuity with the symmetric case. Since $\Delta < \Delta_*$, there exists three marginal branches $\eta_c^{(-)}(a)$, $\eta_c^{(p)}(a)$ and $\eta_c^{(+)}(a)$.

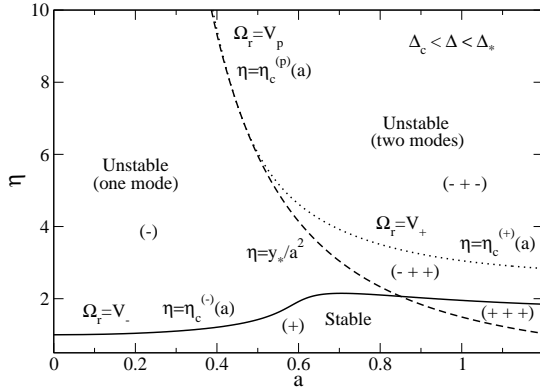


Fig. 35. Stability diagram of the asymmetric double-humped distribution for $\Delta_c < \Delta < \Delta_*$ (specifically $\Delta = 1.5$) showing the disappearance of the re-entrant phase.

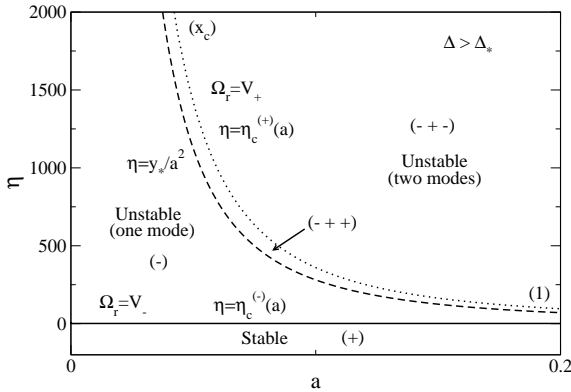


Fig. 36. Stability diagram of the asymmetric double-humped distribution for $\Delta > \Delta_*$ (specifically $\Delta = 10$). Since $\Delta > \Delta_*$, there exists only two marginal branches $\eta_c^{(-)}(a)$ and $\eta_c^{(+)}(a)$.

For $x \rightarrow -1^+$, Eqs. (111) and (112) reduce to

$$y \sim -\frac{1}{2} \ln(1+x) \rightarrow +\infty, \quad (118)$$

and

$$\eta \simeq \frac{1+\Delta}{[W_r(2\sqrt{y}) + \Delta W_r(\sqrt{y}(1+x))]} \quad (119)$$

Using Eqs. (213) and (214), we obtain at leading order

$$\eta \simeq \frac{1+\Delta}{\Delta - \frac{1}{4y}} \simeq \frac{1+\Delta}{\Delta} \left(1 + \frac{1}{4\Delta y}\right) \simeq \frac{1+\Delta}{\Delta} \left(1 + \frac{1}{4\Delta\eta a^2}\right), \quad (120)$$

so that

$$\eta_c^{(-)}(a) = \frac{1+\Delta}{\Delta} + \frac{1}{4\Delta a^2} + \dots \quad (a \rightarrow +\infty). \quad (121)$$

The limit $a \rightarrow 0$ with η finite corresponds to $y \rightarrow 0$, i.e. $x \rightarrow x_0$. We find from Eq. (112) that $\eta \rightarrow 1/W_r(0) = 1$ so that

$$\eta_c^{(-)}(a) \rightarrow 1 \quad (a \rightarrow 0). \quad (122)$$

This returns the critical temperature (46) associated with the Maxwellian distribution (34) corresponding to $a = 0$. The limit $a \rightarrow 0$ with $\eta \rightarrow +\infty$ corresponds to

$$\eta_c^{(P)}(a) \sim \frac{y_c}{a^2}, \quad (a \rightarrow 0), \quad (123)$$

with y_c finite ($P = p$ if $\Delta < \Delta_*$ and $P = +$ if $\Delta > \Delta_*$ as will become clear below). Since $\eta \rightarrow +\infty$, this constant y_c is determined by

$$y_c = \frac{1}{2x_c} \ln\left(\frac{1+x_c}{1-x_c}\right) + \frac{\ln(\Delta)}{2x_c}, \quad (124)$$

$$W_r(\sqrt{y_c}(x_c - 1)) + \Delta W_r(\sqrt{y_c}(x_c + 1)) = 0. \quad (125)$$

Note that there is no physical solution to Eqs. (111)-(113) when $0 < x < x_c$ (η would be negative) so that the branch $\eta_c^{(P)}(a)$ starts at $(0, +\infty)$ corresponding to $x = x_c$. The evolution of x_c and y_c with Δ is studied in Fig. 33 and is compared with the evolution of x_* and y_* . The curves intersect each other at $\Delta_* = 3.3105$. For $\Delta < \Delta_*$, $x_c < x_*$ so that the stability diagram displays three marginal branches $\eta_c^{(-)}(a)$, $\eta_c^{(p)}(a)$ and $\eta_c^{(+)}(a)$ (see Fig. 34). The branches $\eta_c^{(p)}(a)$ and $\eta_c^{(+)}(a)$ connect each other at (a_*, η_*) corresponding to $x = x_*$. At that point they touch the hyperbole $\eta = y_*/a^2$ separating distributions with one or two maxima. Since $y_c > y_*$, the curve $\eta_c^{(p)}(a)$ for $a \rightarrow 0$ is above the hyperbole $\eta = y_*/a^2$. For $\Delta = \Delta_*$, $x_c = x_*$ so that the branch $\eta_c^{(p)}(a)$ is rejected at infinity and only the branches $\eta_c^{(-)}(a)$ and $\eta_c^{(+)}(a)$ remain. Since $y_c = y_*$, the branch $\eta_c^{(+)}(a)$ coincides with the hyperbole $\eta = y_*/a^2$ for $a \rightarrow 0$. For $\Delta > \Delta_*$, $x_c > x_*$ so that the phase diagram displays only two marginal branches $\eta_c^{(-)}(a)$ and $\eta_c^{(+)}(a)$ (see Fig. 36). The curve $\eta_c^{(+)}(a)$ is strictly above the hyperbole $\eta = y_*/a^2$ without any intersection.

6.3 The stability diagram

The critical temperatures $\eta_c(a)$ corresponding to marginal stability determined previously are represented as a function of the separation a in Figs. 34, 35 and 36 for three values of the asymmetry factor Δ . We recall that $\eta_c^{(-)}(a)$ corresponds to the temperature associated with a marginal mode with pulsation $\Omega_r = V_- < 0$, $\eta_c^{(p)}(a)$ corresponds to the temperature associated with a marginal mode with pulsation $\Omega_r = V_p > 0$ and $\eta_c^{(+)}(a)$ corresponds to the temperature associated with a marginal mode with pulsation $\Omega_r = V_+ > 0$. We have also plotted the hyperbole $\eta = y_*/a^2$. Below this curve, the DF has a single maximum at $V_- < 0$ and above this curve, the DF has two maxima at $V_- < 0$ and $V_+ > 0$ and a minimum at $V_p > 0$. In order to investigate the stability of the solutions in the different regions of the parameter space, we have used the Nyquist criterion. There exists a critical value $\Delta_c = 1.09$ of the asymmetry parameter. For $\Delta < \Delta_c$, the stability diagram displays a re-entrant phase (in continuity with the case $\Delta = 1$) but for $\Delta > \Delta_c$ the re-entrant phase disappears. The description of the stability diagram is similar to the one given in Sec. 5.3 and the different possible cases can be understood directly from the reading of Figs. 34, 35 and 36. The best way is to fix a and progressively increase the value of η . Below the dashed line, the distribution has only one maximum at $V_0 = V_-$ so the Nyquist curve has one intersection with the x -axis (in addition to the limit point $(1, 0)$). For $\eta \rightarrow 0$, we find that $\epsilon_r(V_-) > 0$ so the system is stable. As we increase η and pass above the dashed line, the distribution has two maxima at $V_0 = V_-$ and $V_0 = V_+$ and one minimum at $V_0 = V_p$. At each intersection with a marginal line, one of the values $\epsilon_r(V_-)$, $\epsilon_r(V_p)$ or $\epsilon_r(V_+)$ changes sign. We have indicated by symbols like $(- + +)$ the respective signs of $\epsilon_r(V_-)$, $\epsilon_r(V_p)$ and $\epsilon_r(V_+)$. We can then easily draw by hands the corresponding Nyquist curve. Therefore, it is not necessary to show all the possibilities and we have only indicated a few representative cases in Figs. 37-39 for illustration.

7 The repulsive HMF model

7.1 General results

We shall now consider the HMF model with a repulsive interaction between particles. It is described by the Hamiltonian

$$H = \sum_{i=1}^N \frac{v_i^2}{2} + \frac{k}{2\pi} \sum_{i < j} \cos(\theta_i - \theta_j), \quad (126)$$

with $k > 0$. In this paper, we shall investigate the linear dynamical stability¹³ of stationary solutions of the Vlasov

¹³ The nonlinear regime of the repulsive HMF model leading to a bicluster (for low energies) has been studied in [87].

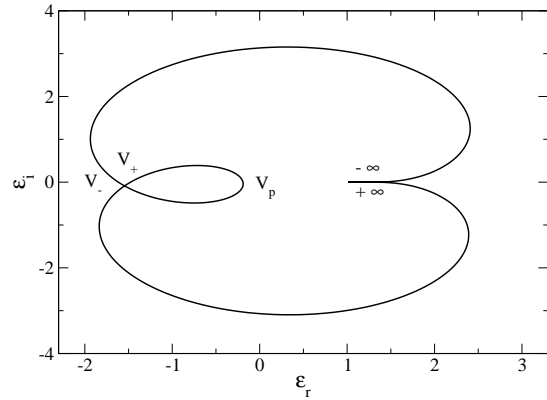


Fig. 37. For $\Delta < \Delta_c < \Delta_*$: Nyquist curve for $a < a_*$ and $y_*/a^2 < \eta < \eta_c^{(p)}$ (specifically $\Delta = 1.02$, $a = 0.4$ and $\eta = 8$). The DF has two maxima at V_- and V_+ and one minimum at V_p . The DF is unstable because the Nyquist curve encircles the origin once. There is $N = 1$ unstable mode. Case $(- - -)$.

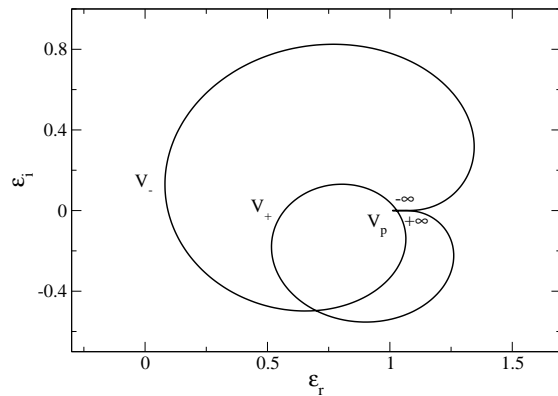


Fig. 38. For $\Delta_c < \Delta < \Delta_*$: Nyquist curve for $y_*/a^2 < \eta < \eta_c^{(-)}$ (specifically $\Delta = 1.5$, $a = 1$ and $\eta = 1.8$). The DF has two maxima at V_- and V_+ and one minimum at V_p . The DF is stable because the Nyquist curve does not encircle the origin. Case $(+ + +)$.

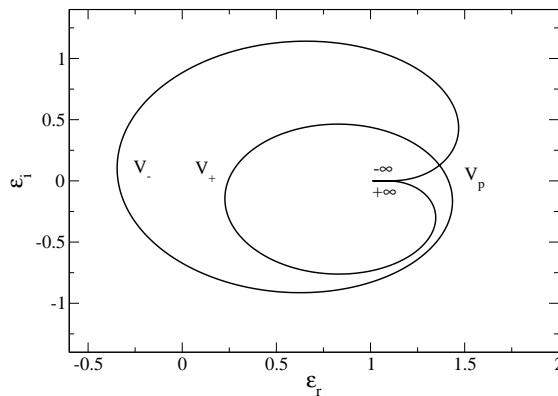


Fig. 39. For $\Delta_c < \Delta < \Delta_*$: Nyquist curve for $y_*/a^2 < \eta_c^{(-)} < \eta < \eta_c^{(+)}$ (specifically $\Delta = 1.5$, $a = 1$ and $\eta = 2.5$). The DF has two maxima at V_- and V_+ and one minimum at V_p . The DF is unstable because the Nyquist curve encircles the origin once. There is $N = 1$ unstable mode. Case $(- + +)$.

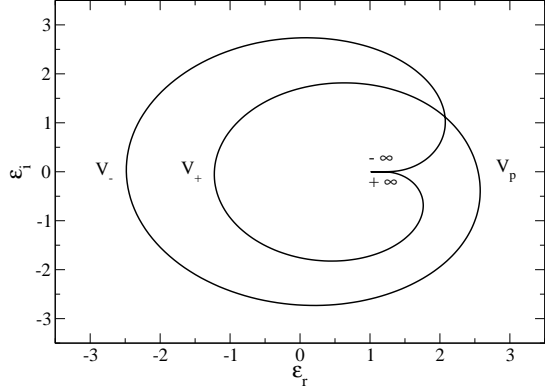


Fig. 40. For $\Delta_c < \Delta < \Delta_*$: Nyquist curve for $\eta > \eta_c^{(+)} > y_*/a^2$ (specifically $\Delta = 1.5$, $a = 1$ and $\eta = 6$). The DF has two maxima at V_- and V_+ and one minimum at V_P . The DF is unstable because the Nyquist curve encircles the origin twice. There are $N = 2$ unstable modes. Case $(- + -)$.

equation of the form $f = f(v)$. In the repulsive case, the dispersion relation becomes

$$\epsilon(\omega) \equiv 1 - \frac{k}{2} \int_C \frac{f'(v)}{v - \omega} dv = 0. \quad (127)$$

When $\omega_i = 0$, the real and imaginary parts of the dielectric function $\epsilon(\omega_r) = \epsilon_r(\omega_r) + i\epsilon_i(\omega_r)$ are

$$\epsilon_r(\omega_r) = 1 - \frac{k}{2} P \int_{-\infty}^{+\infty} \frac{f'(v)}{v - \omega_r} dv, \quad (128)$$

$$\epsilon_i(\omega_r) = -\pi \frac{k}{2} f'(\omega_r). \quad (129)$$

To apply the Nyquist method, we have to plot the curve $(\epsilon_r(\omega_r), \epsilon_i(\omega_r))$ parameterized by ω_r going from $-\infty$ to $+\infty$. Let us consider the asymptotic behavior for $\omega_r \rightarrow \pm\infty$. Since $f(v)$ tends to zero for $v \rightarrow \pm\infty$, we conclude that $\epsilon_i(\omega_r) \rightarrow 0$ for $\omega_r \rightarrow \pm\infty$ and that $\epsilon_i(\omega_r) < 0$ for $\omega_r \rightarrow -\infty$ while $\epsilon_i(\omega_r) > 0$ for $\omega_r \rightarrow +\infty$. On the other hand, for $\omega_r \rightarrow \pm\infty$, we obtain at leading order

$$\epsilon_r(\omega_r) \simeq 1 - \frac{k}{2} \frac{\rho}{\omega_r^2}, \quad (\omega_r \rightarrow \pm\infty). \quad (130)$$

From these results, we conclude that the behavior of the curve close to the point $(1, 0)$ is the one represented in Fig. 41. Let v_{ext} be the velocity corresponding to an extremum of the distribution ($f'(v_{ext}) = 0$). Then, we have

$$\epsilon_r(v_{ext}) = 1 + \frac{k}{2} \int_{-\infty}^{+\infty} \frac{f(v_{ext}) - f(v)}{(v - v_{ext})^2} dv > 1. \quad (131)$$

If v_{Max} denotes the velocity corresponding to the global maximum of the distribution, we clearly have

$$\epsilon_r(v_{Max}) > 1. \quad (132)$$

Finally, for a repulsive interaction, we note that if the zero of $f'(v)$ corresponds to a maximum (resp. minimum) of f then the hodograph crosses the real axis upward (resp. downward).

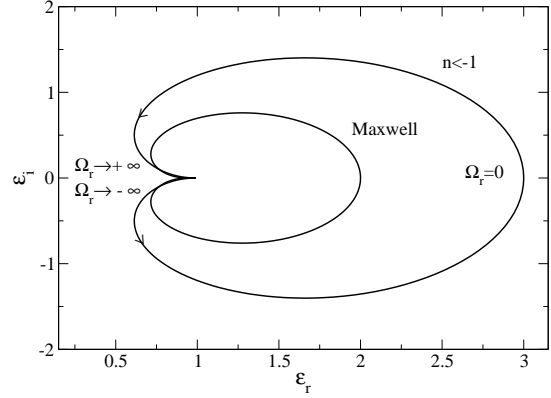


Fig. 41. Nyquist curve for the Maxwell and the Tsallis distribution with $n < -1$ (specifically $n = -2$).

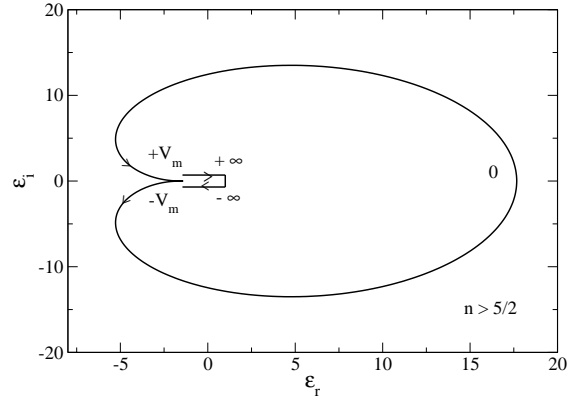


Fig. 42. Nyquist curve for the Tsallis distribution with $n > 5/2$ (specifically $n = 5$).

7.1.1 Single-humped distributions

Let us assume that the distribution $f(v)$ has a single maximum at $v = v_0$ (so that $f'(v_0) = 0$) and tends to zero for $v \rightarrow \pm\infty$. Then, the Nyquist curve cuts the x -axis ($\epsilon_i(\omega_r)$ vanishes) at the limit point $(1, 0)$ when $\omega_r \rightarrow \pm\infty$ and at the point $(\epsilon_r(v_0), 0)$ when $\omega_r = v_0$. Due to its behavior close to the limit point $(1, 0)$, the fact that it rotates in the counterclockwise sense, and the property that $\epsilon_r(v_0) > 1$ according to Eq. (132), the Nyquist curve must necessarily behave like in Fig. 41. Therefore, the Nyquist curve starts on the real axis at $\epsilon_r(\omega_r) = 1$ for $\omega_r \rightarrow -\infty$, then going in counterclockwise sense it crosses the real axis at the point $\epsilon_r(v_0) > 1$ and returns on the real axis at $\epsilon_r(\omega_r) = 1$ for $\omega_r \rightarrow +\infty$. Therefore, it cannot encircle the origin. According to the Nyquist criterion exposed in Sec. 2.4, we conclude that a single-humped distribution is always linearly stable. For illustration, the Nyquist curves for the Maxwell and the Tsallis distributions are represented in Figs. 41-44.

For the water-bag model ($n = 1/2$), we can obtain an analytical expression of the dielectric function in the form

$$\epsilon(\Omega) = 1 + \frac{1}{3} \eta W^{(1/2)}(\sqrt{\eta} \Omega), \quad (133)$$

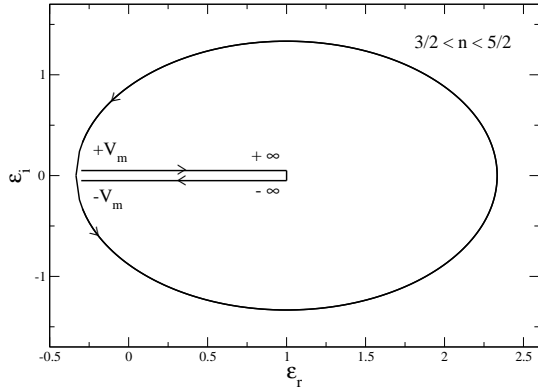


Fig. 43. Nyquist curve for the Tsallis distribution with $3/2 < n < 5/2$ (specifically $n = 2$).

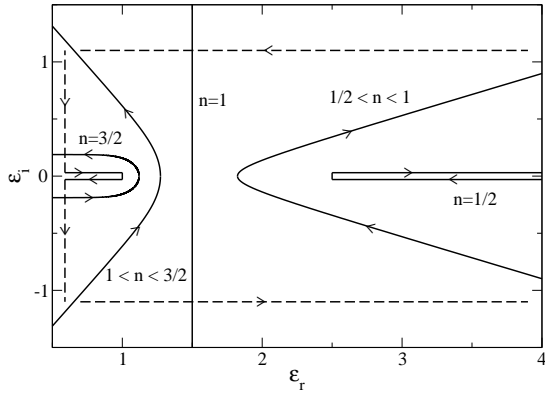


Fig. 44. Nyquist curve for the Tsallis distribution with $1/2 < n < 3/2$ showing the different cases (specifically $n = 3/2$, $n = 1.2$, $n = 1$, $n = 0.7$ and $n = 1/2$).

where $W^{(1/2)}(z)$ is given by Eq. (61). The condition $\epsilon(\omega) = 0$ determines the complex pulsation. We have

$$\omega^2 = \frac{kM}{4\pi} + 3T. \quad (134)$$

The pulsation is real so the mode is purely oscillating without being damped. For $T = 0$, we find that $\omega = \omega_p$ where ω_p is the proper pulsation defined in Eq. (251). Note, in passing, that the dimensionless pulsation can be written $\Omega = \omega/\omega_p$. On the other hand, for $\Omega_i = 0$, we get

$$\epsilon_r(\Omega_r) = 1 + \frac{1}{3}\eta \frac{1}{1 - \frac{1}{3}\eta\Omega_r^2}, \quad \epsilon_i(\Omega_r) = 0. \quad (135)$$

Therefore, the Nyquist curve is made of two segments $] -\infty, 1]$ and $[1 + \eta/3, +\infty[$ as represented in Fig. 44.

7.1.2 Double-humped distributions

Let us consider a double-humped distribution with a global maximum at v_{Max} , a minimum at v_{min} and a local maximum at v_{max} . We assume $v_{Max} < v_{min} < v_{max}$. The

Nyquist curves starts at $(1, 0)$, progresses in the counter-clockwise sense and crosses the x -axis at $\epsilon_r(v_{Max}) > 1$, then at $\epsilon_r(v_{min})$ and $\epsilon_r(v_{max})$. We can convince ourselves by making drawings of the following results. If

$$(+ + +): \epsilon_r(v_{Max}) > 0, \epsilon_r(v_{min}) > 0, \epsilon_r(v_{max}) > 0,$$

$$(+ - -): \epsilon_r(v_{Max}) > 0, \epsilon_r(v_{min}) < 0, \epsilon_r(v_{max}) < 0,$$

$$(+ + -): \epsilon_r(v_{Max}) > 0, \epsilon_r(v_{min}) > 0, \epsilon_r(v_{max}) < 0,$$

the Nyquist curve does not encircle the origin so the system is stable. If

$$(+ - +): \epsilon_r(v_{Max}) > 0, \epsilon_r(v_{min}) < 0, \epsilon_r(v_{max}) > 0,$$

the Nyquist curve rotates one time around the origin so that there is one mode of instability. Since $\epsilon_r(v_{Max}) > 0$ there is no mode of marginal stability with $\omega_r = v_{Max}$. Cases $(+ + +)$, $(+ - +)$ and $(+ - -)$ are observed in Sec. 7.3 for an asymmetric double-humped distribution made of two Maxwellians.

If the double-humped distribution is symmetric with respect to the origin with two maxima at $\pm v_*$ and a minimum at $v = 0$, we get the same results as above with the additional properties $\epsilon_r(v_{Max}) = \epsilon_r(v_{max}) = \epsilon_r(v_*) > 1$ and $\epsilon_r(v_{min}) = \epsilon_r(0)$. We have only two cases $(+ + +)$ and $(+ - +)$. They are observed in Sec. 7.2 for a symmetric double-humped distribution made of two Maxwellians. Since $\epsilon_r(v_*) > 0$, there is no mode of marginal stability with $\omega_r = \pm v_*$.

7.2 The symmetric double-humped distribution

Let us now consider the symmetric double-humped distribution (65). In the repulsive case, the dielectric function is

$$\epsilon(\Omega) = 1 + \frac{\eta}{2} [W(\sqrt{\eta}(\Omega - a)) + W(\sqrt{\eta}(\Omega + a))]. \quad (136)$$

The condition of marginal stability corresponds to $\epsilon(\Omega) = 0$ and $\omega_i = 0$. The condition $\epsilon_i(\omega_r) = 0$ is equivalent to $f'(\omega_r) = 0$ so that the real pulsations correspond to the velocities where the distribution is extremum: $\omega_r = v_0$. Then, the temperatures at which the distribution is marginally stable are obtained by solving $\epsilon_r(\omega_r = v_0) = 0$. Proceeding as in Sec. 5 and introducing the parameters $x = V_0/a$ and $y = \eta a^2$, we find that the equations determining the critical temperatures $\eta_c(a)$ are given by

$$y = \frac{1}{2x} \ln \left(\frac{1+x}{1-x} \right), \quad (137)$$

$$\eta = \frac{-2}{[W_r(\sqrt{y}(x-1)) + W_r(\sqrt{y}(x+1))]}, \quad (138)$$

$$a^2 = \frac{y}{\eta}. \quad (139)$$

We note that only the sign in Eq. (138) changes with respect to the study of the attractive case, so we can readily adapt the results of Sec. 5 to the present situation by simply reverting the sign. For $\Omega_r = \pm v_*$, corresponding to $x \neq 0$, there is no physical solution to Eqs. (137)-(139) with positive temperature $\eta > 0$. Therefore, in the repulsive case, there is no marginal mode with non zero pulsation for the symmetric double-humped distribution (in

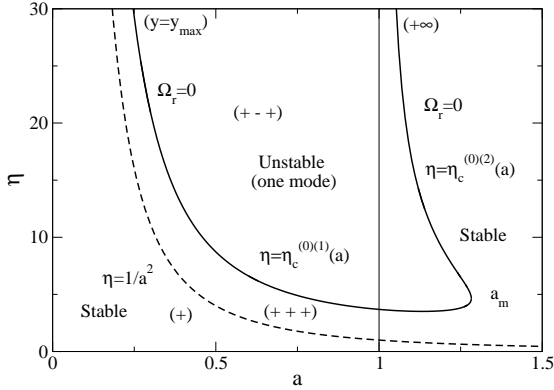


Fig. 45. Stability diagram of the symmetric double-humped distribution for the repulsive HMF model. There is a re-entrant phase for $1 < a < a_m$.

agreement with the general discussion of Sec. 7.1.2). We now consider the marginal mode with $\Omega_r = 0$. This corresponds to the “degenerate” solution $x = 0$ (for any y) for which Eqs. (137)-(139) reduce to

$$\eta = \frac{-1}{W_r(\sqrt{y})}, \quad (140)$$

$$a^2 = \frac{y}{\eta} = -yW_r(\sqrt{y}). \quad (141)$$

According to Fig. 16, physical solutions exist only for $y \geq y_{max} = z_c^2$. We note that the range of parameters that was forbidden in the attractive case is now allowed in the repulsive case and vice versa. We thus consider the range $y \in [y_{max}, +\infty[$. The function (141) has a maximum $a_m = 1.282$ at $y = y_m = 7.642$ and for $y \rightarrow +\infty$ it tends to $a = 1$. Therefore, for $a > a_m$, Eqs. (140)-(141) have no solution. For $a = a_m$, Eq. (141) has one solution $y = y_m$ determining, through Eq. (140), a temperature $\eta_c^{(0)(m)} = 4.647$. For $1 < a < a_m$, Eq. (141) has two solutions $y = y_{1,2}$. Then, Eq. (140) determines two temperatures $\eta_c^{(0)(1)}$ and $\eta_c^{(0)(2)}$ as illustrated in Fig. 17. Finally, for $0 < a < 1$, Eq. (141) has one solution $y = y_1$ determining, through Eq. (140), a temperature $\eta_c^{(0)(1)}$.

The limit $y \rightarrow y_{max}$ corresponds to $a \rightarrow 0$. Since $a^2 \sim -y_{max}W_r(\sqrt{y})$ and $\eta \sim -1/W_r(\sqrt{y})$, we get

$$\eta_c^{(0)(1)}(a) \sim \frac{z_c^2}{a^2}, \quad (a \rightarrow 0). \quad (142)$$

This result is to be expected since, for $a = 0$, the distribution (65) reduces to the Maxwellian that is stable for a repulsive interaction (hence $\eta_c = +\infty$).

Using Eq. (213), the limit $y \rightarrow +\infty$ corresponds to $a \rightarrow 1^+$. Then, we get

$$\eta_c^{(0)(2)}(a) \sim \frac{3}{2(a-1)}, \quad (a \rightarrow 1^+). \quad (143)$$

The critical temperature(s) $\eta_c(a)$ corresponding to marginal stability determined previously are represented

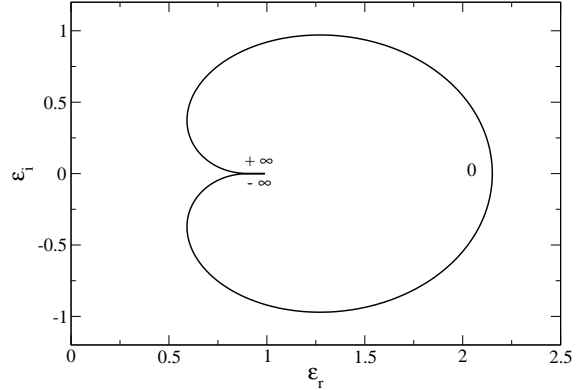


Fig. 46. Nyquist curve for $a < 1$ and $\eta < 1/a^2 < \eta_c^{(0)(1)}(a)$ (specifically $a = 0.5$, $\eta = 2$). The system is stable. Case (+).

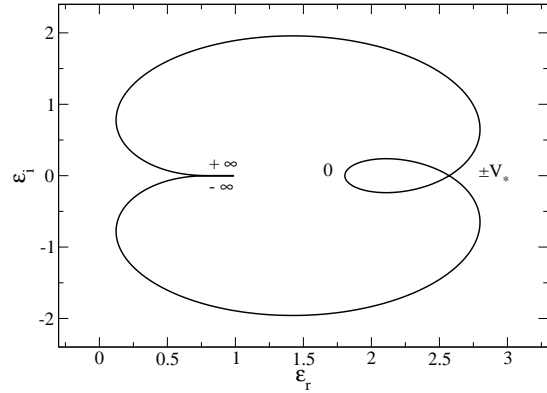


Fig. 47. Nyquist curve for $a < 1$ and $1/a^2 < \eta < \eta_c^{(0)(1)}(a)$ (specifically $a = 0.5$, $\eta = 5$). The system is stable. Case (+++).

as a function of the separation a in Fig. 45. We have also plotted the hyperbole $\eta = 1/a^2$. Below this curve, the distribution has a single maximum at $V_0 = 0$ and above this curve, the distribution has two maxima at $V_0 = \pm V_*$ and a minimum at $V_0 = 0$. In order to investigate the stability of the solutions in the different regions, we have used the Nyquist criterion.

For $a < 1$, there exists one temperature $\eta_c^{(0)(1)}$ at which the distribution is marginally stable. For $\eta = \eta_c^{(0)(1)}$, the distribution has a minimum at $V_0 = 0$ and two maxima at $\pm V_*$. The marginal perturbation has zero pulsation $\Omega_r = 0$. By considering the Nyquist curves in this region (see Figs. 46-48), we find that the DF is stable for $\eta < \eta_c^{(0)(1)}$ and unstable for $\eta > \eta_c^{(0)(1)}$.

For $a > a_m$, there is no marginal mode and the distribution is always stable (see Figs. 49-50). This result is to be expected because, for $a \rightarrow +\infty$, the two humps do not “see” each other and behave as two independent single-humps distributions that are stable in the repulsive case.

For $1 < a < a_m$, there exists two temperatures $\eta_c^{(0)(1)}$, and $\eta_c^{(0)(2)}$ at which the distribution is marginally stable. These two branches merge at the point $(a_m, \eta_c^{(0)(m)})$.

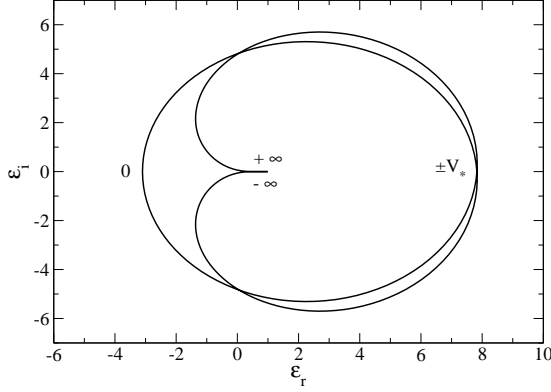


Fig. 48. Nyquist curve for $a < 1$ and $\eta > \eta_c^{(0)(1)}(a) > 1/a^2$ (specifically $a = 0.5$, $\eta = 15$). The system is unstable. Case (+ - +).

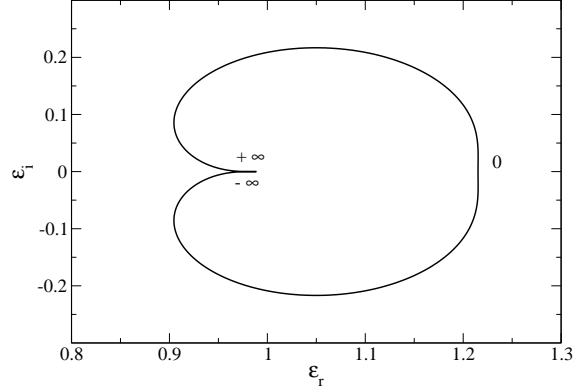


Fig. 51. Nyquist curve for $1 < a < a_m$ and $\eta < 1/a^2$ (specifically $a = 1.2$, $\eta = 0.5$). The system is stable. Case (+).

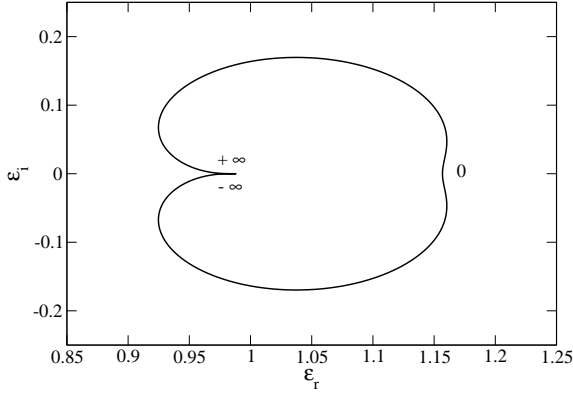


Fig. 49. Nyquist curve for $a > a_m$ and $\eta < 1/a^2$ (specifically $a = 1.4$, $\eta = 0.4$). The system is stable. Case (+).

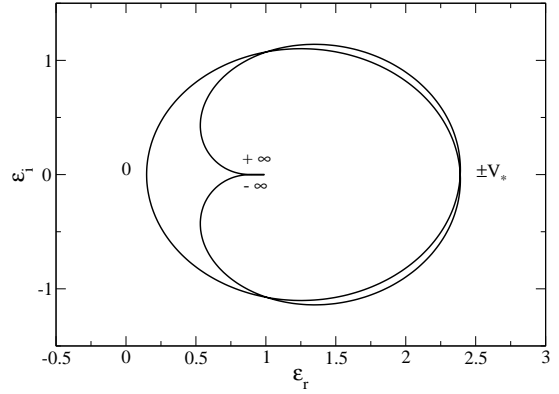


Fig. 52. Nyquist curve for $1 < a < a_m$ and $1/a^2 < \eta < \eta_c^{(0)(1)}(a)$ (specifically $a = 1.2$, $\eta = 3$). The system is stable. Case (+ + +).

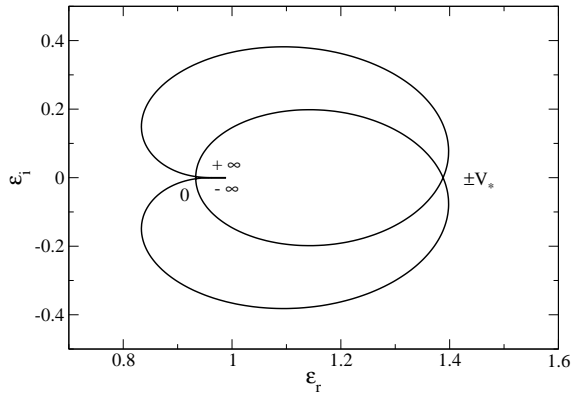


Fig. 50. Nyquist curve for $a > a_m$ and $\eta > 1/a^2$ (specifically $a = 1.4$, $\eta = 1$). The system is stable. Case (+ + +).

For $\eta = \eta_c^{(0)(1)}$ and $\eta = \eta_c^{(0)(2)}$, the DF has a minimum at $V_0 = 0$ and two maxima at $\pm V_*$. The marginal perturbation has zero pulsation $\Omega_r = 0$. By considering the Nyquist curves in this region (see Figs. 51-54), we find that the distribution is stable for $\eta < \eta_c^{(0)(1)}$, unstable for $\eta_c^{(0)(1)} < \eta < \eta_c^{(0)(2)}$ and stable again for $\eta > \eta_c^{(0)(2)}$. This corresponds to a re-entrant phase.

7.3 The asymmetric double-humped distribution

The dielectric function associated to the asymmetric double-humped distribution (93) in the repulsive case is

$$\epsilon(\Omega) = 1 + \frac{\eta}{1 + \Delta} [W(\sqrt{\eta}(\Omega - a)) + \Delta W(\sqrt{\eta}(\Omega + a))]. \quad (144)$$

Proceeding as in Sec. 6 and introducing the parameters $x = V_0/a$ and $y = \eta a^2$, we find that the equations determining the critical temperatures $\eta_c(a)$ are given by

$$y = \frac{1}{2x} \ln \left(\frac{1+x}{1-x} \right) + \frac{\ln(\Delta)}{2x}, \quad (145)$$

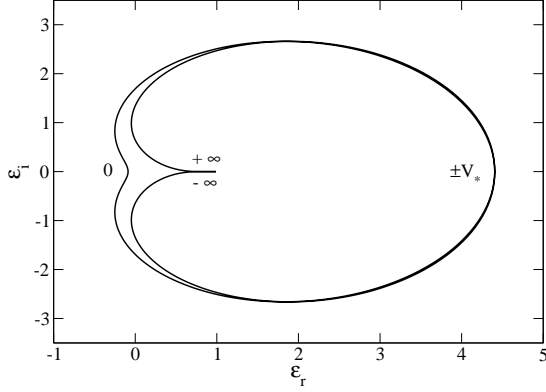


Fig. 53. Nyquist curve for $1 < a < a_m$ and $1/a^2 < \eta_c^{(0)(1)}(a) < \eta < \eta_c^{(0)(2)}(a)$ (specifically $a = 1.2$, $\eta = 7$). The system is unstable. Case $(+ - +)$.

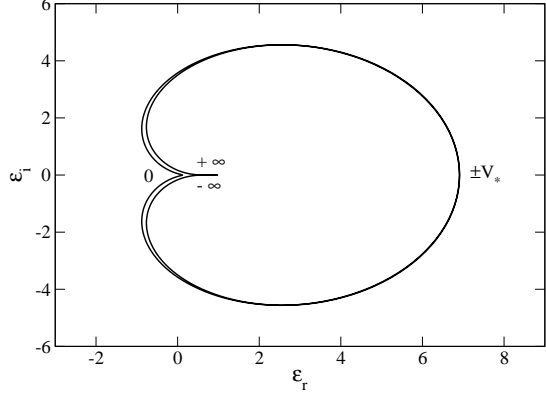


Fig. 54. Nyquist curve for $1 < a < a_m$ and $\eta > \eta_c^{(0)(2)}(a) > 1/a^2$ (specifically $a = 1.2$, $\eta = 12$). The system is stable. Case $(+ + +)$.

$$\eta = -\frac{1 + \Delta}{[W_r(\sqrt{y}(x-1)) + \Delta W_r(\sqrt{y}(x+1))]} \quad (146)$$

$$a^2 = \frac{y}{\eta} \quad (147)$$

Equations (145) and (147) determine the extrema of the distribution and Eq. (146) determines the temperatures corresponding to the modes of marginal stability. As in Sec. 6, the curve $\eta_c(a)$ can be obtained by varying x between -1 and $+1$. In the repulsive case, there exists physical solutions with positive temperature only for $0 < x \leq x_c$. For $\Delta < \Delta_*$, we get only one marginal branch $\eta_c^{(p)}(a)$ corresponding to the mode $\Omega_r = V_p > 0$ (see Fig. 55). For $\Delta > \Delta_*$, we get two marginal branches $\eta_c^{(p)}(a)$ and $\eta_c^{(+)}(a)$ corresponding to the modes $\Omega_r = V_p > 0$ and $\Omega_r = V_+ > 0$ (see Fig. 56). They connect each other at (a_*, η_*) corresponding to $x = x_*$. At that point they touch the hyperbole $\eta = y_*/a^2$ separating distributions with one or two maxima.

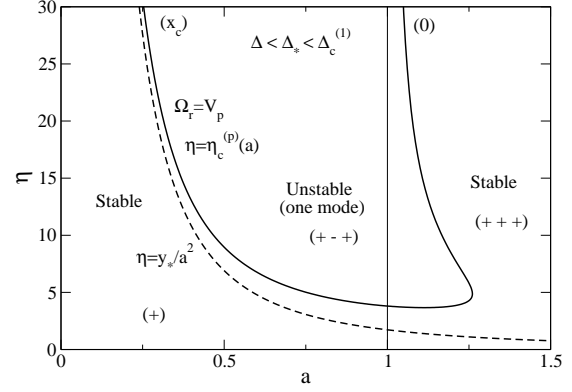


Fig. 55. Stability diagram for the asymmetric double-humped distribution with $\Delta < \Delta_* < \Delta_c^{(1)}$ (specifically $\Delta = 2$). We have also plotted the hyperbole $\eta = y_*/a^2$. Below this curve, the distribution has a single maximum at $V_p > 0$ and above this curve, the distribution has a global maximum at $V_0 = V_- < 0$, a local maximum at $V_0 = V_+ > 0$ and a minimum at $V_p > 0$. Since $\Delta < \Delta_*$, there exists only one marginal branch $\eta_c^{(p)}$ which is always strictly above the hyperbole $\eta = y_*/a^2$.

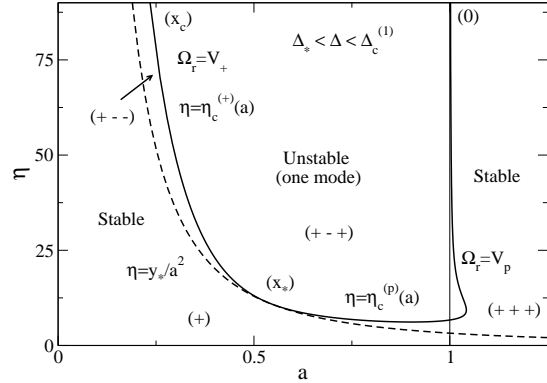


Fig. 56. Stability diagram for the asymmetric double-humped distribution with $\Delta_* < \Delta < \Delta_c^{(1)}$ (specifically $\Delta = 20$). Since $\Delta > \Delta_*$, there exists two marginal branches $\eta_c^{(p)}$ and $\eta_c^{(+)}$ that connect each other at the point of contact with the hyperbole $\eta = y_*/a^2$.

For $x \rightarrow 0^+$, using Eq. (213), we find that $a \rightarrow 1$. Then, proceeding carefully, we get

$$\eta_c^{(p)}(a) \sim \left(\frac{3}{2} + \frac{1 - \Delta \ln \Delta}{1 + \Delta} \frac{1}{2} \right) \frac{1}{a - 1}, \quad (a \rightarrow 1). \quad (148)$$

For $x \rightarrow x_c$, we find that $a \rightarrow 0$ and

$$\eta_c^{(p)}(a) \sim \frac{y_c}{a^2}, \quad (a \rightarrow 0). \quad (149)$$

The stability diagrams corresponding to the asymmetric double-humped distribution with $\Delta = 2$ and $\Delta = 20$ are represented in Figs. 55 and 56. In continuity with the symmetric case $\Delta = 1$, they display a re-entrant phase. Some representative Nyquist curves are represented in Figs. 57-59. In Fig. 60, we determine how the stability

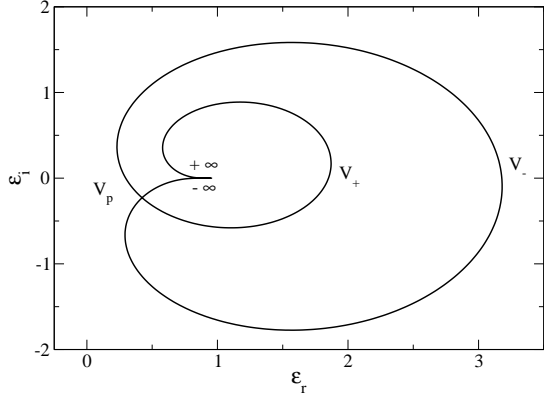


Fig. 57. For $\Delta < \Delta_* < \Delta_c^{(1)}$: Nyquist curve for $y_*/a^2 < \eta < \eta_c^{(p)}(a)$ (specifically $\Delta = 2$, $a = 0.9$ and $\eta = 3.5$). The system is stable. Case (+++).

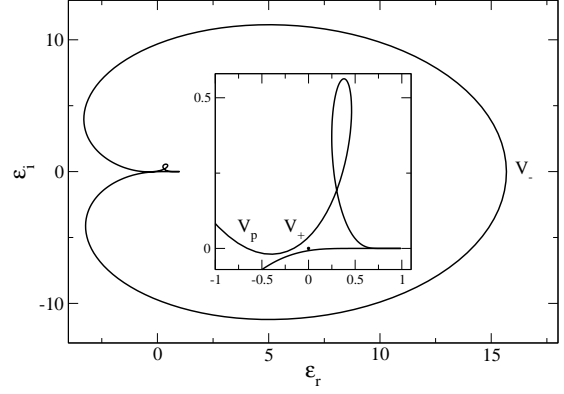


Fig. 59. For $\Delta_* < \Delta < \Delta_c^{(1)}$: Nyquist curve for $y_*/a^2 < \eta < \eta_c^{(+)}(a)$ (specifically $\Delta = 20$, $a = 0.46$ and $\eta = 15.5$). The system is stable. Case (+--).

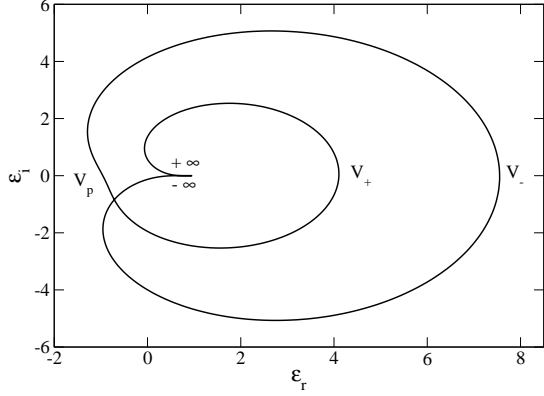


Fig. 58. For $\Delta < \Delta_* < \Delta_c^{(1)}$: Nyquist curve for $y_*/a^2 < \eta_c^{(p)}(a) < \eta$ (specifically $\Delta = 2$, $a = 0.9$ and $\eta = 10$). The system is unstable. Case (+-+).

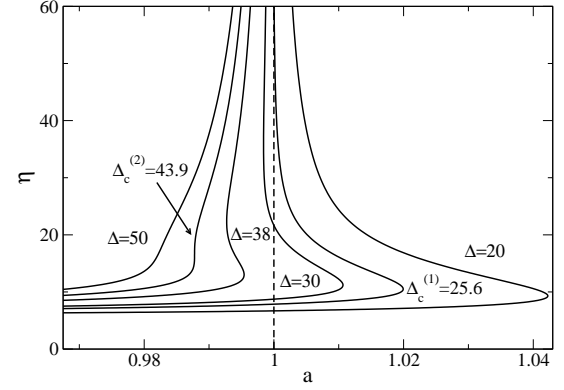


Fig. 60. Stability diagram for different values of the asymmetry Δ showing the appearance of a double re-entrant phase at $\Delta_c^{(1)} = 25.6$ and their disappearance above $\Delta_c^{(2)} = 43.9$.

diagram changes with the asymmetry Δ . We find that a double re-entrant phase appears for $\Delta_c^{(1)} = 25.6$ and that they both disappear above $\Delta_c^{(2)} = 43.9$. In fact, the critical value $\Delta_c^{(1)}$ corresponds to the case where the asymptote passes from $a = 1^+$ to $a = 1^-$. Therefore, it corresponds to the vanishing of the term in parenthesis in Eq. (148). A numerical solution of $3 + \ln \Delta(1 - \Delta)/(1 + \Delta) = 0$ then gives $\Delta_c^{(1)} = 25.6268\dots$

8 General results for an arbitrary potential of interaction

In this section, we show that the previous results obtained for the attractive or repulsive HMF models can have applications for more general potentials of interaction. We also make the connexion between linear and formal nonlinear stability, and between dynamical stability with respect to the the Euler and Vlasov equations.

8.1 Linear stability for the barotropic Euler equation

We consider the dynamics of a gas governed by the Euler equations

$$\frac{\partial \rho}{\partial t} + \nabla \cdot (\rho \mathbf{u}) = 0, \quad (150)$$

$$\rho \left[\frac{\partial \mathbf{u}}{\partial t} + (\mathbf{u} \cdot \nabla) \mathbf{u} \right] = -\nabla p - \rho \nabla \Phi, \quad (151)$$

$$\Phi(\mathbf{r}, t) = \int u(|\mathbf{r} - \mathbf{r}'|) \rho(\mathbf{r}', t) d\mathbf{r}', \quad (152)$$

where $u(|\mathbf{r} - \mathbf{r}'|)$ is an arbitrary binary potential of interaction. We assume that the gas is described by a barotropic equation of state $p = p(\rho)$. Clearly, a spatially homogeneous distribution $\rho = \Phi = \text{Cst.}$ with $\mathbf{u} = \mathbf{0}$ is a stationary solution of Eq. (150)-(152) provided that $\Phi = \rho U$ with $U = \int u(\mathbf{x}) d\mathbf{x}$ (for the gravitational potential, this last condition is not realized and we have to make the Jeans

swindle [21]). We want to investigate the linear dynamical stability of this spatially homogeneous distribution. Linearizing the Euler equations (150)-(152) around this steady state and decomposing the perturbations in normal modes $\delta\rho_{\mathbf{k}\omega} \sim \delta\Phi_{\mathbf{k}\omega} \sim \delta\mathbf{u}_{\mathbf{k}\omega} \sim e^{i(\mathbf{k}\cdot\mathbf{r}-\omega t)}$ we obtain the dispersion relation [29]:

$$\omega^2 = c_s^2 k^2 + (2\pi)^d \hat{u}(k) k^2 \rho, \quad (153)$$

where we have introduced the velocity of sound $c_s^2 = p'(\rho)$. We note that the pulsation ω is either real ($\omega^2 > 0$) or purely imaginary ($\omega^2 < 0$). As a result, the system is linearly stable with respect to a perturbation with wavenumber k if

$$c_s^2 + (2\pi)^d \hat{u}(k) \rho > 0, \quad (154)$$

and linearly unstable otherwise (when $\omega^2 < 0$, the mode $\omega = +i\sqrt{-\omega^2}$ grows exponentially rapidly).

For repulsive potentials satisfying $\hat{u}(k) > 0$, the homogeneous distribution is always stable. For Coulombian plasmas in $d = 3$, using Eq. (240), the dispersion relation can be written [72]:

$$\omega^2 = \omega_p^2 + c_s^2 k^2, \quad (155)$$

where ω_p is the plasma pulsation Eq. (241). For the repulsive HMF model, using $\hat{u}_n = \frac{k}{4\pi} \delta_{n,\pm 1}$, the dispersion relation is [29]:

$$\omega^2 = c_s^2 n^2 + \frac{kM}{4\pi} n^2 \delta_{n,\pm 1}. \quad (156)$$

The modes $n \neq \pm 1$ oscillate with a pulsation $\omega = \pm c_s n$. The pulsation of the modes $n = \pm 1$ is $\omega^2 = \omega_p^2 + c_s^2$ where ω_p is the proper pulsation (251).

For attractive potentials satisfying $\hat{u}(k) < 0$, the homogeneous distribution is linearly stable if

$$c_s^2 > (c_s^2)_{crit} \equiv (2\pi)^d \rho |\hat{u}(k)|_{max}, \quad (157)$$

and linearly unstable if $c_s^2 < (c_s^2)_{crit}$. In this last case, the unstable wavelengths are determined by the converse of inequality (154). For the gravitational interaction in $d = 3$, using Eq. (246), the dispersion relation can be written [21]:

$$\omega^2 = c_s^2 k^2 - 4\pi G \rho. \quad (158)$$

The system is always unstable ($(c_s^2)_{crit} = \infty$) for sufficiently small wavenumbers

$$k < k_J \equiv \left(\frac{4\pi G \rho}{c_s^2} \right)^{1/2}, \quad (159)$$

where k_J is the Jeans wavenumber for a barotropic gas. The growth rate is maximum for $k \rightarrow 0$. For the attractive HMF model, using $\hat{u}_n = -\frac{k}{4\pi} \delta_{n,\pm 1}$, the dispersion relation is [29]:

$$\omega^2 = c_s^2 n^2 - \frac{kM}{4\pi} n^2 \delta_{n,\pm 1}. \quad (160)$$

The modes $n \neq \pm 1$ oscillate with a pulsation $\omega = \pm c_s n$. The complex pulsation of the modes $n = \pm 1$ is $\omega^2 = c_s^2 - \frac{kM}{4\pi}$. The system is stable for $c_s^2 > \frac{kM}{4\pi}$ and unstable for $c_s^2 < \frac{kM}{4\pi}$.

8.2 Formal stability for the barotropic Euler equation

The barotropic Euler equation conserve the mass $M = \int \rho d\mathbf{r}$ and the energy functional [21]:

$$\mathcal{W}[\rho, \mathbf{u}] = \int \rho \int^\rho \frac{p(\rho')}{\rho'^2} d\rho' d\mathbf{r} + \frac{1}{2} \int \rho \Phi d\mathbf{r} + \int \rho \frac{\mathbf{u}^2}{2} d\mathbf{r}. \quad (161)$$

Therefore, a minimum of the energy functional at fixed mass determines a steady state of the Euler equation that is nonlinearly dynamically stable¹⁴. The qualitative idea is the following. If the system is an energy minimum, and since the energy is conserved by the Euler equation, then it cannot evolve away from that point. Therefore, it is dynamically stable. Alternatively, if the flow is a saddle point of energy, then it can evolve away from that point by following an iso-energy line. In that case, it is not dynamically stable. Here, we have stability in the sense of Lyapunov. This means that the size of the perturbation is bounded by the size of the initial perturbation for all times. We are led therefore to considering the minimization problem

$$\min_{\rho, \mathbf{u}} \{ \mathcal{W}[\rho, \mathbf{u}] \mid M[\rho] = M \}. \quad (162)$$

In this paper we shall consider *small* perturbations and determine conditions under which the system is a local minimum of energy ($\delta\mathcal{W} = 0$ and $\delta^2\mathcal{W}$ positive definite). Thus, we restrict ourselves to formal nonlinear stability [73]. Since $\delta^2\mathcal{W}$ provides a norm preserved by the linearized equations, formal stability implies linear stability (which in turn implies spectral stability). However, for infinite dimensional systems, formal nonlinear stability need not imply nonlinear stability.

The critical points of energy at fixed mass are given by $\delta\mathcal{W} - \mu\delta M = 0$ where μ is a Lagrange multiplier. This leads to $\mathbf{u} = \mathbf{0}$ and to the condition of hydrostatic equilibrium

$$\nabla p + \rho \nabla \Phi = \mathbf{0}. \quad (163)$$

Therefore, the critical points of energy at fixed mass are steady states of the Euler equation (150)-(152). For a barotropic gas $p = p(\rho)$, the condition of hydrostatic equilibrium (163) leads to $\rho = \rho(\Phi)$ and $p = p(\Phi)$ with $p'(\Phi) = -\rho(\Phi)$. This leads to the identity

$$p'(\rho) = -\frac{\rho}{\rho'(\Phi)}. \quad (164)$$

Since $p'(\rho) = c_s^2 > 0$, this relation implies that $\rho'(\Phi) < 0$.

A critical point of energy at fixed mass is a (local) minimum iff

$$\delta^2\mathcal{W} = \int \frac{p'(\rho)}{2\rho} (\delta\rho)^2 d\mathbf{r} + \frac{1}{2} \int \delta\rho \delta\Phi d\mathbf{r} > 0 \quad (165)$$

¹⁴ In astrophysics, this is called the Chandrasekhar energy principle [21].

for all perturbations $\delta\rho$ that conserve mass. Using Eq. (164), this can be rewritten

$$\delta^2\mathcal{W} = -\frac{1}{2} \int \frac{(\delta\rho)^2}{\rho'(\Phi)} d\mathbf{r} + \frac{1}{2} \int \delta\rho\delta\Phi d\mathbf{r} > 0 \quad (166)$$

for all perturbations $\delta\rho$ that conserve mass. We are led therefore to considering the eigenvalue equation

$$p'(\rho)\delta\rho + \rho\delta\Phi = \lambda\delta\rho, \quad (167)$$

with $\delta\Phi = u * \delta\rho$, for perturbations such that $\int \delta\rho d\mathbf{r} = 0$. For these eigenmodes, we have

$$\delta^2\mathcal{W} = \frac{1}{2} \lambda \int \frac{(\delta\rho)^2}{\rho} d\mathbf{r}. \quad (168)$$

Therefore, a critical point of energy at fixed mass is a (local) minimum iff all the eigenvalues of the equation (167) are positive.

Let us specifically consider spatially homogeneous systems. Solving Eq. (167) in Fourier space and using $\delta\hat{\Phi} = (2\pi)^d \hat{u}(k) \delta\hat{\rho}$ since the integral in Eq. (152) is a convolution, we find that the eigenvalues are given by

$$\lambda(k) = c_s^2 + (2\pi)^d \hat{u}(k) \rho. \quad (169)$$

Therefore, a spatially homogeneous system is a (local) minimum of energy at fixed mass iff

$$c_s^2 + (2\pi)^d \hat{u}(k) \rho > 0, \quad \forall k. \quad (170)$$

When condition (170) is fulfilled, we conclude that the system is formally nonlinearly stable with respect to the barotropic Euler equations (150)-(152). We see that, for spatially homogeneous systems, the condition of formal stability (170) coincides with the condition of linear stability (154). On the other hand, when condition (170) is not fulfilled the system is linearly unstable according to Sec. 8.1. In conclusion, *for spatially homogeneous systems described by the barotropic Euler equation, formal nonlinear stability coincides with linear stability*¹⁵.

8.3 Linear stability for the Vlasov equation

We consider the dynamics of a kinetic system described by the Vlasov equation

$$\frac{\partial f}{\partial t} + \mathbf{v} \cdot \frac{\partial f}{\partial \mathbf{r}} - \nabla \Phi \cdot \frac{\partial f}{\partial \mathbf{v}} = 0, \quad (171)$$

$$\Phi(\mathbf{r}, t) = \int u(|\mathbf{r} - \mathbf{r}'|) \rho(\mathbf{r}', t) d\mathbf{r}', \quad (172)$$

where $u(|\mathbf{r} - \mathbf{r}'|)$ is an arbitrary binary potential of interaction. Clearly, a distribution function $f = f(\mathbf{v})$ that

¹⁵ This result may remain true for inhomogeneous systems. In particular, it is shown in [88] that the neutral modes of linear and formal stability for barotropic stars are determined by the same condition.

depends only on the velocity is a stationary solution of the Vlasov equation with $\Phi = \rho U$. We want to investigate the linear dynamical stability of this spatially homogeneous distribution. Linearizing the Vlasov equation around this steady state and using Laplace-Fourier transform (writing the perturbations in the form $\delta f_{\mathbf{k}\omega} \sim \delta\Phi_{\mathbf{k}\omega} \sim e^{i(\mathbf{k}\cdot\mathbf{r}-\omega t)}$), we obtain the dispersion relation [29]:

$$\epsilon(\mathbf{k}, \omega) \equiv 1 - (2\pi)^d \hat{u}(\mathbf{k}) \int \frac{\mathbf{k} \cdot \frac{\partial f}{\partial \mathbf{v}}}{\mathbf{k} \cdot \mathbf{v} - \omega} d\mathbf{v} = 0. \quad (173)$$

If we take the wavevector \mathbf{k} along the z -axis¹⁶, the dispersion relation becomes

$$\epsilon(k, \omega) \equiv 1 - (2\pi)^d \hat{u}(k) \int_C \frac{k \frac{\partial f}{\partial v_z}}{k v_z - \omega} dv_x dv_y dv_z = 0, \quad (174)$$

where the integral must be performed along the Landau contour C . We define $g(v_z) = \int f dv_x dv_y$. In the following, we shall note v instead of v_z and f instead of g . With these conventions, the dispersion relation (174) can be rewritten

$$\epsilon(k, \omega) \equiv 1 - (2\pi)^d \hat{u}(k) \int_C \frac{f'(v)}{v - \frac{\omega}{k}} dv = 0. \quad (175)$$

We are led therefore to a one-dimensional problem like the one investigated in the first part of this paper for the HMF model.

For $\omega_i = 0$, the real and imaginary parts of the dielectric function $\epsilon(k, \omega_r) = \epsilon_r(k, \omega_r) + i\epsilon_i(k, \omega_r)$ are given by

$$\epsilon_r(k, \omega_r) = 1 - (2\pi)^d \hat{u}(k) P \int_{-\infty}^{+\infty} \frac{f'(v)}{v - \frac{\omega_r}{k}} dv, \quad (176)$$

$$\epsilon_i(k, \omega_r) = -\pi (2\pi)^d \hat{u}(k) f' \left(\frac{\omega_r}{k} \right). \quad (177)$$

The condition of marginal stability corresponds to $\epsilon_r(k, \omega_r) = \epsilon_i(k, \omega_r) = 0$. The condition $\epsilon_i(k, \omega_r) = 0$ is equivalent to $f' \left(\frac{\omega_r}{k} \right) = 0$ so that $\omega_r/k = v_0$ is equal to a velocity where $f'(v)$ is extremum ($f'(v_0) = 0$). The condition $\epsilon_r(k, \omega_r = v_0) = 0$ then gives

$$1 - (2\pi)^d \hat{u}(k) \int_{-\infty}^{+\infty} \frac{f'(v)}{v - v_0} dv = 0. \quad (178)$$

This determines the wavenumber(s) k_c corresponding to marginal stability.

On the other hand, as a direct consequence of the Nyquist criterion, if $f(v)$ has a unique maximum at $v = v_0$, then the DF is linearly stable with respect to a perturbation with wavenumber k iff $\epsilon_r(k, \omega_r = v_0) > 0$ i.e. iff

$$1 - (2\pi)^d \hat{u}(k) \int_{-\infty}^{+\infty} \frac{f'(v)}{v - v_0} dv > 0. \quad (179)$$

¹⁶ If the distribution function is isotropic, there is no restriction in making this choice.

This stability criterion generalizes Eq. (27) to the case of an arbitrary potential of interaction. If $\hat{u}(k) > 0$ (repulsive potential), a single-humped distribution is always stable. This is the case in particular for a Coulombian plasma [72]. If $\hat{u}(k) < 0$ (attractive potential), the distribution is stable to all wavenumbers if

$$\frac{\rho}{\int_{-\infty}^{+\infty} \frac{f'(v)}{v-v_0} dv} > (2\pi)^d \rho |\hat{u}(k)|_{max}, \quad (180)$$

and unstable otherwise. In that last case, the range of unstable wavenumbers is determined by the converse of inequality (179). For the gravitational interaction in $d = 3$, the stability criterion (179) becomes

$$1 + \frac{4\pi G}{k^2} \int_{-\infty}^{+\infty} \frac{f'(v)}{v-v_0} dv > 0. \quad (181)$$

The system is always unstable for sufficiently small wavenumbers:

$$k < k_J = \left(-4\pi G \int_{-\infty}^{+\infty} \frac{f'(v)}{v-v_0} dv \right)^{1/2}, \quad (182)$$

where k_J is the Jeans wavenumber for a stellar system. We shall make the connexion between the stability of a kinetic system and the stability of the corresponding barotropic gas in the next section. In particular, using identity (204), we will show that Eqs. (179) and (180) are equivalent to Eqs. (154) and (157).

8.4 Formal stability for the Vlasov equation

The Vlasov equation conserves the mass $M = \int f d\mathbf{r}d\mathbf{v}$, the energy $E = \int f \frac{v^2}{2} d\mathbf{r}d\mathbf{v} + \frac{1}{2} \int \rho \Phi d\mathbf{r}$ and the Casimirs $I_h = \int h(f) d\mathbf{r}d\mathbf{v}$ where h is an arbitrary continuous function. Let us introduce the functionals $S = -\int C(f) d\mathbf{r}d\mathbf{v}$ where C is an arbitrary convex function ($C'' > 0$). They will be called ‘‘pseudo entropies’’. We also introduce the ‘‘pseudo free energies’’ $J = S - \beta E$ or $F = E - TS$ and the ‘‘pseudo grand potential’’ $G = S - \beta E - \alpha M$ where $\beta = 1/T$ and α are some constants. Since E , M , I_h , S , J , F and G are conserved by the Vlasov equation, the following optimization principles¹⁷

$$\min_f \{E[f] \mid \text{all the Casimirs } I_h\}, \quad (183)$$

$$\min_f \{E[f] \mid M[f] = M, \quad S[f] = S\}, \quad (184)$$

$$\max_f \{S[f] \mid M[f] = M, \quad E[f] = E\}, \quad (185)$$

$$\max_f \{J[f] \mid M[f] = M\}, \quad (186)$$

¹⁷ A review of these variational principles will be given in a forthcoming paper.

$$\min_f \{F[f] \mid M[f] = M\}, \quad (187)$$

$$\max_f \{G[f]\}, \quad (188)$$

determine steady states of the Vlasov equation that are nonlinearly dynamically stable. The first criterion is the most refined stability criterion that has been introduced in the literature¹⁸. The other criteria provide only *sufficient* conditions of dynamical stability. Since the solution of an optimization problem is always the solution of a more constrained optimization problem, we have the relations

$$(188) \Rightarrow (187) \Leftrightarrow (186) \Rightarrow (185) \Leftrightarrow (184) \Rightarrow (183). \quad (189)$$

We note that (185) is similar to a condition of microcanonical (two constraints) stability, (186) or (187) is similar to a condition of canonical (one constraint) stability, and (188) is similar to a condition of grand canonical (no constraint) stability¹⁹ in thermodynamics [15,88]. Therefore, the inclusion $(188) \Rightarrow (187) \Leftrightarrow (186) \Rightarrow (185)$ is similar to the fact that ‘‘grand canonical stability implies canonical stability which implies microcanonical stability’’ in thermodynamics. However, the reciprocal is wrong in case of ‘‘ensemble inequivalence’’ that is generic for systems with long-range interactions [12,17,18]. In the following, we shall mainly be interested by formal dynamical stability [73]. We shall consider small perturbations and determine under which conditions the first variations of the functional vanish (critical point) and the second variations are positive definite (for problems (183), (184) and (187)) or negative definite (for problems (185), (186) and (188)).

Critical points: considering problem (183), we find that a DF is a critical point of energy for symplectic perturbations (i.e perturbations that conserve all the Casimirs) iff $f(\mathbf{r}, \mathbf{v})$ is a steady state of the Vlasov equation [76,77]. On the other hand, the critical points of problems (184)-(188) lead to DF of the form $f = f(\epsilon)$ with $f'(\epsilon) < 0$, i.e. the DF depends only on the individual energy $\epsilon = v^2/2 + \Phi(\mathbf{r})$ and is monotonically decreasing [88].

Formal stability: considering problem (183), a critical point of energy for symplectic perturbations is a (local) minimum iff

$$-\int \frac{(\delta f)^2}{f'(\epsilon)} d\mathbf{r}d\mathbf{v} + \int \delta f \delta \Phi d\mathbf{r}d\mathbf{v} > 0, \quad (190)$$

for all perturbations δf that conserve the energy and all the Casimirs at first order $\delta E = \delta I_h = 0$. Considering problems (184) and (185), a critical point of energy (resp.

¹⁸ In astrophysics, this is called the Antonov energy principle [21]. Recently, developing these arguments, Lemou *et al.* [78] have proven for the first time that all DF $f = f(\epsilon)$ with $f'(\epsilon) < 0$ are *nonlinearly* stable with respect to the Vlasov-Poisson system.

¹⁹ We could also introduce a grand microcanonical ensemble corresponding to the maximization of $K = S - \alpha M$ at fixed energy [15].

pseudo entropy) at fixed mass and pseudo entropy (resp. energy) is a (local) minimum (resp. maximum) iff inequality (190) is satisfied all perturbations δf that conserve mass and energy at first order $\delta M = \delta E = 0$. Considering problems (186) and (187), a critical point of pseudo free energy J (resp. pseudo free energy F) at fixed mass is a (local) maximum (resp. minimum) if inequality (190) is satisfied for all perturbations δf that conserve mass $\delta M = 0$. Considering problem (188), a critical point of pseudo grand potential G is a (local) maximum if inequality (190) is satisfied for all perturbations. Problem (183) is the most refined stability criterion because it tells that, in order to settle the dynamical stability of the system, we just need considering symplectic (i.e. dynamically accessible) perturbations. Of course, if inequality (190) is satisfied by a larger class of perturbations, as implied by problems (184)-(188), the system will be stable a fortiori. Therefore, we have the implications (189). Problems (184)-(188) provide sufficient (but not necessary) conditions of dynamical stability. A steady state can be stable according to (183) while it does not satisfy (184)-(185), or it can be stable according to (184)-(185) while it does not satisfy (186)-(187), or it can be stable according to (186)-(187) while it does not satisfy (188). Therefore, the stability criterion (183) is more refined than (184)-(185) which is itself more refined than (186)-(187) which is itself more refined than (188).

Let us consider the minimization problem

$$\min_f \{F[f] \mid M[f] = M\}, \quad (191)$$

in more detail. As we have seen, it provides a sufficient condition of dynamical stability for the Vlasov equation. The critical points of pseudo free energy F at fixed mass M are given by

$$\delta F + \alpha T \delta M = 0, \quad (192)$$

where α is a Lagrange multiplier. This yields

$$C'(f) = -\beta\epsilon - \alpha. \quad (193)$$

Since C is convex this relation can be reversed to give

$$f = F(\beta\epsilon + \alpha), \quad (194)$$

where $F(x) = (C')^{-1}(-x)$. Differentiating Eq. (193), we obtain

$$C''(f) = -\frac{\beta}{f'(\epsilon)}, \quad (195)$$

so that $f'(\epsilon)$ is monotonic. We shall assume that $f'(\epsilon) < 0$ so that the pseudo temperature T is positive. A critical point of pseudo free energy at fixed mass is a (local) minimum iff

$$\delta^2 F = \frac{T}{2} \int C''(f) (\delta f)^2 d\mathbf{r} d\mathbf{v} + \frac{1}{2} \int \delta\rho \delta\Phi d\mathbf{r} > 0 \quad (196)$$

for all perturbations that conserve mass. Using Eq. (195), this can be rewritten

$$\delta^2 F = -\frac{1}{2} \int \frac{(\delta f)^2}{f'(\epsilon)} d\mathbf{r} d\mathbf{v} + \frac{1}{2} \int \delta\rho \delta\Phi d\mathbf{r} > 0 \quad (197)$$

for all perturbations that conserve mass.

For any distribution $f = f(\mathbf{r}, \mathbf{v})$, the density and the pressure are given by $\rho = \int f d\mathbf{v}$ and $p = \frac{1}{d} \int f v^2 d\mathbf{v}$. If $f = f(\epsilon)$, we have $\rho = \rho(\Phi)$ and $p = p(\Phi)$. Eliminating $\Phi(\mathbf{r})$ between these expressions we find that the pressure is a function of the density: $p = p(\rho)$. Therefore, to any kinetic system described by a distribution function $f = f(\epsilon)$, we can associate a barotropic gas with an equation of state $p(\rho)$ that is entirely specified by the function $C(f)$. We now introduce the functional

$$F[\rho] = \int \rho \int^\rho \frac{p(\rho')}{\rho'^2} d\rho' d\mathbf{r} + \frac{1}{2} \int \rho \Phi d\mathbf{r}, \quad (198)$$

and consider the minimization problem

$$\min_\rho \{F[\rho] \mid M[\rho] = M\}. \quad (199)$$

It can be shown [88,69] that

$$(191) \Leftrightarrow (199). \quad (200)$$

Therefore, f is a minimum of $F[f]$ at fixed mass iff ρ is a minimum of $F[\rho]$ at fixed mass. As a result, (199) provides a sufficient condition of nonlinear dynamical stability for the Vlasov equation. However, it is not a necessary condition of nonlinear dynamical stability. For example, a DF can be nonlinearly stable according to (183) or (185) although it does not satisfy (191) or (199). This is similar to “ensemble inequivalence” in thermodynamics [12,17,18].

It is also obvious that

$$(162) \Leftrightarrow (199). \quad (201)$$

Therefore, if ρ is nonlinearly stable with respect to the Euler equation then it solves (162) and (199). According to (200), the corresponding distribution function f solves (191) so it is nonlinearly stable with respect to the Vlasov equation. Therefore, *a distribution function $f = f(\epsilon)$ with $f'(\epsilon) < 0$ is nonlinearly stable with respect to the Vlasov equation if the corresponding density profile ρ is nonlinearly stable with respect to the Euler equation*. In astrophysics, this corresponds to the (nonlinear) Antonov first law: “a stellar system $f = f(\epsilon)$ with $f'(\epsilon) < 0$ is (nonlinearly) stable with respect to the Vlasov equation if the corresponding barotropic star with an equation of state $p = p(\rho)$ is (nonlinearly) stable with respect to the Euler equations”. However, the reciprocal is wrong in general. The distribution function f can be nonlinearly stable according to (183) or (185) although it does not satisfy (191) so that the density profile ρ does not satisfy (199) or (162). We see therefore that the nonlinear Antonov first law is similar to the notion of “ensemble inequivalence” in thermodynamics [88].

According to the previous discussion, f is a minimum of $F[f]$ at fixed mass iff ρ is a minimum of $F[\rho]$ or $\mathcal{W}[\rho, \mathbf{u}]$ at fixed mass. We can therefore use the results of Sec. 8.2. In particular, for a spatially homogeneous system, the distribution $f(\mathbf{v})$ is a (local) minimum of $F[f]$ at fixed mass iff

$$c_s^2 + (2\pi)^d \hat{u}(k) \rho > 0, \quad \forall k, \quad (202)$$

where $c_s^2 = p'(\rho)$ is the velocity of sound in the corresponding barotropic gas. Now, using Eq. (164) and the fact that $\rho = \int f(\epsilon) d\mathbf{v}$, we have for any distribution $f = f(\epsilon)$:

$$c_s^2(\mathbf{r}) = -\frac{\rho(\mathbf{r})}{\int f'(\epsilon) d\mathbf{v}} = -\frac{\rho(\mathbf{r})}{\int \frac{\partial f}{\partial v_z} d\mathbf{v}} = -\frac{\rho(\mathbf{r})}{\int_{-\infty}^{+\infty} \frac{\partial g}{\partial v_z} dv_z}, \quad (203)$$

where $g(v_z) = \int f(\mathbf{v}) dv_x dv_y$. For a spatially homogeneous system, we obtain

$$c_s^2 = -\frac{\rho}{\int_{-\infty}^{+\infty} \frac{f'(v)}{v} dv}, \quad (204)$$

where we have noted v for v_z and f for g like in Sec. 8.3. Substituting this relation in Eq. (202), we find that a homogeneous distribution is a (local) minimum of F at fixed mass iff

$$1 - (2\pi)^d \hat{u}(k) \int_{-\infty}^{+\infty} \frac{f'(v)}{v} dv > 0, \quad \forall k. \quad (205)$$

When condition (205) is fulfilled, we conclude that the system is formally nonlinearly stable with respect to the Vlasov equation [according to criterion (187)]. We see that, for spatially homogeneous systems, the condition of formal stability (205) coincides with the condition of linear stability (179)²⁰. When condition (205) is not fulfilled the system is linearly unstable according to Sec. 8.3. Therefore, for homogeneous systems, criterion (187) is a sufficient and necessary condition of dynamical stability (in that case, we have ensemble equivalence). In conclusion, *for spatially homogeneous systems described by the Vlasov equations, formal nonlinear stability coincides with linear stability*. On the other hand, Eq. (204) shows that the integral appearing in Eqs. (205) and (179) is directly related to the sound velocity in the corresponding barotropic gas²¹. This implies that the condition of (linear and formal) dynamical stability for the Vlasov equation coincide with the condition of (linear and formal) dynamical stability for the Euler equation. In conclusion, *a spatially homogeneous system is dynamically stable with respect to the Vlasov equation iff the corresponding barotropic gas is dynamically stable with respect to the Euler equations*. This is the proper formulation of the Antonov first law for homogeneous systems. In that case, we have ‘‘ensemble equivalence’’. This is not true in general for spatially inhomogeneous systems.

Remark: we have obtained the condition of formal stability (205) by a method different from the one developed by Yamaguchi *et al.* [32]. Our result is more general

²⁰ Since $f = f(\epsilon)$ with $f'(\epsilon) < 0$ where $\epsilon = v^2/2 + \Phi(\mathbf{r})$, we deduce that, for a spatially homogeneous system ($\Phi = \text{cst.}$), $f(v)$ is a symmetric function with a single maximum at $v_0 = 0$. Therefore, Eq. (179) reduces to Eq. (205).

²¹ This is true for any distribution function, not only for the Maxwell and Tsallis distributions. However, the relation (204) can be checked explicitly for these simple distributions [29].

because it is valid for an arbitrary potential of interaction. Our method exploits the link between the variational problems acting on the distribution function f and those acting on the spatial density ρ . We have used the fact that a distribution function f is stable with respect to the Vlasov equation if the corresponding density profile ρ is stable with respect to the Euler equation. This is similar to the Antonov first law in astrophysics and this is related to a notion of ensemble inequivalence in thermodynamics (for spatially homogeneous systems, we have ensemble equivalence). As a by-product, our approach gives a physical interpretation of the stability criterion (205) in terms of a condition on the velocity of sound (202) in the corresponding barotropic gas. Furthermore, our method can be extended to spatially inhomogeneous systems (see Appendix F). Indeed, if all the eigenvalues λ of the eigenvalue equation (167) are positive, then ρ is formally stable with respect to the Euler equation, implying by (201) and (200) that the corresponding distribution f is formally stable with respect to the Vlasov equation.

9 Conclusion

In this paper, we have carried out an exhaustive study of the dynamical stability of systems with long-range interactions described by the Vlasov equation. For illustration, we have considered the HMF model and we have treated the case of single-humped (Maxwell, Tsallis,...) as well as double-humped (symmetric and asymmetric) distributions. The stability of the system has been investigated by using the Nyquist method. Interestingly, the stability diagrams of these systems are very rich, exhibiting re-entrant phases in the case of double-humped distributions. For the HMF model, the potential of interaction is truncated to one Fourier mode so that only the modes $n = \pm 1$ can propagate. As a result, the stability of the system is expressed as a condition on the temperature T while for other systems (plasmas, gravitational systems,...) it is expressed as a condition on the wavenumber k (for a given value of the temperature T). On the other hand, for the HMF model, we can consider attractive as well as repulsive interactions and there exists spatially homogeneous distributions in each case allowing the application of the Nyquist method. Therefore, by changing the sign of the interaction, this simple toy model exhibits features similar to Coulombian or gravitational plasmas. Noticably, this is the first time that the Nyquist method is applied to a system with *attractive* interactions without making any (Jeans) swindle. Finally, we have shown that the results and methods developed for the HMF model are in fact applicable to more general potentials of interaction giving further interest to our study. This opens the way to many numerical and/or analytical investigations that will be considered in future works.

A The function $W_r(z)$

Let us study the function

$$W_r(z) = 1 - ze^{-\frac{z^2}{2}} \int_0^z e^{\frac{x^2}{2}} dx, \quad (206)$$

for z real. We clearly have

$$W_r(-z) = W_r(z), \quad (207)$$

so we can restrict ourselves to $z \geq 0$. This function is plotted in Fig. 61. It starts from 1 for $z = 0$, crosses the x -axis for $z = z_c = 1.307$, achieves a minimum value -0.2847 for $z = 2.124$ and tends to 0 for $z \rightarrow +\infty$. In order to determine its asymptotic behavior, let us consider the integral

$$I = \int_0^z e^{\frac{x^2}{2}} dx. \quad (208)$$

It can be rewritten

$$I = e^{\frac{z^2}{2}} \int_0^z e^{-\frac{z^2-x^2}{2}} dx. \quad (209)$$

With the change of variables $y = \sqrt{z^2 - x^2}$, we get

$$I = \frac{1}{z} e^{\frac{z^2}{2}} \int_0^z e^{-\frac{y^2}{2}} \frac{y}{\sqrt{1 - \frac{y^2}{z^2}}} dy. \quad (210)$$

For $z \rightarrow +\infty$, we obtain

$$I = \frac{1}{z} e^{\frac{z^2}{2}} \int_0^z dy e^{-\frac{y^2}{2}} y \left(1 + \frac{y^2}{2z^2} + \frac{3y^4}{8z^4} + \dots \right), \quad (211)$$

so that finally

$$I = \frac{1}{z} e^{\frac{z^2}{2}} \left(1 + \frac{1}{z^2} + \frac{3}{z^4} + \dots \right). \quad (212)$$

Therefore, we get

$$W_r(z) = -\frac{1}{z^2} - \frac{3}{z^4} - \dots, \quad (z \rightarrow +\infty). \quad (213)$$

On the other hand, for $z \rightarrow 0$, we have

$$W_r(z) = 1 - z^2 - \dots, \quad (z \rightarrow 0). \quad (214)$$

B The Tsallis and Cauchy distributions

The Tsallis distributions are usually written in the form [83]:

$$f = C_q \left[1 - (q-1) \frac{v^2}{2\theta} \right]_+^{\frac{1}{q-1}}, \quad (215)$$

where C_q is a normalization constant (see below). The parameter $\theta > 0$ has the dimension of a temperature but it is *not* the kinetic temperature $T = \langle v^2 \rangle$. To arrive at

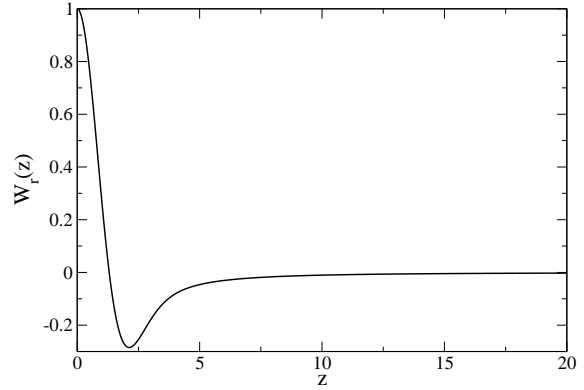


Fig. 61. The function $W_r(z)$ for z real.

the form (47), we can either follow the steps described in [29,83] or directly proceed as follows. First, we introduce notations similar to those used in astrophysics [21] and define the polytropic index n through the relation $1/(q-1) = n - 1/2$. Equation (215) can then be rewritten

$$f = A_n \frac{\rho}{\sqrt{2\pi\theta}} \left[1 - \frac{1}{n - \frac{1}{2}} \frac{v^2}{2\theta} \right]_+^{n-1/2}. \quad (216)$$

This distribution is normalizable provided that $n > 1/2$ or $n < 0$. Using $\rho = \int f dv$, we get

$$A_n = \frac{\Gamma(n+1)}{\Gamma(n+1/2)(n-1/2)^{1/2}}, \quad n > \frac{1}{2}, \quad (217)$$

$$A_n = \frac{\Gamma(1/2-n)}{\Gamma(-n)[-(n-1/2)]^{1/2}}, \quad n < 0. \quad (218)$$

According to criterion (28), the Tsallis distributions (216) are linearly stable with respect to the Vlasov equation iff

$$\theta \geq \theta_c \equiv \frac{n}{n-1/2} \frac{kM}{4\pi}. \quad (219)$$

On the other hand, the kinetic temperature (variance) $T = \langle v^2 \rangle$ exists if $n > 1/2$ or $n < -1$. In that case, we have

$$T = \frac{n-1/2}{n+1} \theta. \quad (220)$$

Substituting this relation in Eq. (216) yields expression (47) of the distribution function where T has a clear physical meaning as being the kinetic temperature (or the velocity dispersion).

The Tsallis distributions with index $-1 < n < 0$ have not been considered in Sec. 4 because they have infinite kinetic energy $K = N \langle v^2 \rangle / 2$, so they are not physical. Yet, they can be studied at a mathematical level. For these distributions, the stability criterion is given by Eq. (219) and the Nyquist curves are similar to those reported in Sec. 4 for $n < -1$. Of particular interest is the Cauchy distribution corresponding to $n = -1/2$. The Cauchy distribution is

$$f = \frac{1}{\pi} \frac{\rho}{\sqrt{2\theta}} \frac{1}{1 + \frac{v^2}{2\theta}}, \quad (221)$$

and the corresponding dielectric function (9) can be written

$$\epsilon(\omega) = 1 - \frac{kM}{4\pi^2\theta} \int_C \frac{x}{(1+x^2)^2(x - \frac{\omega}{\sqrt{2\theta}})} dx. \quad (222)$$

The integral can be computed analytically by completing the domain of integration by a large semi-circle in the lower-half plane of the complex plane and using the Cauchy residue theorem for a function with a pole of order 2 at $x = -i$. This yields

$$\epsilon(\omega) = 1 + \frac{kM}{8\pi\theta} \frac{1}{\left(i + \frac{\omega}{\sqrt{2\theta}}\right)^2}. \quad (223)$$

The condition $\epsilon(\omega) = 0$ gives the complex pulsations

$$\omega_{\pm} = -i\sqrt{2\theta} \left(1 \pm \sqrt{\frac{kM}{8\pi\theta}}\right). \quad (224)$$

For the attractive HMF model (see Sec. 2), the pulsations are purely imaginary. The mode ω_+ is always damped (stable). The mode ω_- is damped (stable) if $\theta > \theta_c$ while it grows exponentially with time (unstable) if $\theta < \theta_c$ with

$$\theta_c = \frac{kM}{8\pi}, \quad (225)$$

in agreement with Eq. (219). On the other hand, if we take $\omega_i = 0$, we find that

$$\epsilon_r(\omega_r) = 1 - \frac{kM}{8\pi\theta} \frac{1 - \frac{\omega_r^2}{2\theta}}{\left(1 + \frac{\omega_r^2}{2\theta}\right)^2}, \quad (226)$$

$$\epsilon_i(\omega_r) = -\frac{kM}{4\pi\theta} \frac{\frac{\omega_r}{\sqrt{2\theta}}}{\left(1 + \frac{\omega_r^2}{2\theta}\right)^2}. \quad (227)$$

The corresponding Nyquist curve is represented in Fig. 62. It is very similar to the one obtained for other values of $n < 0$ but, for the Cauchy distribution, it is obtained analytically.

The case of the repulsive HMF model (see Sec. 7) is obtained by changing $+k$ in $-k$ in the preceding relations. The condition $\epsilon(\omega) = 0$ gives the complex pulsations

$$\omega_{\pm} = \pm\sqrt{\frac{kM}{4\pi}} - i\sqrt{2\theta}. \quad (228)$$

These modes are always stable. They evolve with the (proper) pulsation $\omega_p = \pm\sqrt{kM/(4\pi)}$ (see Appendix E) independent on the temperature and they are damped at a rate $\gamma = \sqrt{2\theta}$. For $\omega_i = 0$, the real and imaginary parts of the dielectric function are given by Eqs. (226) and (227) with k replaced by $-k$. The corresponding Nyquist curve is represented in Fig. 62.

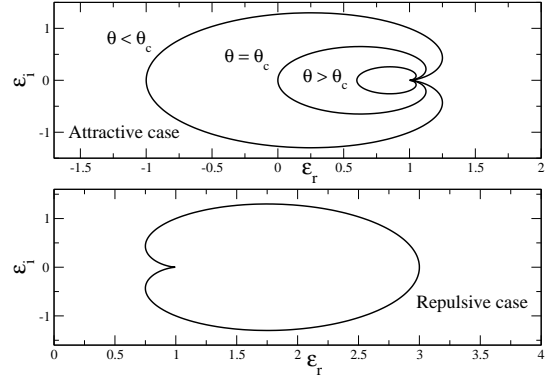


Fig. 62. Nyquist curve (analytical) for the Cauchy distribution for the attractive and repulsive HMF models.

C The function $W_r^{(n)}(z)$

Let us consider the function

$$W_r^{(n)}(z) = \frac{1}{\sqrt{2\pi}} \frac{B_n}{n} \left(n - \frac{1}{2}\right) P \int_{-\infty}^{+\infty} \frac{x \left[1 - \frac{x^2}{2(n+1)}\right]_+^{n-3/2}}{x - z} dx, \quad (229)$$

for z real and $n < -1$ or $n > 1/2$. We clearly have $W_r^{(n)}(-z) = W_r^{(n)}(z)$. For $n < -1$ and $n > 5/2$, this function is defined for any z and its derivative is continuous. For $3/2 < n \leq 5/2$, this function is defined for any z but its derivative is discontinuous at $z = \sqrt{2(n+1)}$. For $1/2 < n \leq 3/2$, this function diverges at $z = \sqrt{2(n+1)}$. This leads to the behaviors represented in Figs. 63 and 64. For $n > 3/2$, we define $\zeta_n \equiv -W_r^{(n)}(\sqrt{2(n+1)})$ or, explicitly,

$$\zeta_n = \frac{1}{\sqrt{2\pi}} \frac{B_n}{n} \left(n - \frac{1}{2}\right) \int_{-\sqrt{2(n+1)}}^{\sqrt{2(n+1)}} \frac{x \left[1 - \frac{x^2}{2(n+1)}\right]_+^{n-3/2}}{\sqrt{2(n+1)} - x} dx. \quad (230)$$

Note that the principal value is not needed in that case. Note also that $\zeta_n \geq 0$. This inequality can be obtained from Eq. (25) by taking $v_{ext} = \sqrt{2(n+1)}$ and recalling that $f(v_{ext}) = 0$. Setting $y = x/\sqrt{2(n+1)}$, Eq. (230) can be rewritten

$$\zeta_n = \frac{1}{\sqrt{2\pi}} \frac{B_n}{n} \left(n - \frac{1}{2}\right) \sqrt{2(n+1)} I_n, \quad (231)$$

with

$$I_n = \int_{-1}^{+1} y(1-y)^{n-5/2}(1+y)^{n-3/2} dy. \quad (232)$$

It turns out that this integral can be computed analytically yielding

$$I_n = \frac{1}{4} \Gamma(n-3/2) \left[\frac{4^n \Gamma(n+1/2)}{\Gamma(2n-1)} - \frac{4\sqrt{\pi}}{\Gamma(n-1)} \right]. \quad (233)$$

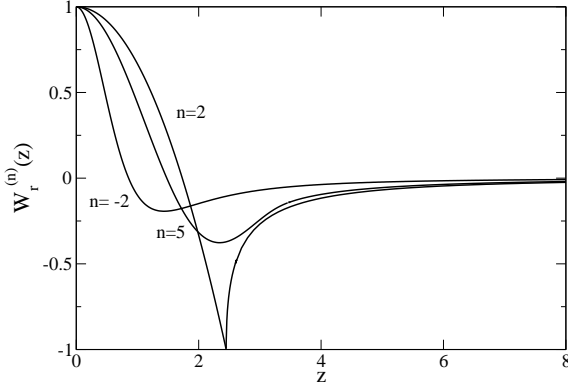


Fig. 63. The function $W_r^{(n)}(z)$ for $n < -1$ and $n > 3/2$.

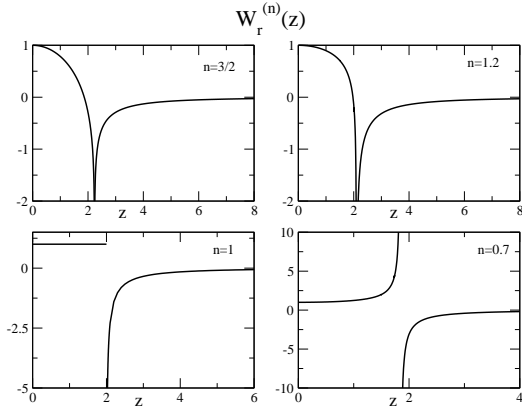


Fig. 64. The function $W_r^{(n)}(z)$ for $1/2 < n < 3/2$.

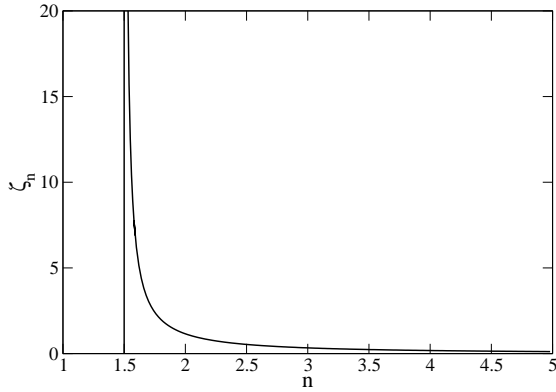


Fig. 65. The parameter $\zeta_n = -W_r^{(n)}(\sqrt{2(n+1)})$ as a function of the polytropic index $n > 3/2$.

For $n \rightarrow 3/2^+$, we have the equivalent $\zeta_n \sim 1/[2(n-3/2)]$. For $n \rightarrow +\infty$, $\zeta_n \rightarrow 0$. This parameter is plotted as a function of n in Fig. 65.

Finally, for the index $n = 3/2$, the functions (57)-(58) can be calculated analytically. For any real $z \neq \pm\sqrt{5}$, we find

$$W_r^{(3/2)}(z) = 1 + \frac{z}{2\sqrt{5}} \ln \left| \frac{\sqrt{5}-z}{\sqrt{5}+z} \right|. \quad (234)$$

On the other hand, for $z \in [-\sqrt{5}, \sqrt{5}]$, we have

$$W_i^{(3/2)}(z) = \frac{\pi}{2\sqrt{5}} z, \quad (235)$$

while $W_i^{(3/2)}(z) = 0$ otherwise. Using these results, the Nyquist curve in Fig. 9 can be obtained analytically.

Finally, for the index $n = 3/2$ and for $z = i\gamma$ where γ is a real number, the function (54) can be calculated analytically. For $\gamma > 0$, using Eq. (10), we get

$$W^{(3/2)}(i\gamma) = 1 - \frac{\gamma}{\sqrt{5}} \arctan \left(\frac{\sqrt{5}}{\gamma} \right). \quad (236)$$

For $\gamma < 0$, using Eq. (12), we get

$$W^{(3/2)}(i\gamma) = 1 - \frac{\gamma}{\sqrt{5}} \left[\arctan \left(\frac{\sqrt{5}}{\gamma} \right) + \pi \right]. \quad (237)$$

Finally, for $\gamma = 0$, using Eq. (11), we have $W^{(3/2)}(0) = 0$. Therefore, looking for a solution of the equation $\epsilon(\Omega) \equiv 1 - (\eta/\eta_c)W^{(3/2)}(\sqrt{\eta}\Omega) = 0$ of the form $\Omega = i\Omega_i$, we find that for $\eta > \eta_c = 5/3$ (unstable), the perturbation grows with a rate $\Omega_i > 0$ given by

$$1 - \frac{\eta}{\eta_c} \left[1 - \frac{\sqrt{\eta}\Omega_i}{\sqrt{5}} \arctan \left(\frac{\sqrt{5}}{\sqrt{\eta}\Omega_i} \right) \right] = 0, \quad (238)$$

while for $\eta < \eta_c = 5/3$ (stable), the perturbation is damped with a rate $\Omega_i < 0$ given by

$$1 - \frac{\eta}{\eta_c} \left[1 - \frac{\sqrt{\eta}\Omega_i}{\sqrt{5}} \left\{ \arctan \left(\frac{\sqrt{5}}{\sqrt{\eta}\Omega_i} \right) + \pi \right\} \right] = 0. \quad (239)$$

Finally, for $\eta = \eta_c = 5/3$, we recover the case of marginal stability $\Omega_i = 0$. For $\eta \rightarrow +\infty$, we recover Eq. (276) and for $\eta \rightarrow 0$, we find $\Omega_i \sim -5\sqrt{5}/(3\pi\eta^{3/2})$.

D Analogies and differences between the HMF model, Coulombian plasmas and self-gravitating systems

For Coulombian plasmas, the potential of interaction is determined by the Poisson equation $\Delta u = -4\pi(e^2/m^2)\delta(\mathbf{x})$ yielding

$$(2\pi)^3 \hat{u}(k) = \frac{4\pi e^2}{m^2 k^2} > 0. \quad (240)$$

We introduce the plasma frequency

$$\omega_p^2 \equiv \frac{4\pi\rho e^2}{m^2}, \quad (241)$$

and the Debye wavenumber

$$k_D^2 \equiv \frac{4\pi e^2 \beta \rho}{m} = \beta m \omega_p^2. \quad (242)$$

The dispersion relation (175) can be written

$$\epsilon(k, \omega) = 1 - \frac{4\pi e^2}{m^2 k^2} \int_C \frac{f'(v)}{v - \frac{\omega}{k}} dv. \quad (243)$$

Comparing this expression with Eq. (127), we make the link between Coulombian plasmas and the repulsive HMF model by setting

$$\frac{4\pi e^2}{m^2 k^2} = \frac{\tilde{k}}{2}, \quad \beta m = \tilde{\beta}, \quad \frac{\omega}{k} = \tilde{\omega}, \quad \frac{\omega_p}{k} = \tilde{\omega}_p, \quad (244)$$

where the tilde variables refer to the HMF model and the un-tilde variables to the plasmas. Then, we find that the dimensionless parameters for the plasmas are

$$\eta = \frac{k_D^2}{k^2}, \quad \Omega = \frac{\omega}{\omega_p}, \quad a = \frac{1}{\sqrt{\eta}} \sqrt{\beta m} v_a. \quad (245)$$

The results obtained in Sec. 7 for the repulsive HMF model can be applied to Coulombian plasmas provided that we interpret η as a normalized squared wavelength and Ω as a normalized pulsation according to Eq. (245). In particular, single-humped distributions are stable to all wavelengths [72] and the Nyquist curves for Maxwell and Tsallis distributions are given in Sec. 7.1.1. By contrast, the phase diagrams of the double-humped distribution (in Sec. 7.1.2) are not directly applicable to plasmas because, according to Eq. (245), the dimensionless parameter $a \propto 1/\sqrt{\eta}$ depends on k . Therefore, this is not the correct dimensionless separation. For plasmas, the correct dimensionless separation (which must be independent on the wavenumber k) is $y = \eta a^2 = \beta m v_a^2$ instead of a . Therefore, the correct stability diagram corresponds to the curve(s) $\eta_c(y)$ obtained from Eqs. (137)-(138). This will be discussed in more detail in a specific paper.

For self-gravitating systems, the potential of interaction is determined by $\Delta u = 4\pi G \delta(\mathbf{x})$ yielding

$$(2\pi)^3 \hat{u}(k) = -\frac{4\pi G}{k^2} < 0. \quad (246)$$

We introduce the Jeans wavenumber

$$k_J^2 = 4\pi G \beta \rho m. \quad (247)$$

The dispersion relation (175) can be written

$$\epsilon(k, \omega) = 1 + \frac{4\pi G}{k^2} \int_C \frac{f'(v)}{v - \frac{\omega}{k}} dv. \quad (248)$$

Comparing this expression with Eq. (9), we make the link with the attractive HMF model by setting

$$\frac{4\pi G}{k^2} = \frac{\tilde{k}}{2}, \quad \beta m = \tilde{\beta}, \quad \frac{\omega}{k} = \tilde{\omega}, \quad (249)$$

where the tilde variables refer the HMF model and the un-tilde variables to self-gravitating systems. Then, we find that the dimensionless parameters for self-gravitating systems are

$$\eta = \frac{k_J^2}{k^2}, \quad \Omega = \frac{\omega}{\sqrt{4\pi G \rho}}, \quad a = \frac{1}{\sqrt{\eta}} \sqrt{\beta m} v_a. \quad (250)$$

The results obtained in Sec. 2 for the attractive HMF model can be applied to (uniform) self-gravitating systems provided that we interpret η as a normalized squared wavelength and Ω as a normalized pulsation according to Eq. (250). In particular, the Maxwell distribution is stable for $k > k_J$ (i.e. $\eta < 1$) and unstable for $k < k_J$ (i.e. $\eta > 1$) and the Tsallis distributions are stable for $k > (\frac{n}{n+1})^{1/2} k_J$ (i.e. $\eta < \eta_c$) and unstable for $k < (\frac{n}{n+1})^{1/2} k_J$ (i.e. $\eta > \eta_c$). The Nyquist curves for the Maxwell and Tsallis distributions are given in Secs. 3 and 4. By contrast, the phase diagrams of the double-humped distribution (in Secs. 2.6 and 2.7) are not directly applicable to self-gravitating systems because, according to Eq. (250), the dimensionless parameter $a \propto 1/\sqrt{\eta}$ depends on k . Therefore, this is not the correct dimensionless separation. For self-gravitating systems, the correct dimensionless separation (which must be independent on the wavenumber k) is $y = \eta a^2 = \beta m v_a^2$ instead of a . Therefore, the correct stability diagram corresponds to the curve(s) $\eta_c(y)$ obtained from Eqs. (111)-(112). This will be discussed in more detail in a specific paper.

E Landau damping and Landau growth for the repulsive and attractive HMF models

Like for Coulombian plasmas, the repulsive HMF model leads to Landau damping at low temperatures. On the other hand, the attractive HMF model can lead to ‘‘Landau growth’’ associated to the phase transition (collapse) at low temperatures.

E.1 The limit $T \rightarrow 0$

Let us first consider the limit $T \rightarrow 0$ for the repulsive HMF model. The case $T = 0$ corresponds to $f = \rho \delta(v)$. In that case, we obtain $\epsilon(\omega) = 1 - \frac{k\rho}{2\omega^2}$. The condition $\epsilon(\omega) = 0$ yields $\omega = \pm(k\rho/2)^{1/2} = \pm\omega_p$ where ω_p is the proper pulsation

$$\omega_p^2 = \frac{k\rho}{2} = \frac{kM}{4\pi}. \quad (251)$$

This is the equivalent of the plasma pulsation in plasma physics. Therefore, for $T = 0$ the system is stable and the perturbation oscillates with the pulsation ω_p without attenuation. To determine the damping rate $\gamma = -\omega_i$ for $T \ll 1$, we shall solve the equation (127) for the complex pulsation $\omega = \omega_r + i\omega_i$ by assuming $\omega_i \ll \omega_r$ (we adapt the method of plasma physics given in [72]). Expanding the dielectric function in Taylor series as $\epsilon(\omega) = \epsilon(\omega_r + i\omega_i) \simeq \epsilon(\omega_r) + i\epsilon'(\omega_r)\omega_i$, the condition $\epsilon(\omega) = 0$ gives to leading order

$$\epsilon_r(\omega_r) = 0, \quad (252)$$

$$\epsilon_i(\omega_r) + \epsilon'_r(\omega_r)\omega_i = 0, \quad (253)$$

where $\epsilon_r(\omega_r)$ and $\epsilon_i(\omega_r)$ are defined in Eqs. (128) and (129). Integrating by parts, Eq. (128) can be rewritten

$$\epsilon_r(\omega_r) = 1 - \frac{k}{2} P \int_{-\infty}^{+\infty} \frac{f(v)}{(v - \omega_r)^2} dv. \quad (254)$$

For $v/\omega_r \ll 1$, we get

$$\epsilon_r(\omega_r) = 1 - \frac{k\rho}{2\omega_r^2} \left(1 + \frac{2\langle v \rangle}{\omega_r} + \frac{3\langle v^2 \rangle}{\omega_r^2} + \dots \right). \quad (255)$$

If the distribution is symmetrical with respect to the origin and if the variance is finite, we obtain

$$\epsilon_r(\omega_r) = 1 - \frac{k\rho}{2\omega_r^2} \left(1 + \frac{3\langle v^2 \rangle}{\omega_r^2} + \dots \right), \quad (256)$$

and

$$\epsilon_r'(\omega_r) = \frac{k\rho}{\omega_r^3}. \quad (257)$$

Substituting these relations in Eqs. (252)-(253), we find that

$$1 - \frac{k\rho}{2\omega_r^2} \left(1 + \frac{3\langle v^2 \rangle}{\omega_r^2} \right) = 0, \quad (258)$$

$$- \pi \frac{k}{2} f'(\omega_r) + \frac{k\rho}{\omega_r^3} \omega_i = 0. \quad (259)$$

This expansion is valid for $T = \langle v^2 \rangle \rightarrow 0$. For $T = 0$, Eq. (258) gives $\omega_r = \omega_p$. Then, to next order, Eq. (258) gives

$$\omega_r^2 = \omega_p^2 + 3T + \dots \quad (T \rightarrow 0). \quad (260)$$

This asymptotic expansion for $T \rightarrow 0$ also gives the exact pulsation (valid at any temperature) for the water-bag distribution (see Sec. 7.1.1). Using the dimensionless variables introduced in Sec. 3, Eq. (260) can be rewritten²²

$$\Omega_r^2 = 1 + \frac{3}{\eta} + \dots \quad (\eta \rightarrow +\infty). \quad (261)$$

On the other hand, to leading order when $T \rightarrow 0$ (or $\eta \rightarrow +\infty$), Eq. (259) gives the damping rate²³

$$\omega_i = \frac{\pi\omega_p^3}{2\rho} f'(\omega_p). \quad (262)$$

When $f'(\omega_p) < 0$, we obtain the expression of the Landau damping for the repulsive HMF model. We stress that the relation (260) is the same for *any* distribution. By contrast, the damping coefficient (262) strongly depends on

²² Let us recall that this solution only exists for the repulsive HMF model. For the attractive HMF model, there is collapse when $T \rightarrow 0$ (see below).

²³ A more accurate expression is obtained by replacing $f'(\omega_p)$ by $f'(\omega_r)$.

the form of the distribution. For the Maxwellian distribution (34), we find that

$$\Omega_i = -\sqrt{\frac{\pi}{8}} \eta^{3/2} e^{-\eta/2}. \quad (263)$$

For the asymmetric double-humped distribution (93), we get

$$\Omega_i = -\frac{1}{1+\Delta} \sqrt{\frac{\pi}{8}} \eta^{3/2} \left[(1-a)e^{-\frac{\eta}{2}(1-a)^2} + \Delta(1+a)e^{-\frac{\eta}{2}(1+a)^2} \right]. \quad (264)$$

For the Tsallis distributions (47), we obtain

$$\Omega_i = -\sqrt{\frac{\pi}{8}} B_n \eta^{3/2} \left(n - \frac{1}{2} \right) \frac{1}{n+1} \left[1 - \frac{\eta}{2(n+1)} \right]_+^{n-3/2}. \quad (265)$$

For $n \rightarrow \pm\infty$, we recover Eq. (263). For $n > 1/2$, the damping is zero if $\omega_p > v_m$, i.e. $\eta > 2(n+1)$. For fixed n in the range $]-\infty, -1[$ and $\eta \rightarrow +\infty$, Eq. (265) becomes

$$\Omega_i = \sqrt{\frac{\pi}{8}} B_n \frac{1}{2^{n-\frac{3}{2}}} \left(n - \frac{1}{2} \right) \frac{1}{[-(n+1)]^{n-\frac{1}{2}}} \eta^n, \quad (266)$$

so the damping rate behaves like $\Omega_i \propto -1/\eta^{n|}$ for $\eta \rightarrow +\infty$. Let us consider for illustration the index $n = -3/2$ corresponding to the distribution

$$f = \frac{2\rho}{\pi\sqrt{T}} \frac{1}{\left(1 + \frac{v^2}{T}\right)^2}. \quad (267)$$

In that case, we have

$$\Omega_i = -\frac{4}{\eta^{3/2}}. \quad (268)$$

Using the correspondance between Coulombian plasmas and the repulsive HMF model (see Appendix D), we find that the equivalent of Eqs. (260) and (262) are

$$\omega_r^2 = \omega_p^2 + 3Tk^2, \quad \omega_i = \frac{\pi\omega_p^3}{2\rho k^2} f' \left(\frac{\omega_p}{k} \right). \quad (269)$$

These expressions are valid for $k/k_D \rightarrow 0$. For the Maxwellian distribution, we get

$$\omega_i = -\sqrt{\frac{\pi}{8}} \omega_p \left(\frac{k_D}{k} \right)^3 e^{-\frac{\beta m \omega_p^2}{2k^2}}. \quad (270)$$

For the Tsallis distributions, we get

$$\omega_i = -\sqrt{\frac{\pi}{8}} B_n \omega_p \left(\frac{k_D}{k} \right)^3 \times \left(n - \frac{1}{2} \right) \frac{1}{n+1} \left[1 - \frac{\beta m \omega_p^2}{2(n+1)k^2} \right]_+^{n-3/2}. \quad (271)$$

For $n \rightarrow \pm\infty$, we recover Eq. (270). For $n > 1/2$, the damping is zero if $\omega_p/k > v_m$, i.e. if $k/k_J < 1/\sqrt{2(n+1)}$. For fixed n in the interval $] -\infty, -1[$ and $k/k_D \rightarrow 0$, we obtain

$$\omega_i = \sqrt{\frac{\pi}{8}} B_n \omega_p \frac{1}{2^{n-\frac{3}{2}}} \left(n - \frac{1}{2}\right) \frac{1}{[-(n+1)]^{n-\frac{1}{2}}} \left(\frac{k_D}{k}\right)^{2n}, \quad (272)$$

so the damping behaves like $\omega_i \propto -k^{2|n|}$ for $k/k_D \rightarrow 0$. For the distribution (267) corresponding to $n = -3/2$, we have

$$\omega_i = -\frac{4\omega_p}{k_D^3} k^3. \quad (273)$$

Let us now consider the limit $T \rightarrow 0$ for the attractive HMF model. The case $T = 0$ corresponds to $f = \rho \delta(v)$. In that case, we obtain $\epsilon(\omega) = 1 + \frac{k\rho}{2\omega^2} = 0$ yielding $\omega = \pm i(k\rho/2)^{1/2}$. Therefore, for $T = 0$ the system is unstable and the perturbation grows with a growth rate $\omega_i = (kM/4\pi)^{1/2}$. Let us now consider the case $T \ll 1$. We anticipate a solution with $\omega_r = 0$ and $\omega_i > 0$. In that case, the perturbation grows ($\omega_i > 0$) without oscillating. The growth rate is given by Eq. (30). Integrating Eq. (30) by parts, we obtain

$$1 - \frac{k}{2} \int_{-\infty}^{+\infty} \frac{f(v)(\omega_i^2 - v^2)}{(v^2 + \omega_i^2)^2} dv = 0. \quad (274)$$

Expanding the integrand in powers of $v/\omega_i \ll 1$ for $T \rightarrow 0$, we find that

$$\omega_i^2 = \frac{kM}{4\pi} - 3T - \dots \quad (T \rightarrow 0), \quad (275)$$

with $T = \langle v^2 \rangle$. This asymptotic expansion for $T \rightarrow 0$ also gives the exact pulsation (valid at any temperature $T < T_c = kM/12\pi$) for the water-bag distribution (see Sec. 4). Introducing dimensionless variables, we get

$$\Omega_i^2 = 1 - \frac{3}{\eta} - \dots \quad (\eta \rightarrow +\infty). \quad (276)$$

For the Maxwellian distribution, we recover Eq. (136) of [29].

E.2 The limit $T \rightarrow +\infty$

Let us consider the limit $T \rightarrow +\infty$ for the repulsive HMF model (we adapt the method of plasma physics given in [70]). We look for a solution of the equation $\epsilon(\omega) = 0$ of the form $\omega = \omega_r + i\omega_i$ with $\omega_i < 0$ (damping) and $\omega_i/\omega_r \gg 1$. Using Eq. (12) for $\omega_i < 0$, Eq. (127) can be written

$$1 - \frac{k}{2} \int_{-\infty}^{+\infty} \frac{f'(v)}{v - \omega} dv - ik\pi f'(\omega) = 0. \quad (277)$$

If f decreases exponentially rapidly for large v , then for $\omega_i/\omega_r \gg 1$, the foregoing equation reduces to

$$1 - ik\pi f'(\omega) = 0. \quad (278)$$

Separating real and imaginary parts, we obtain two transcendental equations

$$\text{Re}[ik\pi f'(\omega_r + i\omega_i)] = 1, \quad (279)$$

$$\text{Im}[if'(\omega_r + i\omega_i)] = 0, \quad (280)$$

which strongly depend on the form of the distribution. For the Maxwellian (34), they can be rewritten to leading order in the limit $\omega_i/\omega_r \gg 1$ as

$$k\pi \left(\frac{\beta}{2\pi}\right)^{1/2} \rho\beta\omega_i e^{\frac{\beta}{2}\omega_i^2} \cos(\beta\omega_r\omega_i) = 1, \quad (281)$$

$$\sin(\beta\omega_r\omega_i) = 0. \quad (282)$$

Equation (282) implies $\beta\omega_r\omega_i = m\pi$. Eq. (281) will have a solution provided that m is even. Let us take $\beta\omega_r\omega_i = \pi$. Then, Eq. (281) gives

$$-k\pi \left(\frac{\beta}{2\pi}\right)^{1/2} \rho\beta\omega_i e^{\frac{\beta}{2}\omega_i^2} = 1, \quad (283)$$

which determines ω_i . By a graphical construction, it is easy to see that $|\omega_i|$ is an increasing function of T . For $T \rightarrow +\infty$, we find the asymptotic behavior

$$\omega_i = -\sqrt{2T \ln T}, \quad \omega_r = -\pi \sqrt{\frac{T}{2 \ln T}}. \quad (284)$$

Since $\omega_i/\omega_r \sim \ln T \rightarrow +\infty$, our basic assumption is satisfied. We also note that $\omega_r < 0$ in the repulsive case. Introducing dimensionless variables, we have for $\eta \rightarrow 0$:

$$\Omega_i = -\sqrt{\frac{2|\ln \eta|}{\eta}}, \quad \Omega_r = \frac{-\pi}{\sqrt{2\eta|\ln \eta|}}. \quad (285)$$

Using the correspondance (245) between the repulsive HMF model and Coulombian plasmas, we recover the results of plasma physics [70] for $k/k_D \rightarrow +\infty$:

$$\omega_i = -\frac{2\omega_p}{k_D} k \sqrt{\ln k}, \quad \omega_r = -\frac{\pi\omega_p}{2k_D} \frac{k}{\sqrt{\ln k}}. \quad (286)$$

Let us consider the limit $T \rightarrow +\infty$ for the attractive HMF model. We again look for a solution of the equation $\epsilon(\omega) = 0$ of the form $\omega = \omega_r + i\omega_i$ with $\omega_i < 0$ (damping) and $\omega_i/\omega_r \gg 1$. Repeating the procedure followed previously, we obtain two transcendental equations

$$\text{Re}[ik\pi f'(\omega_r + i\omega_i)] = -1, \quad (287)$$

$$\text{Im}[if'(\omega_r + i\omega_i)] = 0. \quad (288)$$

For the Maxwellian (34), they can be rewritten to leading order in the limit $\omega_i/\omega_r \gg 1$ as

$$k\pi \left(\frac{\beta}{2\pi}\right)^{1/2} \rho\beta\omega_i e^{\frac{\beta}{2}\omega_i^2} \cos(\beta\omega_r\omega_i) = -1, \quad (289)$$

$$\sin(\beta\omega_r\omega_i) = 0. \quad (290)$$

Equation (290) implies $\beta\omega_r\omega_i = m\pi$. Eq. (289) will have a solution provided that m is odd. Let us take $\omega_r = 0$. Then, Eq. (289) reduces to Eq. (283). Therefore, for $T \rightarrow +\infty$, we find the asymptotic behavior

$$\omega_i = -\sqrt{2T \ln T}, \quad \omega_r = 0. \quad (291)$$

This returns Eq. (141) of [29].

F Marginal stability of spatially inhomogeneous states

For the HMF model, the eigenvalue equation associated with the minimization problem (162) can be written (see Eq. (77) of [29])

$$\frac{d}{d\theta} \left(\frac{p'(\rho)}{\rho} \frac{dq}{d\theta} \right) + \frac{k}{2\pi} \int_0^{2\pi} q(\theta') \cos(\theta - \theta') d\theta' = -2\lambda q, \quad (292)$$

with $q(0) = q(2\pi) = 0$, where $q(\theta) = \int_0^\theta \delta\rho(\theta') d\theta'$ is the perturbed integrated density²⁴. This equation is valid for homogeneous and inhomogeneous equilibrium density profiles $\rho(\theta)$. We have $\delta^2\mathcal{W} = \frac{1}{2} \int \mathcal{L}[q]q d\theta$ where \mathcal{L} is the operator defined by the r.h.s. of Eq. (292). Therefore, a critical point of energy $\mathcal{W}[\rho, \mathbf{u}]$ at fixed mass is a (local) minimum iff all the eigenvalues λ are positive. In that case, the density profile $\rho(\theta)$ is formally nonlinearly stable with respect to the Euler equation. On the other hand, since (162) \Leftrightarrow (199) \Leftrightarrow (191), the corresponding distribution function $f(\theta, v)$ (leading to an equation of state $p(\rho)$) is a (local) minimum of pseudo free energy $F[f]$ at fixed mass, so that it is formally nonlinearly stable with respect to the Vlasov equation. Therefore, the positiveness of the eigenvalues of Eq. (292) is a sufficient condition of formal nonlinear stability for the Vlasov equation. Unfortunately, it does not appear feasible to solve Eq. (292) analytically in the general case. However, it is possible to solve it analytically for the marginal case $\lambda = 0$. This criterion will give the point at which the series of equilibria of the inhomogeneous equilibrium states becomes unstable. This is the first result concerning the stability of *inhomogeneous* states of the HMF model. The eigenvalue equation (292) can be rewritten

$$\frac{d}{d\theta} \left(\frac{p'(\rho)}{\rho} \frac{dq}{d\theta} \right) - b_x \cos \theta - b_y \sin \theta = \frac{\lambda^2}{\rho} q, \quad (293)$$

with

$$b_x = -\frac{k}{2\pi} \int_0^{2\pi} q(\theta) \cos \theta d\theta = \frac{k}{2\pi} \int_0^{2\pi} q'(\theta) \sin \theta d\theta, \quad (294)$$

²⁴ Note that the eigenvalue equation associated with the linear stability problem (see Eq. (85) of [29]) has a similar form as Eq. (292) and that they both coincide at the neutral point $\lambda = 0$.

$$b_y = -\frac{k}{2\pi} \int_0^{2\pi} q(\theta) \sin \theta d\theta = -\frac{k}{2\pi} \int_0^{2\pi} q'(\theta) \cos \theta d\theta, \quad (295)$$

where we have used an integration by parts to obtain the second equalities. For $\lambda = 0$, Eq. (293) is readily integrated to yield

$$\frac{dq}{d\theta} = \frac{\rho}{p'(\rho)} (b_x \sin \theta - b_y \cos \theta + C), \quad (296)$$

where C is a constant of integration. Another integration with the boundary condition $q(0) = 0$ yields

$$q(\theta) = b_x \int_0^\theta \frac{\rho}{p'(\rho)} \sin \theta' d\theta' - b_y \int_0^\theta \frac{\rho}{p'(\rho)} \cos \theta' d\theta' + C \int_0^\theta \frac{\rho}{p'(\rho)} d\theta'. \quad (297)$$

Then, the condition $q(2\pi) = 0$ determines the constant

$$C = b_y \frac{\int_0^{2\pi} \frac{\rho}{p'(\rho)} \cos \theta d\theta}{\int_0^{2\pi} \frac{\rho}{p'(\rho)} d\theta}, \quad (298)$$

where we have assumed that the density profile $\rho(\theta)$ is symmetric with respect to $\theta = 0$ to simplify some terms²⁵. Substituting Eq. (296) into Eq. (294), we find either that $b_x = 0$ or that

$$1 = \frac{k}{2\pi} \int_0^{2\pi} \frac{\rho}{p'(\rho)} \sin^2 \theta d\theta. \quad (299)$$

Substituting Eq. (296) into Eq. (295) we find either that $b_y = 0$ or that

$$1 = \frac{k}{2\pi} \int_0^{2\pi} \frac{\rho}{p'(\rho)} \cos^2 \theta d\theta - \frac{k}{2\pi} \frac{\left(\int_0^{2\pi} \frac{\rho}{p'(\rho)} \cos \theta d\theta \right)^2}{\int_0^{2\pi} \frac{\rho}{p'(\rho)} d\theta}. \quad (300)$$

Therefore, if we restrict ourselves to even perturbations ($b_y = 0$ and $b_x \neq 0$) the condition of marginal stability is given by Eq. (299) and if we restrict ourselves to odd perturbations ($b_x = 0$ and $b_y \neq 0$) the condition of marginal stability is given by Eq. (300). For general perturbations, we must satisfy both Eqs. (299) and (300). Note that using Eq. (203), which becomes for the HMF model

$$\frac{\rho}{p'(\rho)} = - \int \frac{\partial f}{\partial v}(\theta, v) dv, \quad (301)$$

we can express the criteria of marginal stability (299) and (300) directly in terms of the distribution function $f(\theta, v) = f(\epsilon)$.

²⁵ Since $\rho = \rho(\Phi)$ at equilibrium with $\Phi = B_x \cos \theta + B_y \sin \theta$ (where B_x, B_y are the two components of the magnetization), it is always possible to choose the x -axis such that the distribution profile is even ($B_y = 0$).

For homogeneous distributions $\rho = \text{const.}$, we immediately find that Eqs. (299) and (300) both reduce to the condition of marginal stability

$$c_s^2 = \frac{kM}{4\pi}, \quad \text{or} \quad 1 + \frac{k}{2} \int_{-\infty}^{+\infty} \frac{f'(v)}{v} dv = 0. \quad (302)$$

For inhomogeneous isothermal distributions (see Eq. (20) of [29]) for which $p = \rho T$, using Eqs. (21) and (26) of [29] and the relation $I_2(t) = I_0(t) - \frac{2}{t} I_1(t)$, we find that Eq. (299) is always satisfied. This implies that an inhomogeneous isothermal distribution is always marginally stable with respect to even perturbations ($b_y = 0$ and $b_x \neq 0$) of the form (297), for any temperature T . This can be checked explicitly. For an isothermal distribution, these perturbations can be written

$$q(\theta) = e^{-\beta B \cos \theta} - 1, \quad (303)$$

and a direct substitution shows that they are solution of Eq. (293) with $\lambda = 0$. Finally, for inhomogeneous isothermal distributions, using Eqs. (20), (21) and (26) of [29], we find that Eq. (300) is equivalent to

$$\left(\frac{I_1(x)}{I_0(x)} \right)^2 + \frac{2}{x} \frac{I_1(x)}{I_0(x)} = 1, \quad (304)$$

with $x = \beta B$. The only solution of this equation is $x = 0$ leading to $T = \frac{kM}{4\pi} = T_c$. Indeed, it is shown in [29] that the inhomogeneous isothermal distributions are always stable ($\lambda \geq 0$) so that the point of marginal stability corresponds to the point $x = 0$ where the branch of inhomogeneous states begins. At the temperature $T = T_c$, the branch of homogeneous states becomes unstable and bifurcates to the branch of inhomogeneous states (second order phase transition). Therefore, in that case, the marginal stability condition for homogeneous and inhomogeneous states coincides. However, this is not necessarily the case for more general distributions like for example the Lynden-Bell (or Fermi-Dirac) distribution where a first order phase transition takes place [57,58]. In that case, the new stability criteria (299) and (300) can give information about the stability/instability of the inhomogeneous states.

References

1. *Dynamics and thermodynamics of systems with long range interactions*, edited by T. Dauxois *et al.*, Lecture Notes in Physics **602**, (Springer, 2002).
2. *Dynamics and thermodynamics of systems with long range interactions: Theory and experiments*, edited by A. Campa *et al.*, AIP Conf. Proc. **970** (AIP, 2008).
3. P.H. Chavanis, *Statistical mechanics of two-dimensional vortices and stellar systems* in [1]
4. P.H. Chavanis, M. Ribot, C. Rosier, C. Sire, Banach Center Publ. **66**, 103 (2004)
5. P.H. Chavanis, C. R. Physique **7**, 318 (2006)
6. D. Lynden-Bell, R. Wood, MNRAS **138**, 495 (1968)
7. W. Thirring, Z. Phys. **235**, 339 (1970)
8. D.H.E. Gross, *Microcanonical Thermodynamics: Phase Transitions in "Small" Systems*, Lecture Notes in Physics **66** (World Scientific, Singapore, 2001)
9. M. Kiessling, PNAS **100**, 1510 (2003)
10. R.A. Smith, T.M. O'Neil, Phys. Fluids B **2**, 2961 (1990)
11. T. Padmanabhan, Phys. Rep. **188**, 285 (1990)
12. R. Ellis, K. Haven, B. Turkington, J. Stat. Phys. **101**, 999 (2000)
13. J. Barré, D. Mukamel, S. Ruffo, Phys. Rev. Lett. **87**, 030601 (2001)
14. P.H. Chavanis, Phys. Rev. E **65**, 056123 (2002)
15. P.H. Chavanis, A&A **401**, 15 (2003)
16. H. Touchette, R.S. Ellis, B. Turkington, Physica A **340**, 138 (2004)
17. F. Bouchet, J. Barré, J. Stat. Phys. **118**, 1073 (2005)
18. P.H. Chavanis, Int J. Mod. Phys. B **20**, 3113 (2006)
19. S. Chandrasekhar *Principles of Stellar Dynamics* (University of Chicago Press, 1942)
20. W.C. Saslaw, *Gravitational Physics of Stellar and Galactic Systems* (Cambridge Univ. Press, 1985)
21. J. Binney, S. Tremaine, *Galactic Dynamics* (Princeton Series in Astrophysics, 1987)
22. L. Spitzer, *Dynamical Evolution of Globular Clusters* (Princeton University Press 1987)
23. D. Heggie, P. Hut *The Gravitational Million-Body Problem: A Multidisciplinary Approach to Star Cluster Dynamics* (Cambridge Univ. Press, 2003)
24. P.H. Chavanis, Physica A **387**, 787 (2008)
25. P.H. Chavanis, Physica A **387**, 1123 (2008)
26. P.H. Chavanis, Phys. Rev. E **64**, 026309 (2001)
27. D. Dubin, Phys. Plasmas **10**, 1338 (2003)
28. F. Bouchet, T. Dauxois, Phys. Rev. E **72**, 5103 (2005)
29. P.H. Chavanis, J. Vatteville, F. Bouchet, Eur. Phys. J. B **46**, 61 (2005)
30. P.H. Chavanis, M. Lemou, Eur. Phys. J. B **59**, 217 (2007)
31. V. Latora, A. Rapisarda, C. Tsallis, Phys. Rev. E **64**, 056134 (2001)
32. Y.Y. Yamaguchi, J. Barré, F. Bouchet, T. Dauxois, S. Ruffo, Physica A **337**, 36 (2004)
33. A. Campa, A. Giansanti, G. Morelli, Phys. Rev. E **76**, 041117 (2007)
34. M. Antoni, S. Ruffo, A. Torcini, Europhys. Lett. **66**, 645 (2004)
35. P.H. Chavanis, A&A **432**, 117 (2005)
36. A. Pluchino, V. Latora, A. Rapisarda, Physica A **338**, 60 (2004)
37. A. Rapisarda, A. Pluchino, Europhysics News **36**, 202 (2005)
38. Y. Yamaguchi, F. Bouchet, T. Dauxois, J. Stat. Mech. **1**, 01020 (2007)
39. P.H. Chavanis, M. Lemou, Phys. Rev. E **72**, 061106 (2005)
40. X.P. Huang, C.F. Driscoll, Phys. Rev. Lett. **72**, 2187 (1994)
41. H. Brands, P.H. Chavanis, R. Pasmantier, J. Sommeria, Phys. Fluids **11**, 3465 (1999)
42. P.H. Chavanis, Physica A **387**, 1504 (2008)
43. D. Lynden-Bell, MNRAS **136**, 101 (1967)
44. J. Miller, Phys. Rev. Lett. **65**, 2137 (1990)
45. R. Robert, J. Sommeria, JFM **229**, 291 (1991)
46. P.H. Chavanis, J. Sommeria, R. Robert, ApJ **471**, 385 (1996)
47. J. Barré, T. Dauxois, G. de Ninno, D. Fanelli, S. Ruffo, Phys. Rev. E **69**, 045501 (2004)

48. A. Antoniazzi, F. Califano, D. Fanelli, S. Ruffo, Phys. Rev. Lett. **98**, 150602 (2007)
49. Y. Levin, R. Pakter, F.B. Rizzato, Phys. Rev. E **78**, 021130 (2008)
50. Y. Yamaguchi, Phys. Rev. E **78**, 041114 (2008)
51. R. Bachelard, C. Chandre, D. Fanelli, X. Leoncini, S. Ruffo, [arXiv:0809.3400]
52. P.H. Chavanis, J. Sommeria, JFM **314**, 267 (1996)
53. P.H. Chavanis, J. Sommeria, MNRAS **296**, 569 (1998)
54. R. Ellis, K. Haven, B. Turkington, Nonlinearity **15**, 239 (2002)
55. P.H. Chavanis, Eur. Phys. J. B **53**, 487 (2006)
56. A. Antoniazzi, D. Fanelli, J. Barré, P.H. Chavanis, T. Dauxois, S. Ruffo, Phys. Rev. E **75**, 011112 (2007)
57. A. Antoniazzi, D. Fanelli, S. Ruffo, Y. Yamaguchi Phys. Rev. Lett. **99**, 040601 (2007)
58. P.H. Chavanis, G. De Ninno, D. Fanelli, S. Ruffo, in *Chaos, Complexity and Transport*, edited by C. Chandre, X. Leoncini and G. Zaslavsky (World Scientific, Singapore, 2008) p. 3 [arXiv:0712.1752]
59. A. Venaille, F. Bouchet, [arXiv:0710.5606]
60. A. Campa, P.H. Chavanis, A. Giansanti, G. Morelli, Phys. Rev. E **78**, 040102(R) (2008)
61. P.H. Chavanis, Eur. Phys. J. B **52**, 47 (2006)
62. K.R. Yawn, B.N. Miller, Phys. Rev. E **56**, 2429 (1997)
63. A. Pluchino, A. Rapisarda, C. Tsallis, Europhys. Lett. **80**, 26002 (2007)
64. F. Bouchet, T. Dauxois, D. Mukamel, S. Ruffo, Phys. Rev. E **77**, 1125 (2008)
65. A. Pluchino, V. Latora, A. Rapisarda, Physica A **340**, 187 (2004)
66. F. Baldovin, E. Orlandini, Phys. Rev. Lett. **96**, 240602 (2006); **97**, 100601 (2006)
67. F. Baldovin, E. Orlandini, Int. J. Mod. Phys. B **21**, 4000 (2007)
68. F. Baldovin, P.H. Chavanis, E. Orlandini, Phys. Rev. E (in press) [arXiv:0804.0612]
69. P.H. Chavanis, *Dynamics and thermodynamics of systems with long-range interactions : interpretation of the different functionals*, in [2]
70. R. Balescu, *Statistical Mechanics of Charged Particles* (Interscience, New York, 1963)
71. S. Ichimaru *Basic Principles of Plasma Physics* (W.A. Benjamin, Reading, MA, 1973)
72. D.R. Nicholson, *Introduction to Plasma Theory* (Krieger Publishing Company, Florida, 1992)
73. D.D. Holm, J.E. Marsden, T. Ratiu & A. Weinstein, Phys. Rep. **123**, 1 (1985)
74. H. Nyquist, Bell System Tech. J. **11**, 126 (1932)
75. V.A. Antonov, Astr. Zh. **37**, 918 (1960) (translated in: Sov. Astron. **4**, 859 (1961))
76. P. Bartholomew, MNRAS **151**, 333 (1971)
77. H. Kandrup, ApJ **370**, 312 (1991)
78. M. Lemou, F. Méhats, P. Raphaël, preprint
79. M. Antoni, S. Ruffo, Phys. Rev. E **52**, 2361 (1995)
80. W. Braun, K. Hepp, Commun. Math. Phys. **56**, 101 (1977)
81. Inagaki, S. & Konishi, T. 1993, Publ. Astron. Soc. Japan **45**, 733
82. Choi, M.Y. & Choi, J. 2003, Phys. Rev. Lett., **91**, 124101
83. P.H. Chavanis, C. Sire, Physica A **356**, 419 (2005)
84. H.C. Plummer, MNRAS **71**, 460 (1911)
85. A.S. Eddington, MNRAS **76**, 572 (1916)
86. M. Le Bellac, *Des phénomènes critiques aux champs de jauge* (InterEditions/Editions du CNRS, 1988)
87. J. Barré, F. Bouchet, T. Dauxois, S. Ruffo Eur. Phys. J. B **29**, 577 (2002)
88. P.H. Chavanis, A&A **451**, 109 (2006)